2022

Distributed Detection in Energy Harvesting Wireless Sensor Networks

Ghazaleh Ardeshiri
University of Central Florida

DISTRIBUTED DETECTION IN ENERGY HARVESTING WIRELESS SENSOR NETWORKS

by

GHAZALEH ARDESHIRI
B.S. in Electrical Engineering, Shiraz University, Shiraz, Iran, 2013
M.S. in Electrical Engineering, Shiraz University, Shiraz, Iran, 2017

A dissertation submitted in partial fulfilment of the requirements
for the degree of Doctor of Philosophy
in the Department of Electrical and Computer Engineering
in the College of Engineering and Computer Science
at the University of Central Florida
Orlando, Florida

Fall Term
2022

Major Professor: Azadeh Vosoughi

ABSTRACT

A conventional wireless sensor networks (WSN), consisting of sensors powered by non-rechargeable batteries, has a strictly limited lifetime. Energy harvesting (EH) from the environment is a promising solution to address the energy constraint problem in conventional WSNs, and to render these networks to self-sustainable networks with perpetual lifetimes. In EH-powered WSNs, where sensors are capable of harvesting and storing energy, power control is necessary to balance the rates of energy harvesting and energy consumption for data transmission. In addition, wireless communication channels change randomly in time due to fading. These together prompt the need for developing new power control strategies for an EH-enabled transmitter that can best exploit and adapt to the random energy arrivals and time-varying fading channels.

We consider parallel structure EH-powered WSNs tasked with solving a binary distributed detection problem. Sensors process locally their observations, adapt their transmission according to the battery and fading channel states, and transmit their data symbols to the fusion center (FC) over orthogonal fading channels. We study adaptive transmission schemes that optimize detection performance metrics at the FC, subject to certain battery and transmit power constraints. In the first part, modeling the random energy arrival as a Poisson process, we propose a novel transmit power control strategy that is parameterized in terms of the channel gain quantization thresholds and the scale factors corresponding to the quantization intervals and we find the jointly optimal quantization thresholds and the scale factors such that detection metric at the FC is maximized. We have assumed that the battery operates at the steady-state and the energy arrival and channel models are independent and identically distributed across transmission blocks. In the second part, we assume the battery is not at the steady-state and both the channel and the energy arrival are modeled as

homogeneous finite-state Markov chains. Therefore, the power control optimization problem at hand becomes a multistage stochastic optimization problem and can be solved via the Markov decision process (MDP) framework. This is the first work that develops MDP-based channel-dependent power control policy for distributed detection in EH-powered WSNs.

To my love, Mohsen, who never gave up on me, for his endless support,

and to my parents and my sisters.

ACKNOWLEDGMENTS

I would like to express my sincere gratitude to my advisor Prof. Azadeh Vosoughi of the Electrical and Computer Engineering department at UCF for her insightful guidance, immense knowledge, and continuous support of my PhD study and research. She was incessantly encouraging, supportive, and ready to provide practical help and advice.

I am also grateful to my committee members for their great support and invaluable advice: Dr. Nazanin Rahnavard, Dr. Yaser Fallah, Dr. George Atia of the Electrical and Computer Engineering program and Dr. Kein Hua of Department the Computer Science program.

I am grateful to my close friends for providing support and friendship that I needed in my PhD life. I also want to thank my lab mates for the stimulating discussions and brainstorms we did and for sharing their valuable ideas in research related problems I encountered along the way.

I am also grateful to have my parents for their never ending love, kindness and support. There are not enough words to describe how thankful I am to have both of you. Thank you for always being there for me. I would also like to thank my sisters whose voices over the phone make me forget everything and just smile.

Words cannot express how grateful I am to my beloved husband, who always supports me with his unconditional love through thick and thin. Thank you for taking care of me beyond my dreams.

TABLE OF CONTENTS

LIST OF FIGURES

LIST OF TABLES

CHAPTER 1: INTRODUCTION AND LITERATURE REVIEW[1][2][3].

The classical problem of binary distributed detection in a network, consisting of multiple distributed sensors and a fusion center (FC), has a long and rich history [4–7]. In this problem, each sensor sends its locally processed observation to the FC, that is tasked with making a reliable global decision about the underlying binary hypothesis testing problem. Distributed detection using wireless sensor network (WSN) has applications in diverse domains, including environmental monitoring, surveillance, healthcare, and transportation [8]. The classical studies in [4–7] cannot be directly applied to WSNs, since the results are obtained based on the assumption that the rate-constrained communication channels between sensors and FC are error-free. The designs of wireless sensor networks to perform the task of distributed detection are often based on the conventional battery-powered sensors, leading into designs with a short lifetime, due to battery depletion [9–11]. Recently, energy harvesting, which can collect energy from renewable resources in ambient environment (e.g., solar, wind, and geothermal energy) has attracted much attention [12, 13]. Energy harvesting technology in wireless sensor networks promises a self-sustainable system with a lifetime that is not limited by the lifetime of the conventional batteries [10, 14]. Due to this reason, researchers have studied how to re-design the local decision rules at the sensors and the fusion rule at the FC, such that the effect of wireless communication channels between the sensors and the FC is integrated into the designs [15–17]. Another challenge of performing distributed detection task using a WSN is to provide an *unvarying detection performance*. In conventional WSNs,

[1] © 2018 IEEE. Part of this chapter is reprinted, with permission, from [1]

[2] © 2019 IEEE. Part of this chapter is reprinted, with permission, from [2]

[3] © 2022 IEEE. Part of this chapter is reprinted, with permission, from [3]

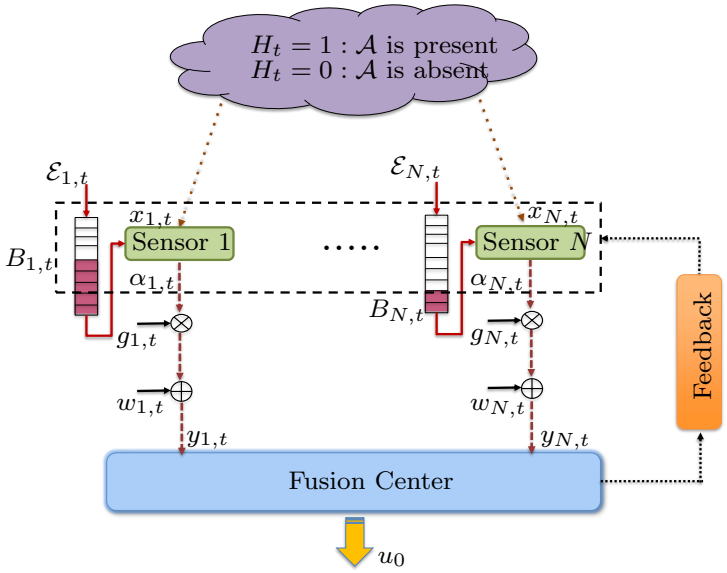

Figure 1.1: Our system model and the schematic of battery state in time slot t.

sensors are powered by non-rechargeable batteries. A major limitation of these networks is their limited lifetimes, due to the fact that sensors become inactive when the energy stored in their batteries is exhausted. Motivated by this challenge, researchers have developed novel adaptive signal transmission strategies that improve the energy efficiency and hence extend the lifetimes of these networks. These transmission strategies include optimal channel-dependent power control [18, 19], censoring [17, 20], node sleep/wake mechanisms [21], and ordered transmission [22], that attempt to curtail sensors' transmission to the FC. However, regardless of the adopted transmission strategy, the lifetime of a conventional WSN is still bounded, leading to a detection performance degradation, due to discontinuities in sensor-FC communication. Recently, the technology of harnessing energy from the renewable resources of energy in ambient environment has attracted attention of many researchers, as a promising solution to address the challenging energy constraint problem in WSNs, and to render these networks to self sustainable networks with perpetual lifetimes. In particular, energy harvesting (EH)-powered sensors offer potential for transforming design and performance of

WSNs. In practice, the energy arrival of ambient energy sources is intrinsically time-variant and often sporadic. To flatten the randomness of the energy arrival, the harvested energy is stored in a battery, to balance the energy arrival and the energy consumption. Power/energy management in EH-enabled WSNs with finite size batteries is necessary, in order to balance the rates of energy harvesting and energy consumption for transmission. If the energy management policy is overly aggressive, sensors may stop functioning, due to energy outage. On the other hand, if the policy is overly conservative, sensors may fail to utilize the excess energy, due to energy overflow, leading into a performance degradation [23].

1.1 Literature Survey and Related Works

Energy harvesting has been also considered in the contexts of cooperative data communication [24], cognitive radio systems [25], distributed estimation [26], and distributed detection [1–3,8,10,27]. The authors in [18,19] have designed the optimal channel-dependent transmit power control strategies that maximize J-divergence based detection metric for binary-hypothesis and multiple-hypothesis distributed detection problems, respectively. Modeling sensor-FC channels as deterministic and assuming each sensor knows its CSI in full precision, the power control strategies in [18, 19] allow each sensor to adapt its transmit power based on its CSI. However, CSI acquisition at the sensors in WSNs is difficult. In time division duplexing systems, sensors need to perform training-based channel estimation to acquire CSI [28–30]. In frequency division duplexing systems, sensors can acquire quantized CSI via a limited feedback channel from the FC [31]. We note that signal adaptation at the sensors according to the quantized CSI received from a limited feedback channel has been considered before for data communications [32] and distributed estimation of a signal source [33]. It is worth pointing out that, while the studies in [18, 19] on optimal channel-dependent transmit

power control strategies for distributed detection problem can be applied to conventional WSNs, they cannot be applied to EH-enabled WSNs. These works have not considered the new challenges related to energy management imposed by the random nature of the energy arrival and harvesting, i.e., the available energy for transmission in [18, 19] is fixed (non-random). In the context of distributed detection, there are only few studies that consider EH-powered sensors [8, 10, 27], among which [10] is the closest work to ours. Considering an EH-powered node, that is deployed to monitor the change in its environment, the authors in [27] formulated a quickest change detection problem, where the goal is to detect the time at which the underlying distribution of sensor observation changes. Choosing error probability as the detection performance metric, the authors in [8] proposed ordered transmission schemes, that can lead to a smaller average number of transmitting sensors, without comprising the detection performance. Modeling the randomly arriving energy units during a time slot as a Bernoulli process, the battery state as a K-state Markov chain, and choosing Bhattacharya distance as the detection performance metric, the authors in [10] have investigated the optimal local decision thresholds at the sensors, such that the detection performance is optimized. We note that [8, 27] assumed sensor-FC channels are error-free and [10] considered a binary asymmetric channel model for sensor-FC links. The high level channel model in [10], combined with the Bernoulli process model for random energy arrival is limiting. Specifically, it does not allow one to study channel-dependent transmit power control strategies. Such a study requires a more realistic channel model and a different stochastic energy arrival model that matches the energy needed for a channel-dependent transmission. In the following we provide a concise review of the most related literature to our work, highlight how our present work fills the knowledge gap in the literature, and how it is different from our previous works in [1, 2]. In our preliminary works [1, 2] we attempted to fill this knowledge gap, and studied channel-dependent transmit power control policies, considering fading channel model with additive Gaussian noise. In particular, in [1] we modeled random energy

arrival as a Bernoulli process and assumed each sensor knows its CSI in full precision and adapts its transmit power according to the channel-inversion power control policy in wireless communications (i.e., allocated power is inversely proportional to CSI). We found the optimal decision thresholds at sensors such that Kullback-Leibler (KL) distance detection metric at the FC is maximized. In [2], we modeled random energy arrival as an exponential process. Similar to our present work, we assumed each sensor only knows its quantized CSI and adapts its transmit power according to its battery state and its quantized CSI, such that J-divergence based detection metric at the FC is maximized. However, the form of the power control strategy in [2] is completely different from here, i.e., given the quantization thresholds each sensor employs an offline determined lookup table that provides a power value for each battery state and quantized CSI. We found the optimal lookup table through an exhaustive (deterministic) search method. In [3], we consider a parallel network, consisting of several distributed sensors and a FC, tasked with solving a binary distributed detection problem. Each sensor is capable of harvesting energy from the ambient environment and is equipped with a battery of finite size to store the harvested energy. Sensors process locally their observations and communicate directly with the FC over orthogonal fading channels Each sensor only knows the quantized channel state information (CSI), via a limited feedback channel from the FC. Our proposed transmission strategy combines the concepts of censoring and channel-dependent power control, i.e., when the local log-likelihood ratio (LLR) is below a given threshold, sensor is silent, when the LLR exceeds the threshold, sensor transmits a symbol (one information bit), where the symbol power is variable (adaptive) and chosen according to sensor's battery state and its quantized CSI. The FC jointly processes the received signals from all sensors and makes a reliable global decision about the underlying hypotheses (see Fig. 1.1). Given our adopted WSN model (see Fig. 1.1), we aimed at developing an adaptive channel-dependent transmit power control strategy for sensors such that a detection performance metric is optimized. We chose the J-divergence between the distributions

of the detection statistics at the FC under two hypotheses, as the detection performance metric. Our choice is motivated by the fact that J-divergence is a widely adopted metric for designing distributed detection systems [18, 19, 30, 31]. This is because the Bayesian error probability P_e corresponding to the optimal Bayesian fusion rule at the FC for most problems does not have a closed-form expression, and minimizing P_e does not render a tractable procedure for system design, even for small sized networks. We note that J-divergence and P_e are related through $P_e > \Pi_0\Pi_1 e^{-J/2}$, where Π_0, Π_1 are the a-priori probabilities of the null and the alternative hypotheses, respectively [18, 19, 30, 31]. Hence, maximizing the J-divergence is equivalent to minimizing the lower bound on P_e. Also, J-divergence is related to Bhattacharya distance [10] and KL distance [1] that are used as optimization criteria for distributed detection system designs. Furthermore, when sensors' observations conditioned on the true hypothesis are statistically independent, the *total J-divergence of a parallel network at the FC is the summation of the individual J-divergence corresponding to individual sensors*. Therefore, maximizing the total J-divergence at the FC is equivalent to maximizing the individual J-divergence, i.e., maximizing the total J-divergence at the FC enables *distributed implementation* of the design procedure at each sensor. This is different from P_e, which *cannot be decomposed* into the individual error probabilities corresponding to individual sensors.

In [3] We modeled the randomly arriving energy units during a time slot as a Poisson process and the dynamics of the battery as a K-state Markov chain, and consider fading channel model with additive Gaussian noise. Our proposed power control strategy in [3] is parameterized in terms of the channel gain quantization thresholds and the scale factors (corresponding to the quantization intervals). The scale factors play key roles in balancing the rates of energy harvesting and energy consumption for transmission. We sought the jointly optimal scale factors and and the quantization thresholds such that the J-divergence

at the FC is maximized, subject to an average transmit power per sensor constraint. This optimization problem can be solved *offline* at the FC and each sensor, given the statistical information of fading channels and the energy arrival, and the solution is available *a priori* at each sensor, such that each sensor can adapt its transmit power according to its battery state and its quantized CSI that is received from the FC via the feedback channel.

Our work in [34] is different from our prior works in [1–3] in several aspects. The transmit power control strategies in these works are intrinsically different from this work, since in [1–3] we have assumed that the battery operates at the steady-state and the energy arrival and channel models are independent and identically distributed (i.i.d) across transmission blocks. Consequently, the power optimization problem in [1–3] became a deterministic optimization problem, in terms of the optimization variables, and the obtained solutions are different. In this work, the battery is not at the steady-state. Also, both the channel and the energy arrival are modeled as homogeneous finite-state Markov chains (FSMCs). Therefore, the power control optimization problem at hand becomes a multistage stochastic optimization problem, and can be solved via the MDP framework. To the best of our knowledge, this is the first work that develops MDP-based channel-dependent power control policy for distributed detection in EH-WSNs. The MDP framework has been utilized before in [35, 36] to address a quickest change detection problem.

1.2 Motivation, Contributions and Dissertation Organization

Our main contributions can be summarized as follow:

In the Chapter 2, we consider the distributed detection of a known signal using a wireless network with N energy harvesting sensors and a FC. Each sensor makes a noisy observation,

corrupted additive and multiplicative observation noises. Each sensor applies an energy detector, to compare its test statistic against a local decision threshold θ_n (to be optimized), and transmits only if the test statistic exceeds θ_n, its channel gain exceeds a minimum threshold ζ_n, and its battery state can afford transmission. Given our transmission and battery state models, our goal is to investigate the optimal θ_n's that optimize the detection performance metric, subject to average transmit symbol energy constraint.

The main contributions of Chapter 3 can be summarized as follows:

- Given our adopted system model, we propose a novel parameterized channel-dependent transmit power control strategy and formulate a constrained optimization problem to optimize the parameters such that the J-divergence at the FC is maximized, subject to an average transmit power per sensor constraint. Since the proposed problem is not concave with respect to the optimization variables, and the objective function and the constraints of the problem are not differentiable with respect to these variables, we resort to grid-based search methods. In particular, we consider deterministic, random, and hybrid deterministic-random search methods, and explore the trade-offs in their performance and computational complexity. We show that the proposed hybrid search methods have the lowest computational complexity and provide a close-to-optimal performance.

- We derive an approximate expression for P_e, relying on Lindeberg Central Limit Theorem (CLT) for large number of sensors.

- Our simulations reveal the importance of optimizing the parameters of the channel-dependent transmit power control strategy, to maximize the detection performance. We demonstrate that the optimized transmit power level is not a monotonically increasing or decreasing function of the channel gain (given the battery state), i.e., it

is different from water-filling or channel-inversion power control strategies in wireless communication. We also numerically illustrate the trade-off between average transmit power and detection performance, i.e., we show how much average transmit power is required to provide a certain P_e value at the FC.

The main contributions of Chapter 4 can be summarized as follows:

- Modeling the channel fading process as a time- homogeneous finite-state Markov chain and assuming that each sensor knows its current battery state and its quantized channel state information (CSI) obtained by a limited feedback from the FC, our goal is to find the optimal transmit power control policy such that the detection performance metric of interest is maximized. We formulate the problem at hand as a finite-horizon Markov decision process (MDP) problem and obtain the optimal policy via finite-horizon dynamic programming.

The main contributions of Chapter 5 can be summarized as follows:

- Given our adopted system model, we develop the optimal power control policy, using dynamic programming and utilizing the Lagrangian approach to transform the constrained MDP problem into an equivalent unconstrained MDP problem. For the optimal policy, the local action (i.e., a sensor's transmit power) depends on the network state (i.e., all sensors' battery states, quantized CSIs, and the arrived energies), and the computational complexity of the algorithm grows exponentially in number of sensors N. Implementing this solution requires each sensor to report its battery state and arrived energy to the FC, which imposes a significant signaling overhead to the sensors.

• To eliminate the signaling overhead, we develop a sub-optimal power control policy, using a uniform Lagrangian multiplier to transform the constrained MDP problem into N unconstrained MDP problems. For the sub-optimal policy, the local action depends on only the local state (i.e., a sensor's battery state, quantized CSI, and the arrived energy), and the computational complexity of the algorithm grows linearly in N.

- We numerically study the performance of our proposed algorithms and we show that, the performance of the sub-optimal power control policy is very close to that of the optimal policy.

- We study how our system setup and proposed solutions can be extended to the scenario where sensors are randomly deployed in the field.

The main contributions of Chapter 6 can be summarized as follows:

- We extended our work in Chapter 3 to temporally correlated MIMO. Sensors communicate directly with a FC with limited feedback in a time-correlated channel. Markov models are introduced for analyzing the effect of Doppler frequency on limited feedback rate in a MIMO system with channel gain feedback.

CHAPTER 2: OPTIMAL LOCAL THRESHOLDS FOR DISTRIBUTED DETECTION IN ENERGY HARVESTING WIRELESS SENSOR NETWORKS[1]

We consider a wireless sensor network, consisting of N heterogeneous sensors and a fusion center (FC), that is tasked with solving a binary distributed detection problem. Each sensor is capable of harvesting and storing energy for communication with the FC. For energy efficiency, a sensor transmits only if the sensor test statistic exceeds a local threshold θ_n, its channel gain exceeds a minimum threshold, and its battery state can afford the transmission. Our proposed transmission model at each sensor is motivated by the channel inversion power control strategy in the wireless communication community. Considering a constraint on the average energy of transmit symbols, we study the optimal θ_n's that optimize two detection performance metrics: (i) the detection probability P_D at the FC, assuming that the FC utilizes the optimal fusion rule based on Neyman-Pearson optimality criterion, and (ii) Kullback-Leibler distance (KL) between the two distributions of the received signals at the FC conditioned by each hypothesis. Our numerical results indicate that θ_n's obtained from maximizing the KL distance are near-optimal. Finding these thresholds is computationally efficient, as it requires only N one-dimensional searches, as opposed to a N-dimensional search required to find the thresholds that maximize P_D.

2.1 Our system model and problem Statement

Let x_n denote the local observation at sensor n during an observation period. We assume the following signal model

$$H_1 : x_n = \mathcal{A} g_n + w_n, \quad H_0 : x_n = v_n \tag{2.1}$$

where v_n and g_n are additive and multiplicative observation noises, respectively. We assume $v_n \sim \mathcal{N}(0, \sigma_{v_n}^2)$, $g_n \sim \mathcal{N}(0, \gamma_{g_n})$ and all observation noises are independent over time and among N sensors. During each observation period, sensor n takes L samples of x_n to measure the received signal energy and applies an energy detector to make a binary decision, i.e., sensor n decides whether or not signal $\mathcal{A}$ is present. Let d_n denote the binary decision of sensor k, where $d_n = 0$ and $d_n = 1$, respectively, correspond to H_0 and H_1. The test statistic for sensor n is

$$\Lambda_n = \frac{1}{L} \sum_{l=1}^{L} |x_{n,l}|^2 \gtrless_{d_n=0}^{d_n=1} \theta_n \tag{2.2}$$

where θ_n is local decision threshold to be optimized. For the signal model in (2.1)), conditioned on each hypothesis x_n is Gaussian, that is, $x_n | H_0 \sim \mathcal{N}\left(0, \sigma_{v_n}^2\right)$ and $x_n | H_1 \sim \mathcal{N}\left(\mathcal{A}\gamma_{g_n}, \sigma_{v_n}^2\right)$. The test statistic Λ_n in (2.2) has non-central Chi-square distribution [14] as given below

$$H_1 : \Lambda_n \sim \chi_L^2(\eta_n), \quad H_0 : \Lambda_n \sim \chi_L^2 \tag{2.3}$$

where $\eta_n = \mathcal{A}^2\mathbb{E}\{g_{n,l}^2\} = \mathcal{A}^2\gamma_{g_n}$ is the non-centrality parameter. Using (2.3), the false-alarm probability P_{f_n} and detection probability P_{d_n} can be derived as following

$$P_{\mathrm{f}_n} = \Pr(\Lambda_n > \theta_n | H_0) = \frac{\Gamma\big(L/2, \frac{L\theta_n}{\sigma_{v_n}^2}\big)}{\Gamma\left(L/2\right)} \tag{2.4}$$

$$P_{\mathrm{d}_n} = \Pr(\Lambda_n > \theta_n | H_1) = Q_{L/2}\big(\frac{\sqrt{\eta_n}}{\sigma_{v_n}}, \frac{\sqrt{L\theta_n}}{\sigma_{v_n}}\big) \tag{2.5}$$

where $\Gamma(l)$ is the gamma function, $\Gamma(l,x) = \int_x^\infty t^{l-1}e^{-t}dt$ is the upper incomplete gamma function, $Q_n(a,b) = \int_b^\infty x(\frac{x}{a})^{l-1}\exp(\frac{x^2+a^2}{-2})I_{l-1}(ax)dx$ is the generalized Marcum-Q function, and $I_{l-1}(\cdot)$ is modified Bessel function of order $l-1$ [37].

We assume each sensor is able to harvest energy from the environment and stores this harvested energy in a battery that has the capacity of storing at most K units of energy. The sensors communicate with the FC through orthogonal fading channels with channel gains $|h_k|$'s that are independent and have Rayleigh distribution with parameters γ_{h_n}. The sensors employ on-off keying (OOK) signaling for communication, where a $d_n = 1$ decision at sensor n is conveyed at the cost of spending one or more energy units and a $d_n = 0$ decision is conveyed through a no-transmission with no energy cost. We assume that only sending a message costs units of energy, and the energy of making the observation and processing is negligible. The number of energy units spent to convey a $d_n = 1$ decision depends on the quality of the channel gain $|h_n|$ and the battery state of sensor n. Motivated by the channel-inversion power control strategy developed in the wireless communication community [38] we try to compensate for the fading and let the number of energy units spent to convey a $d_n = 1$ decision be (roughly) inversely proportional to $|h_n|$ (i.e., a smaller $|h_n|$ corresponds to a larger number of energy units), albeit if the battery has sufficient number of stored energy units. To avoid the battery depletion when $|h_n|$ is too small, we impose an extra constraint inspired by the channel truncation technique in the channel-inversion power control strategy [38],

to ensure that a $d_n = 1$ decision is conveyed only if $|h_n|$ exceeds a minimum threshold ζ_n (choice of ζ_n will be discussed later). Let t indicate the index of the observation period and $b_{n,t}$ denote the battery state of sensor n in the observation period t. Let $u_{n,t}$ represent the sensor output corresponding to the observation period t. Based on the above explanations, we define $u_{n,t}$ as

$$u_{n,t} = \begin{cases} \lceil \frac{\lambda}{|h_n|} \rceil & \Lambda_n > \theta_n,\ b_{n,t} > \lceil \frac{\lambda}{|h_n|} \rceil,\ |h_n|^2 > \zeta_n \\ 0 & \text{Otherwise} \end{cases} \tag{2.6}$$

where λ is a power regulation constant (that depends on the battery structure). We use the round function $\lceil . \rceil$ toward $+\infty$, to ensure that $u_{n,t}$ is a discrete symbol and the energy of this symbol is equal to the number of consumed energy units to convey $d_n = 1$. The constraint $\Lambda_n > \theta_n$ in (2.6) comes directly from (2.2). We assume the average energy of the transmitted symbol $u_{n,t}$ is constrained, i.e., $P_{av_n} = \mathbb{E}\{\lceil \frac{\lambda}{|h_n|} \rceil^2 \big| u_n = \lceil \frac{\lambda}{|h_n|} \rceil\}$, where the expectation is taken with respect to $|h_n|$. We model $b_{n,t}$ in (2.6) as the following

$$b_{n,t} = \min\big\{ b_{n,t-1} - \lceil \frac{\lambda}{|h_n|} \rceil I_{u_{n,t-1}} + \Omega_{n,t}\ ,\ K \big\} \tag{2.7}$$

where $b_{n,t-1}$ is the battery state of the previous observation period and $\Omega_{n,t} \in \{0, 1\}$ is a binary random variable, indicating whether or not sensor n harvests one unit of energy. We assume $\Omega_{n,t}$ is a Bernoulli random variable, with $\Pr(\Omega_{n,t} = 1) = p_e$, where p_e depends on the harvesting structure. This assumption is repeatedly used in the literature (see [39] and references therein). The indicator function $I_{u_{n,t-1}}$ in (2.7) is defined as

$$I_{u_{n,t-1}} = \begin{cases} 1 & u_{n,t-1} > 0 \\ 0 & \text{Otherwise} \end{cases} \tag{2.8}$$

In the remaining, we focus on one observation period and we drop the subscript t from the battery state $b_{n,t}$ and the sensor output $u_{n,t}$. Given our system model description above, our goal is to investigate the optimal local decision thresholds θ_n's in (2.2) that optimizes the detection performance metric.

2.2 Optimizing Local Decision Thresholds

We consider two detection performance metrics to find the optimal θ_n's: (i) the detection probability at the FC, assuming that the FC utilizes the optimal fusion rule based on Neyman-Pearson optimality criterion, and (ii) the KL distance between the two distributions of the received signals at the FC conditioned on hypothesis H_0, H_1. In Section 2.2.1 we derive the optimal fusion rule and the expressions for the detection and false alarm probabilities P_D, P_F at the FC. In Section 2.2.2 we derive two approximate expressions for the KL distance at the FC. In Section 2.2.3 we discuss the choice of the threshold ζ_n in (2.6).

2.2.1 Optimal LRT Fusion Rule and P_D, P_F Expressions

The received signal at the FC from sensor n is $y_n = h_n u_n + w_n$, where the additive communication channel noise $w_n \sim \mathcal{N}\left(0, \sigma_{w_n}^2\right)$. The likelihood ratio at the FC is [40]

$$\Delta_{\text{LRT}} = \log\left(\frac{f\left(y_1, ..., y_N | H_1\right)}{f\left(y_1, ..., y_N | H_0\right)}\right) = \sum_{n=1}^{N} \log\left(\frac{\sum_{u_n} f\left(y_n | u_n, H_1\right) \Pr\left(u_n | H_1\right)}{\sum_{u_n} f\left(y_n | u_n, H_0\right) \Pr\left(u_n | H_0\right)}\right) \tag{2.9}$$

in which we use the fact that, given H_i the received signals at the FC are independent, i.e., $f(y_1, ..., y_N | H_i) = \prod_{n=1}^{N} f(y_n | H_i)$. Examining (2.9), we note given u_n, y_n and H_i are

independent and hence $f\left(y_n|u_n, H_i\right) = f\left(y_n|u_n\right)$ for $i = 0, 1$. Also, given u_n, y_n is Gaussian, i.e., $y_n|_{u_n=0} \sim \mathcal{N}\left(0, \sigma_{n_n}^2\right)$ and $y_n|_{u_n=\lceil \frac{\lambda}{|h_n|} \rceil} \sim \mathcal{N}\left(\lceil \frac{\lambda}{|h_n|} \rceil h_n, \sigma_{n_n}^2\right)$. The probabilities $\Pr(u_n|H_1)$, $\Pr(u_n|H_0)$ in (2.9) are

$$\begin{aligned} & \Pr\left(u_n = \lceil \frac{\lambda}{|h_n|} \rceil \middle| H_1\right) = \Pr\left(\Lambda_n > \theta_n,\ b_n > \lceil \frac{\lambda}{|h_n|} \rceil,\ |h_n|^2 > \zeta_n \middle| H_1\right) \\ = \ & \Pr\left(\Lambda_n > \theta_n | H_1\right) \Pr\left(b_n > \lceil \frac{\lambda}{|h_n|} \rceil\right) \Pr\left(|h_n|^2 > \zeta_n\right) = P_{\mathrm{d}_n} \rho_n q_n = \alpha_n \qquad (2.10) \\ & \Pr\left(u_n = \lceil \frac{\lambda}{|h_n|} \rceil | H_0\right) = \Pr\left(\Lambda_n > \theta_n \middle| H_0\right) \Pr\left(b_n > \lceil \frac{\lambda}{|h_n|} \rceil\right) \Pr\left(|h_n|^2 > \zeta_n\right) \\ = \ & P_{\mathrm{f}_n} \rho_n q_n = \beta_n \qquad (2.11) \end{aligned}$$

where $P_{\mathrm{f}_n}, P_{\mathrm{d}_n}$ are given in (2.4), (2.5), $\rho_n = \Pr(b_n > \lceil \frac{\lambda}{|h_n|} \rceil)$ and $q_n = \Pr(|h_n|^2 > \zeta_n) = \exp(-\zeta_n/\gamma_{h_n})$.

Assuming b_n in (2.7) is a stationary random process, one can compute the cumulative distribution function (CDF) and the probability mass function (pmf) of b_n in terms of K, p_e, γ_{h_n}. Fig. 2.1a shows CDF of b_n for $K = 20$ and $p_e = 0.5, 0.75, 0.82$, and Fig. 2.1b depicts pmf of b_n for $K = 50$ and $p_e = 0.8$. For our numerical results in Section 2.3 we use pmf of b_n to find ρ_n in (2.10) and (2.11). Combing all, we can rewrite Δ_{LRT} as the following [29]

$$\begin{aligned} \Delta_{\mathrm{LRT}} &= \sum_{n=1}^{N} \log \left(\frac{\alpha_n f(y_n|u_n = \lceil \frac{\lambda}{|h_n|} \rceil) + (1-\alpha_n) f(y_n|u_n = 0)}{\beta_n f(y_n|u_n = \lceil \frac{\lambda}{|h_n|} \rceil) + (1-\beta_n) f(y_n|u_n = 0)} \right) \\ &= \sum_{n=1}^{n} \log \frac{\alpha_n \exp\left(-\frac{(y_n - \lceil \frac{\lambda}{|h_n|} \rceil h_n)^2}{2\sigma_{w_n}^2}\right) + (1-\alpha_n) \exp\left(-\frac{y_n^2}{2\sigma_{w_n}^2}\right)}{\beta_n \exp\left(-\frac{(y_n - \lceil \frac{\lambda}{|h_n|} \rceil h_n)^2}{2\sigma_{w_n}^2}\right) + (1-\beta_n) \exp\left(-\frac{y_n^2}{2\sigma_{w_n}^2}\right)} \end{aligned}$$

In low SNR regime as $\sigma_{w_n}^2 \to \infty$ taking a logarithm from Δ_{LRT} and using the approximations $e^{-x} \approx 1 - x$ and $\log(1 + x)$ for small x, we can simplify Δ_{LRT} to $\Delta_{\mathrm{LRT}} \approx -T_n + \sum_{n=1}^{N} \nu_n y_n$

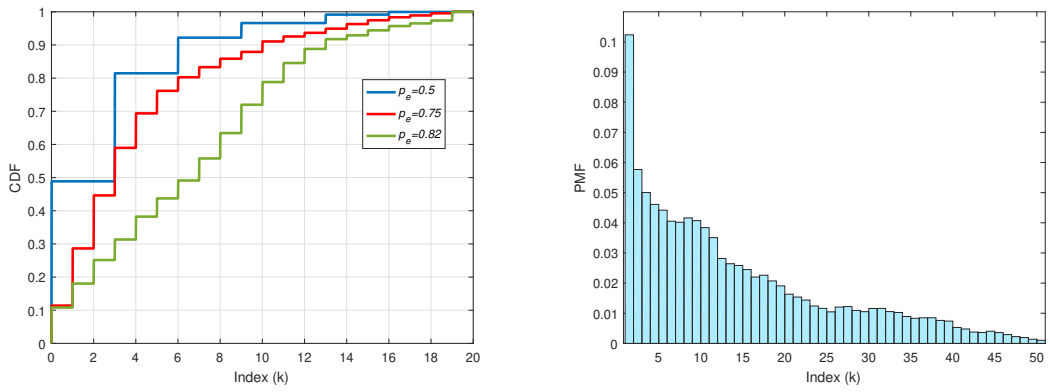

(a) (b)

Figure 2.1: CDF of b_n for $K=20$ and $p_e=0.5, 0.75, 0.82$, pmf of b_n for $K=50$ and $p_e=0.8$.

where $T_n=\sum_{n=1}^{K}\lceil\frac{\lambda}{|h_n|}\rceil^2 h_n^2(\alpha_n-\beta_n)/2\sigma_{w_n}^2$ and $\nu_n=\lceil\frac{\lambda}{|h_n|}\rceil h_n(\alpha_n-\beta_n)/\sigma_{w_n}^2$. Given a threshold τ, the optimal likelihood ratio test (LRT) is $\Delta_{\text{LRT}} \underset{H_0}{\overset{H_1}{\gtrless}} \tau$. The false alarm and detection probabilities P_F, P_D at the FC are

$$P_F = \Pr\left(\Delta_{\text{LRT}} > \tau | H_0\right) = Q\Big(\frac{\tau-\mu_{\Delta|H_0}}{\sigma_{\Delta|H_0}}\Big) \tag{2.12}$$

$$P_D = \Pr\left(\Delta_{\text{LRT}} > \tau | H_1\right) = Q\left(\frac{Q^{-1}(a)\sigma_{\Delta|H_0}+\mu_{\Delta|H_0}-\mu_{\Delta|H_1}}{\sigma_{\Delta|H_1}}\right) \tag{2.13}$$

where

$$\mu_{\Delta|H_i}=-T_n+\sum_{n=1}^{N}\nu_n\mu_{y_n|H_i}, \quad \sigma^2_{\Delta|H_i}=\sum_{n=1}^{n}\nu_n^2\sigma^2_{y_n|H_i}, i=0,1$$

$$\mu_{y_n|H_0}=\lceil\frac{\lambda}{|h_n|}\rceil h_n\beta_n, \quad \sigma^2_{y_n|H_0}=\lceil\frac{\lambda}{|h_n|}\rceil^2 h_n^2\beta_n(1-\beta_n)+\sigma^2_{n_n}$$

$$\mu_{y_n|H_1}=\lceil\frac{\lambda}{|h_n|}\rceil h_n\alpha_n, \quad \sigma^2_{y_n|H_1}=\lceil\frac{\lambda}{|h_n|}\rceil^2 h_n^2\alpha_n(1-\alpha_n)+\sigma^2_{n_n}$$

The threshold τ is determined from the constraint on $P_F \leq a$ in terms of a. We note that

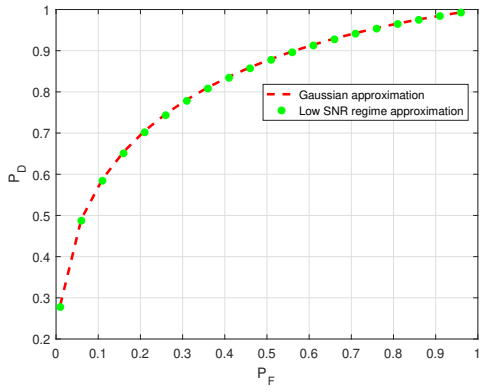

Figure 2.2: P_D vs. P_F, $K = 20, p_e = 0.75, P_{av} = 1$dB.

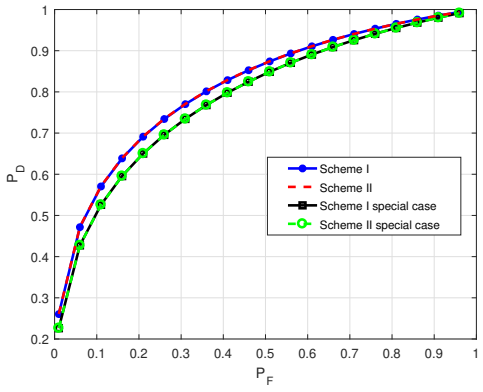

Figure 2.3: P_D vs. P_F, $K = 20, p_e = 0.75, P_{av} = 1$ dB.

P_D expression depends on all our optimization variables θ_n's through α_n, β_n's in $\mu_{\Delta H_i}$ and $\sigma^2_{\Delta|H_i}$.

2.2.2 KL Expression

Let KL_{tot} denote the KL distance between distributions $f(y_1, ..., y_N|H_1)$ and $f(y_1, ..., y_N|H_0)$ at the FC. Since $f(y_1, ..., y_N|H_i) = \prod_{n=1}^{N} f(y_n|H_i)$, we have $KL_{tot} = \sum_{n=1}^{N} KL_n$ where KL_n by definition is [41]

$$KL_n = \int_{y_n} f(y_n|H_1) \log\left(\frac{f(y_n|H_1)}{f(y_n|H_0)}\right) dy_n \tag{2.14}$$

We note that the distributions $f(y_n|H_i), i = 0, 1$ are Gaussian mixtures and thus KL_n in (2.14) does not have a general closed-form expression [18] and approximations must be made. One can approximate KL_n in (2.14) by the KL distance of two Gaussian distributions with the means $\mu_{y_n|H_0}$, $\mu_{y_n|H_1}$, and the variances $\sigma^2_{y_n|H_0}$ and $\sigma^2_{y_n|H_1}$, respectively, i.e., KL_n can be approximated as [42]

$$KL_n \approx \frac{1}{2}\log(\frac{\sigma^2_{y_n|H_0}}{\sigma^2_{y_n|H_1}}) + \frac{\sigma^2_{y_n|H_1} - \sigma^2_{y_n|H_0} + (\mu_{y_n|H_1} - \mu_{y_n|H_0})^2}{2\sigma^2_{y_n|H_0}} \tag{2.15}$$

Another approximation for KL_n in (2.14) can be found using the low SNR regime approximation in Section 2.2.1, as the following

$$KL_n \approx c_n(\beta_n - \alpha_n)\Bigg\{ c_n\sqrt{\frac{\pi}{2\sigma^2_{w_n}}}\Big((1-\alpha_n)(Q(\frac{y_n}{\sigma_{w_n}}) - 0.5) \\ +\alpha_n Q(\frac{y_n - c_n}{\sigma_{w_n}})\Big) + \alpha_n \exp\big(\frac{(c_n - y_n)^2}{-2\sigma^2_{w_n}}\big) + (1-\alpha_n)\exp\big(\frac{-y_n^2}{2\sigma^2_{n_n}}\big)\Bigg\} \tag{2.16}$$

where $c_n = \lceil \frac{\lambda}{|h_n|} \rceil h_n$. Different from P_D expression that depends on all θ_n's, KL_{tot} is decoupled such that KL_n depends on θ_n only through α_n, β_n's in $\mu_{y_n|H_i}$ and $\sigma^2_{y_n|H_i}$.

2.2.3 Choosing Threshold ζ_n in (2.6)

We find ζ_n in (2.6) via solving the constraint $P_{av_n} = \mathbb{E}\{\lceil \frac{\lambda}{|h_n|} \rceil^2 \big| u_n = \lceil \frac{\lambda}{|h_n|} \rceil\}$.

Recall h_n has Rayleigh distribution. After some algebraic manipulations we obtain

$$P_{av_n} = \alpha_n \sum_{i=1}^{\infty}(i+1)\left(e^{\frac{-1}{\gamma h_n}\max\left\{\zeta_n, \frac{\lambda^2}{i+1}\right\}} - e^{\frac{-\lambda^2}{i\gamma h_n}}\right) u\big[\frac{\lambda^2}{i} - \zeta_n\big] \tag{2.17}$$

where $u[.]$ is the step function and α_n is given in (2.10). Note α_n depends on ζ_n through q_n. Although there is no explicit expression for ζ_n, for our numerical results in Section 2.3 we use (2.17) to find ζ_n given P_{av_n} via the interpolation technique.

2.3 Simulation results and Conclusions

In this section, we numerically (i) find θ_n's which maximize P_D in (2.13). Finding θ_n's in this case requires N-dimensional search, as N grows the computational complexity grows

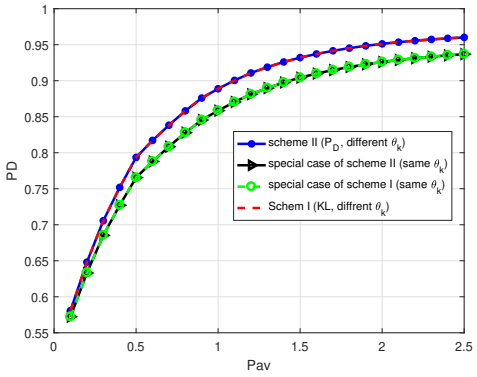

Figure 2.4: P_D vs. P_{av}, $K = 20, p_e = 0.75, P_F = 0.5$.

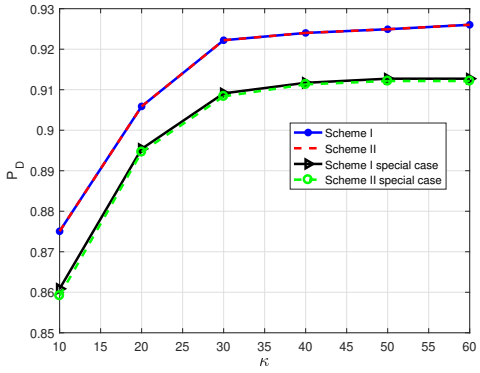

Figure 2.5: P_D vs. K, $p_e = 0.8, P_{av} = 1$ dB, $P_F = 0.5$.

exponentially; (ii) θ_n's which maximize $KL_{tot} = \sum_{n=1}^{N} KL_n$, using the KL_n approximations in (2.16), (2.16). Finding θ_n in this case requires only one dimensional search and is computationally very efficient. We then compare P_D evaluated at the θ_n's obtained from maximizing P_D (refer to as scheme I in the plots), with P_D evaluated at the θ_n's obtained from maximizing KL_{tot} (refer to as scheme II in the plots). Our simulation parameters are $N=3$, $\mathcal{A}=1$, $L=100$, $\lambda=1$, $\gamma_h = [1.5, 0.8, 1.4]$, $\gamma_g = [1.3, 2, 0.9]$ and $\sigma_n^2 = [0.9, 1.2, 0.8]$. Note that sensors are heterogeneous, in the sense that their statistical information parameters are different. Given $P_{av_n} = P_{av}$ we first obtain numerically ζ_n's using (2.17), where ζ_n's are still different since α_n's are different.

Fig. 2.2 plots P_D versus P_F, where for each P_F we evaluate P_D using θ_n's which maximize KL_{tot}, based on the KL_n approximations in (2.16) and (2.16). The fixed parameters in Fig. (2.2) are $K = 20$ units, $p_e = 0.75$, $P_{av} = 1$ dB. This figure shows that, these two approximations have similar $P_D - P_F$ behavior. Therefore, in the remaining figures, we use the KL_n approximation in (2.16).

Fig. 2.3 depicts P_D versus P_F for $K = 20$ units, $p_e = 0.75$, $P_{av} = 1$ dB. To plot Fig. 2.3, for each P_F we evaluate P_D using θ_n's that maximize P_D (scheme I) and KL_{tot} (scheme II).

Comparing schemes I and II in Fig. 2.3, we observe that these schemes perform very closely, indicating that using θ_n's that are obtained from maximizing KL_{tot} are near-optimal. In Fig. 2.3, we also compare schemes I and II for the special case where we assume all sensors employ the same local threshold $\theta_n = \theta$. For this special case, finding θ maximizing P_D or KL_{tot} only needs one dimensional search. The performance gap between each scheme and its corresponding special case indicates that when sensors are heterogeneous, it is advantageous to use different local thresholds according to sensors' statistics (i.e., $\gamma_{h_n}, \gamma_{g_n}, \sigma_{w_n}$).

Fig. 2.4 plots P_D versus P_{av} for $K = 20$ units, $p_e = 0.75$, $P_F = 0.5$. As expected, P_D increases as P_{av} increases. The reason is as P_{av} increases ζ_n's decrease, and sensors can afford to transmit even when their channel gains are weaker.

Fig. 2.5 illustrates P_D versus K for $p_e = 0.8$, $P_{av} = 1$ dB, $P_F = 0.5$. As expected, P_D increases as K increases and it saturates after certain K, since P_D is not limited by the battery size anymore and instead is limited by the sensors' statistics.

Comparing schemes I and II and their corresponding special cases in Figs. 2.4 and 2.5, we make similar observations to those in Fig. 2.3. In summary, we studied a distributed detection problem in a wireless network with N heterogeneous energy harvesting sensors and investigated the optimal local decision thresholds for given transmission and battery state models. Our numerical results indicate that the thresholds obtained from maximizing the KL distance are near-optimal. Finding these thresholds is computationally very efficient, as it requires only N one-dimensional searches, as opposed to a N-dimensional search required to find the thresholds that maximize the detection probability.

CHAPTER 3: ON ADAPTIVE TRANSMISSION FOR DISTRIBUTED DETECTION IN ENERGY HARVESTING WIRELESS SENSOR NETWORKS WITH LIMITED FUSION CENTER FEEDBACK[1]

We consider a wireless sensor network tasked with solving a binary distributed detection problem. Sensors communicate directly with a fusion center (FC) over orthogonal fading channels, with additive Gaussian noise. Each sensor can harvest randomly arriving energy units and store them in a battery. Also, it knows its quantized channel state information (CSI), acquired via a limited feedback channel from the FC. Modeling the randomly arriving energy units during a time slot as a Poisson process and the battery dynamics as a K-state Markov chain (where K is the battery size), we propose a channel-dependent transmit power control strategy such that the J-divergence based detection metric is maximized at the FC, subject to an average transmit power per sensor constraint. The proposed strategy is parameterized in terms of the channel gain quantization thresholds and the scale factors corresponding to the quantization intervals. This strategy allows each sensor to adapt its transmit power based on its battery state and its qunatized CSI. Finding optimal strategy requires solving a non-convex optimization problem that is not differentiable with respect to the optimization variables. We propose near-optimal strategies based on random search methods that have a low-computational complexity and provide a close-to-optimal performance.

3.1 System Model

3.1.1 Observation Model at Sensors

To describe our signal processing blocks at sensors and the FC as well as energy harvesting model, we divide time horizon into slots of equal length T_s. Each time slot is indexed by an integer t for $t = 1, 2, ..., \infty$. We model the underlying binary hypothesis H_t in time slot t as a binary random variable $H_t \in \{0, 1\}$ with a-priori probabilities $\Pi_0 = \Pr(H_t = 0)$ and $\Pi_1 = \Pr(H_t = 1) = 1 - \Pi_0$. We assume that the hypothesis H_t varies over time slots in an independent and identically distributed (i.i.d.) manner. Let $x_{n,t}$ denote the local observation at sensor n in time slot t. We assume that sensors' observations given each hypothesis with conditional distribution $f(x_{n,t}|H_t = h_t)$ for $h_t \in \{0, 1\}$ are independent across sensors. This model is relevant for WSNs that are tasked with detection of a known signal in uncorrelated Gaussian noises with the following signal model

$$H_t = 1 : \ x_{n,t} = \mathcal{A} + v_{n,t}, \qquad H_t = 0 : \ x_{n,t} = v_{n,t}, \quad \text{for } n = 1, \ldots, N \tag{3.1}$$

where Gaussian observation noises $v_{n,t} \sim \mathcal{N}(0, \sigma_{v_n}^2)$ are independent over time slots and across sensors. Given observation $x_{n,t}$ sensor n forms local log-likelihood ratio (LLR)

$$\Gamma_n(x_{n,t}) \triangleq \log\left(\frac{f(x_{n,t}|h_t = 1)}{f(x_{n,t}|h_t = 0)}\right), \tag{3.2}$$

and uses its value to choose its non-negative transmission symbol $\alpha_{n,t}$ to be sent to the FC. In particular, when LLR is below a given local threshold θ_n, sensor n does not transmit and let $\alpha_{n,t} = 0$. When LLR exceeds the given local threshold θ_n, sensor n chooses $\alpha_{n,t}$ according to its battery state and the feedback information about its communication channel. choice of $\alpha_{n,t}$ will be explained later in Section 3.1.2.

3.1.2 Battery State, Harvesting and Transmission Models

We assume sensors are equipped with identical batteries of finite size K cells (units), where each cell corresponds to b_u Joules of stored energy. Therefore, each battery is capable of storing at most Kb_u Joules of harvested energy. Let $B_{n,t} \in \{0, 1, ..., K\}$ denote the discrete random process indicating the battery state of sensor n at the beginning slot t. Note that $B_{n,t} = 0$ and $B_{n,t} = K$ represent the empty battery and full battery levels, respectively. Also, $B_{n,t} = k$ implies that the battery is at state k, i.e., k cells of the battery is charged and the amount of stored energy in the battery is kb_u Joules.

Let $\mathcal{E}_{n,t}$ denote the randomly arriving energy units[2] during time slot t at sensor n. We assume $\mathcal{E}_{n,t}$'s are i.i.d. over time slots and across sensors. We model $\mathcal{E}_{n,t}$ as a Poisson random variable with parameter ρ, and probability mass function (pmf) $p_m \triangleq \Pr(\mathcal{E}_{n,t} = m) = e^{-\rho}\rho^m/m!$ for $m = 0, 1, \ldots, \infty$. Note that parameter ρ is the average number of arriving energy units during one time slot at each sensor. Let $\mathcal{S}_{n,t}$ be the number of stored (harvested) energy units in the battery at sensor n during time slot t. Note that the harvested energy $\mathcal{S}_{n,t}$ cannot be used during slot t. Since the battery has a finite capacity of K cells, we have $\mathcal{S}_{n,t} \in \{0, 1, ..., K\}$. Also, $\mathcal{S}_{n,t}$ are i.i.d. over time slots and across sensors. The two random variables $\mathcal{S}_{n,t}$ and $\mathcal{E}_{n,t}$ are related as the following

$$\mathcal{S}_{n,t} = \begin{cases} \mathcal{E}_{n,t}, & \text{if } 0 \leq \mathcal{E}_{n,t} \leq K-1, \\ K, & \text{if } \mathcal{E}_{n,t} \geq K. \end{cases} \tag{3.3}$$

Based on (3.3) we can find the pmf of $\mathcal{S}_{n,t}$ in terms of the pmf of $\mathcal{E}_{n,t}$. Let $q_e \triangleq \Pr(\mathcal{S}_{n,t} = e)$

[2]Suppose each arriving energy unit measured in Joules is b_u Joules.

for $e = 0, 1, \ldots, K$. We have [3]

$$q_e = \begin{cases} p_e, & \text{if } 0 \leq e \leq K-1, \\ \sum_{m=K}^{\infty} p_m, & \text{if } e = K. \end{cases} \tag{3.4}$$

Let $g_{n,t}$ indicate the fading channel gain between sensor n and the FC during time slot t. We assume block fading model and $g_{n,t}$'s are i.i.d. over time slots and independent across sensors. We assume there is a limited feedback channel from the FC to the sensors [31], through which sensor n is informed of the quantization interval to which $g_{n,t}$ belongs. In particular, suppose the positive real line is partitioned into L disjoint intervals $\mathcal{I}_{n,l} = [\mu_{n,l}, \mu_{n,l+1})$ for $l = 0, ..., L-1$, using the quantization thresholds $\{\mu_{n,l}\}_{l=0}^{L}$, where $0 = \mu_{n,0} < \mu_{n,1} < \ldots < \mu_{n,L} = \infty$ (to be optimized). The quantization mapping rule follows: if the quantizer input $g_{n,t}$ lies in the interval $\mathcal{I}_{n,l}$ then the quantizer output is $\mu_{n,l}$. Let $\pi_{n,l} = \Pr(g_{n,t} \in \mathcal{I}_{n,l})$ be the probability that $g_{n,t}$ lies in the interval $\mathcal{I}_{n,l}$. This probability depends on the distribution of fading model. For instance, for Rayleigh fading model $g_{n,t}^2$ has exponential distribution with the mean $\mathbb{E}\{g_{n,t}^2\} = \gamma_{g_n}$ and we have

$$\pi_{n,l} = \Pr\left((g_{n,t}^2 \in [\mu_{n,l}^2, \mu_{n,l+1}^2)\right) = e^{\frac{-\mu_{n,l}^2}{\gamma_{g_n}}} - e^{\frac{-\mu_{n,l+1}^2}{\gamma_{g_n}}}. \tag{3.5}$$

Let $\mathcal{P}_{n,t}$ denote the transmit power of sensor n in time slot t. When LLR is below a given local threshold θ_n, sensor n does not transmit, i.e., $\mathcal{P}_{n,t} = 0$. When LLR exceeds θ_n, sensor n chooses $\mathcal{P}_{n,t}$ according to its battery state k and its quantized CSI, received through a limited feedback channel from FC. In particular, we choose a transmit power control strategy

[3] Equation (3.4) assumes that the energy storage process is lossless. For a lossy storage process, one needs to model such loss via establishing a functional relationship between $\mathcal{S}_{n,t}$ and $\mathcal{E}_{n,t}$, i.e., $\mathcal{S}_{n,t} = f_n(\mathcal{E}_{n,t})$, where the function $f_n(.)$ can be approximated using the battery type and specifications. Knowing $f_n(.)$ and the pmf of $\mathcal{E}_{n,t}$, one can find the pmf of $\mathcal{S}_{n,t}$ using transformation method.

where $\mathcal{P}_{n,t}$ is proportional to the amount of stored energy in the battery, i.e., kb_u Joules, and the scale factor depends on the feedback information. Mathematically, we express $\mathcal{P}_{n,t}$ as the following

$$\mathcal{P}_{n,t} = \begin{cases} 0, & \Gamma_n(x_{n,t}) < \theta_n, \\ \lfloor c_{n,0}k \rfloor b_u/T_s, & \Gamma_n(x_{n,t}) \geq \theta_n,\ g_{n,t} \in \mathcal{I}_{n,0}, \\ \vdots & \vdots \\ \lfloor c_{n,L-1}k \rfloor b_u/T_s, & \Gamma_n(x_{n,t}) \geq \theta_n,\ g_{n,t} \in \mathcal{I}_{n,L-1}, \end{cases} \tag{3.6}$$

where $\lfloor . \rfloor$ is the floor function and the scale factors $\{c_{n,l}\}_{l=0}^{L-1}$ are between zero and one. The number of scale factors is equal to the number of quantization levels and scale factor $c_{n,l}$ corresponds to the quantization interval $\mathcal{I}_{n,l} = [\mu_{n,l}, \mu_{n,l+1})$. Given θ_n, the problem of optimizing transmit power control strategy reduces to finding the best scale factors $\{c_{n,l}\}_{l=0}^{L-1}$ and the quantization thresholds $\{\mu_{n,l}\}_{l=1}^{L-1}$ such that a specified performance metric is optimized. We let the transmit symbol $\alpha_{n,t} = \sqrt{\mathcal{P}_{n,t}}$. Considering the power control strategy in (3.6), we note that the number of energy units consumed for transmitting symbol $\alpha_{n,t}$ is $\lfloor c_{n,l}k \rfloor$, which is an integer between zero and K and is always smaller than k. In other words, the energy consumption for transmission cannot exceed the stored energy in the battery, and the battery cannot be fully depleted after a transmission. It also implies that when $\lfloor c_{n,l}k \rfloor = 0$ the sensor will not transmit. Note that the scale factors $\{c_{n,l}\}_{l=0}^{L-1}$ in (3.6) play key roles in balancing the rates of energy harvesting and energy consumption for transmission. Given the quantization thresholds $\mu_{n,l}$'s, when $c_{n,l}$'s are closer to one, such that the rate of energy consumption for transmission is greater than the rate of energy harvesting, sensors may stop functioning, due to energy outage, leading into discontinuities in sensor-FC communication. When $c_{n,l}$'s are closer to zero, such that the rate of energy consumption for transmission is smaller than the rate of energy harvesting, sensors may fail to utilize the excess energy,

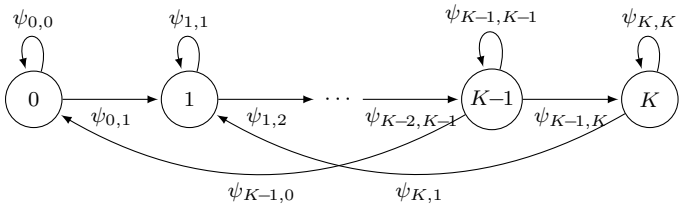

Figure 3.1: Schematics of Markov chain corresponding to the battery state random process $B_{n,t}$.

due to energy overflow, leading into a performance degradation. The battery state at the beginning of slot $t+1$ depends on the battery state at the beginning of slot t, the harvested energy during slot t, and the number of stored energy units that is consumed for transmitting symbol $\alpha_{n,t}$, i.e., $\mathcal{P}_{n,t}T_s/b_u$. Mathematically, we express $B_{n,t+1}$ as the following

$$B_{n,t+1} = \min\left\{[B_{n,t} + \mathcal{S}_{n,t} - \mathcal{P}_{n,t}T_s/b_u]^+, K\right\}, \tag{3.7}$$

where $[x]^+ = \max\{0, x\}$. Considering the dynamic battery state model in (3.7) we note that, conditioned on $\mathcal{S}_{n,t}$ and $\mathcal{P}_{n,t}$ the value of $B_{n,t+1}$ only depends on the value of $B_{n,t}$ (and not the battery states of time slots before t). Hence, the process $B_{n,t}$ can be modeled as a Markov chain. Fig. 3.1 is the schematic representation of this $(K+1)$-state Markov chain. Let $\mathbf{\Phi}_{n,t}$ be the probability vector of battery state in slot t

$$\mathbf{\Phi}_{n,t} \triangleq \Big[\Pr(B_{n,t}=0), \ldots, \Pr(B_{n,t}=K)\Big]^T, \tag{3.8}$$

where the superscript T indicates transposition. We note that $\Pr(B_{n,t}=k)$ in (3.8) depends on $B_{n,t-1}$, $\mathcal{S}_{n,t-1}$ and $\mathcal{P}_{n,t-1}$. Assuming that the Markov chain is time-homogeneous[4], we let $\mathbf{\Psi}_n$ be the corresponding $(K+1)\times(K+1)$ transition probability matrix of this chain with

[4]A Markov chain is time-homogeneous (stationary) if and only if its transition probability matrix is time-invariant. Adopting homogeneous Markov chain model for studying EH-enabled communication systems is widely common [43].

its (i,j)-th entry $\psi_{i,j} \triangleq \Pr(B_{n,t}=j|B_{n,t-1}=i)$ for $i,j=0,\ldots,K$. Defining the indicator function $I_{i\to j}(\mathcal{S}_{n,t},\mathcal{P}_{n,t}T_s/b_u)$ as

$$I_{i\to j}(\mathcal{S}_{n,t},\mathcal{P}_{n,t}T_s/b_u)=\begin{cases}1, & \text{if } j=\min\left\{[i+\mathcal{S}_{n,t}-\mathcal{P}_{n,t}T_s/b_u]^+,K\right\},\\ 0, & \text{o.w.}\end{cases} \tag{3.9}$$

We can express $\psi_{i,j}$ as below

$$\psi_{i,j}=\widehat{\Pi}_{n,1}\sum_{k=0}^{K}\sum_{l=0}^{L}\pi_{n,l}q_k I_{i\to j}(\mathcal{S}_{n,t},\lfloor c_{n,l}i\rfloor)+\widehat{\Pi}_{n,0}\sum_{k=0}^{K}q_k I_{i\to j}(\mathcal{S}_{n,t},0). \tag{3.10}$$

The symbols $\widehat{\Pi}_{n,0}$ and $\widehat{\Pi}_{n,1}$ in (3.10) refer to the probabilities of events $\mathcal{P}_{n,t}=0$ and $\mathcal{P}_{n,t}\neq 0$, respectively. In particular, we have

$$\widehat{\Pi}_{n,0}=\Pr(\mathcal{P}_{n,t}=0)=\Pi_0(1-P_{\mathrm{f}_n})+\Pi_1(1-P_{\mathrm{d}_n}),\ \widehat{\Pi}_{n,1}=\Pr(\mathcal{P}_{n,t}\neq 0)=\Pi_0P_{\mathrm{f}_n}+\Pi_1P_{\mathrm{d}_n}, \tag{3.11}$$

where the probabilities P_{f_n} and P_{d_n} can be determined using our signal model in (3.1) and given the local threshold θ_n

$$P_{\mathrm{f}_n}=\Pr(\mathcal{P}_{n,t}\neq 0|h_t=0)=Q\Big(\frac{\theta_n+\mathcal{A}^2/2\sigma_{v_n}^2}{\sqrt{\mathcal{A}^2/\sigma_{v_n}^2}}\Big),\ P_{\mathrm{d}_n}=\Pr(\mathcal{P}_{n,t}\neq 0|h_t=1)=Q\Big(\frac{\theta_n-\mathcal{A}^2/2\sigma_{v_n}^2}{\sqrt{\mathcal{A}^2/\sigma_{v_n}^2}}\Big). \tag{3.12}$$

Instead of fixing θ_n, one can fix P_{d_n} and let $P_{\mathrm{d}_n}=\overline{P}_{\mathrm{d}},\forall n$. Then the false alarm probability in can be written as $P_{\mathrm{f}_n}=Q\left(Q^{-1}(\overline{P}_{\mathrm{d}})+\mathcal{A}/\sigma_{v_n}\right)$. From a practical perspective, this implies that our optimized power control strategy guarantees fixed detection and false alarm probabilities at the sensors [5]. Going back to the transition probability matrix $\mathbf{\Psi}_n$, since the

[5]Our signal model in (3.1) can be extended to include temporally correlated observation noises. Suppose during time slot t sensor n makes M samples, where the observation noises of these M samples are correlated. The absence and presence of $\mathcal{A}$ can be represented by $H_t=1:\boldsymbol{x}_{n,t}\sim\mathcal{N}(\mathcal{A}\mathbf{1},\boldsymbol{C}),H_t=0:\boldsymbol{x}_{n,t}\sim\mathcal{N}(0,\boldsymbol{C}),\forall n$, where $\boldsymbol{x}_{n,t}$ and $\boldsymbol{C}$, respectively, are $M\times 1$ observation vector and $M\times M$ covariance matrix. One can show $H_t=1:\Gamma_n(\boldsymbol{x}_{n,t})\sim\mathcal{N}(\mu_1,\sigma^2),H_t=0:\Gamma_n(\boldsymbol{x}_{n,t})\sim\mathcal{N}(\mu_0,\sigma^2),\forall n$, where $\mu_0=-\frac{\mathcal{A}^2}{2s^2},\mu_1=\frac{\mathcal{A}^2}{2s^2},\sigma^2=\frac{\mathcal{A}^2}{s^2},s^{-2}=\mathbf{1}^T\Sigma^{-1}\mathbf{1}$. Hence, we find $P_{\mathrm{f}_n}=Q\big(\frac{\theta_n+\mathcal{A}^2/2s^2}{\mathcal{A}/s}\big),P_{\mathrm{d}_n}=Q\big(\frac{\theta_n-\mathcal{A}^2/2s^2}{\mathcal{A}/s}\big)$. Comparing these with $P_{\mathrm{f}_n},P_{\mathrm{d}_n}$ in (3.12) we realize that if σ_v^2 in (3.1) is equal to s^2, then these two different signal models lead to the same channel-dependent transmit power control strategy and the same detection performance at the FC.

Markov chain characterized by $\mathbf{\Psi}_n$ is irreducible and aperiodic, there exists a unique steady state distribution, regardless of the initial state [43]. Let $\mathbf{\Phi}_n = [\phi_{n,0}, \phi_{n,1}, ..., \phi_{n,K}]^T$ be the unique steady state probability vector with the entries $\phi_{n,k} = \lim_{t\to\infty} \Pr(B_{n,t} = k)$. Note that this vector satisfies the following eigenvalue equation

$$\mathbf{\Phi}_n = \mathbf{\Phi}_n \mathbf{\Psi}_n. \tag{3.13}$$

In particular, we let $\mathbf{\Phi}_n$ be the normalized eigenvector of $\mathbf{\Psi}_n$ corresponding to the unit eigenvalue, such that the sum of its entries is one [10]. The closed-form expression for $\mathbf{\Phi}_n$ can be written as [25]

$$\mathbf{\Phi}_n = -(\mathbf{\Psi}_n^T - \mathbf{I} - \mathbf{B})^{-1}\mathbf{1}, \tag{3.14}$$

where $\mathbf{B}$ is an all-ones matrix, $\mathbf{I}$ is the identity matrix, and $\mathbf{1}$ is an all-ones column vector. From this point forward, we assume that the battery operates at its steady state and we drop the superscript t.

For clarity of the presentation and to illustrate our transmit power control strategy in (3.6), we consider the following simple example consisting of one sensor, i.e., $N = 1$, and let $L = 4,\ K = 6,\ \rho = 2$ and $\gamma_{g_1} = 1$. To examine the effect of variations of the scale factors and the quantization thresholds on $\mathbf{\Psi}_n$ and $\mathbf{\Phi}_n$ and transmit power, we consider two sets of values $c_1^{(a)} = [0.1,\ 0.3,\ 0.5,\ 0.7]$, $\mu_1^{(a)} = [0,\ 0.2,\ 1.4,\ 3.6,\ \infty]$ and $c_1^{(b)} = [0.3,\ 0.5,\ 0.7,\ 0.9]$, $\mu_1^{(b)} = [0,\ 0.3,\ 2.5,\ 4.7,\ \infty]$. The corresponding 7×7 transition matrices, denoted as $\mathbf{\Psi}_1^{(a)}$ and $\mathbf{\Psi}_1^{(b)}$, as well as the corresponding 7×1 steady state probability vectors, denoted as $\mathbf{\Phi}_1^{(a)}$ and $\mathbf{\Phi}_1^{(b)}$ are

$$\boldsymbol{\Psi}_1^{(a)} = \begin{pmatrix} 0.13 & 0.27 & 0.27 & 0.17 & 0.09 & 0.03 & 0.04 \\ 0 & 0.13 & 0.27 & 0.27 & 0.18 & 0.09 & 0.06 \\ 0 & 0.02 & 0.15 & 0.27 & 0.25 & 0.16 & 0.15 \\ 0 & 0 & 0.02 & 0.15 & 0.27 & 0.26 & 0.30 \\ 0 & 0 & 0.02 & 0.09 & 0.21 & 0.25 & 0.43 \\ 0 & 0 & 0 & 0.02 & 0.09 & 0.21 & 0.68 \\ 0 & 0 & 0 & 0.02 & 0.04 & 0.09 & 0.85 \end{pmatrix},$$

$$\boldsymbol{\Psi}_1^{(b)} = \begin{pmatrix} 0.14 & 0.28 & 0.28 & 0.16 & 0.07 & 0.04 & 0.03 \\ 0 & 0.14 & 0.28 & 0.28 & 0.16 & 0.09 & 0.05 \\ 0 & 0.06 & 0.19 & 0.27 & 0.22 & 0.13 & 0.13 \\ 0 & 0 & 0.07 & 0.20 & 0.27 & 0.22 & 0.24 \\ 0 & 0 & 0.06 & 0.15 & 0.22 & 0.22 & 0.35 \\ 0 & 0 & 0 & 0.07 & 0.15 & 0.21 & 0.57 \\ 0 & 0 & 0 & 0.07 & 0.12 & 0.14 & 0.67 \end{pmatrix}.$$

$$\boldsymbol{\Phi}_n^{(a)} = [0, 0.0004, 0.0027, 0.0290, 0.0640, 0.1195, 0.7844],$$

$$\boldsymbol{\Phi}_n^{(b)} = [0, 0.0015, 0.0209, 0.1002, 0.1582, 0.1723, 0.5469]$$

Given these two sets of values, Fig. 3.2 illustrates the two corresponding transmit power maps assuming $b_u = 10$ mJ and $T_s = 10$ sec. The transmit power maps in (3.6) show how much power the sensor should spend for its data transmission, given its battery state k and the feedback information (i.e., the quantization interval to which the channel gain $g_{1,t}$ belongs). For instance, for the parameters in Fig. 3.2a, when $g_{1,t} \in \mathcal{I}_{1,2}$ and $B_{1,t} = 3$, then $\mathcal{P}_{1,t} = 1$ mW, whereas for the parameters in Fig. 3.2b, when $g_{1,t} \in \mathcal{I}_{1,2}$ and $B_{1,t} = 3$, then $\mathcal{P}_{1,t} = 2$ mW.

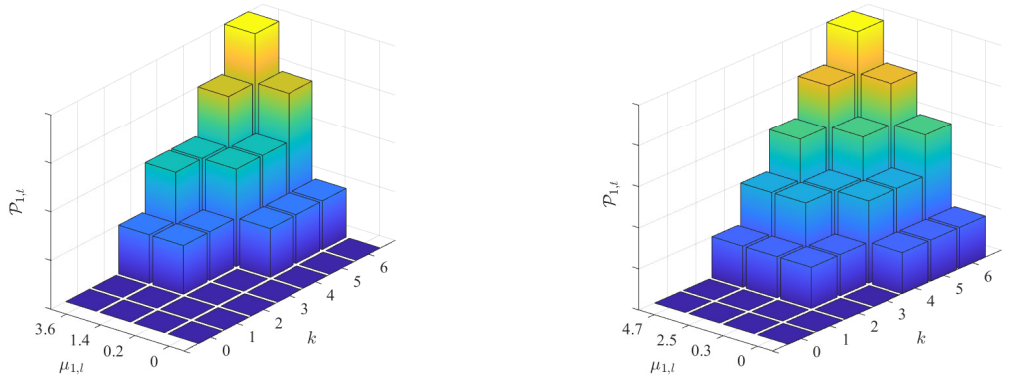

(a) $\mu_1^{(a)} = [0, 0.2, 1.4, 3.6]$, $c_1^{(a)} = [0.1, 0.3, 0.5, 0.7]$

(b) $\mu_1^{(b)} = [0, 0.3, 2.5, 4.7]$, $c_1^{(b)} = [0.3, 0.5, 0.7, 0.9]$

Figure 3.2: This example shows how much power $\mathcal{P}_{1,t}$ the single sensor should spend for its data transmission, given its battery state and the feedback information.

3.1.3 Received Signals at FC and Optimal Bayesian Fusion Rule

In each time slot sensors send their data symbols to the FC over orthogonal fading channels. The received signal at the FC from sensor n corresponding to time slot t is

$$y_{n,t} = g_{n,t}\,\alpha_{n,t} + w_{n,t}, \qquad \text{for } n = 1, \ldots, N \tag{3.15}$$

where $w_{n,t} \sim \mathcal{N}(0, \sigma_{w_n}^2)$ is the additive Gaussian noise and $\alpha_{n,t} = \sqrt{\mathcal{P}_{n,t}}$. We assume $w_{n,t}$'s are i.i.d. over time slots and independent across sensors. Let $\boldsymbol{y}_t = [y_{1,t}, y_{2,t}, \ldots, y_{N,t}]$ denote the vector that includes the received signals at the FC from all sensors in time slot t. The FC applies the optimal Bayesian fusion rule $\Gamma_0(.)$ to the received vector $\boldsymbol{y}_t$ and obtains a global decision $u_{0,t} = \Gamma_0(\boldsymbol{y}_t)$, where $u_{0,t} \in \{0, 1\}$ [16]. In particular, we have

$$u_{0,t} = \Gamma_0(\boldsymbol{y}_t) = \begin{cases} 1, & \Delta_t > \tau, \\ 0, & \Delta_t < \tau, \end{cases} \tag{3.16}$$

where the decision threshold $\tau = \log(\frac{\Pi_0}{\Pi_1})$ and

$$\Delta_t = \log\left(\frac{f(\boldsymbol{y}_t|h_t=1)}{f(\boldsymbol{y}_t|h_t=0)}\right), \tag{3.17}$$

and $f(\boldsymbol{y}_t|h_t)$ is conditional probability density function (pdf) of the received vector $\boldsymbol{y}_t$ at FC.

3.1.4 Our Proposed Constrained Optimization Problem

From Bayesian perspective, the natural choice to measure the detection performance corresponding to the global decision $u_{0,t}$ at the FC is the error probability, defined as

$$P_e = \Pi_0 \Pr(u_{0,t}=1|h_t=0) + \Pi_1 \Pr(u_{0,t}=0|h_t=1) = \Pi_0 \Pr(\Delta_t > \tau|h_t=0) + \Pi_1 \Pr(\Delta_t < \tau|h_t=1). \tag{3.18}$$

However, finding a closed form expression for P_e is often mathematically intractable. Instead, we choose the total J-divergence between the distributions of the detection statistics at the FC under different hypotheses (which will be defined in Section 3.2), as our detection performance metric. This choice allows us to provide a more tractable analysis. Recall that the J-divergence and P_e are related through $P_e > \Pi_0\Pi_1 e^{-J/2}$ [18]. Hence, maximizing the J-divergence is equivalent to minimizing the lower bound on P_e.

Our goal is to find the scale factors $\{c_{n,l}\}_{l=0}^{L-1}$ and the quantization thresholds $\{\mu_{n,l}\}_{l=1}^{L-1}$ in the transmit power control strategy (3.6) for all sensors such that the total J-divergence at the FC is maximized, subject to an average transmit power per sensor constraint. We assume that this optimization problem is solved *offline* at the FC, given (i) the statistical information of fading channels and noises (including communication channel noise and observation noise) and randomly arriving energy units, and (ii) the battery parameter K, the number

of quantization levels L, and the given $\overline{P}_{\rm d}$ for local detectors at the sensors. The solutions to this optimization problem is available a *a priori* at the FC and the sensors, to be utilized for controlling and adapting transmit power according to (3.6). The idea of offline power control optimization with a limited feedback channel has been used before for distributed detection systems in WSNs [31]. Note that, from this point forward, we assume that the battery operates at its steady state and we drop the superscript t.

3.2 Characterization of Total J-divergence and Error Probability

In this section, first we define the total J-divergence and then derive a closed-form expression for it in Section III.A, using Gaussian distribution approximation. Next, considering P_e in (3.18) we provide a closed-form approximate expression for it in Section III.B, using the same Gaussian distribution approximation and Lindeberg central limit theorem (CLT).

3.2.1 Total J-Divergence Derivation

We start with the definition of J-divergence. Consider two pdfs of a continuous random variable x, denoted as $\eta_1(x)$ and $\eta_2(x)$. By definition [18], [30], the J-divergence between $\eta_1(x)$ and $\eta_0(x)$, denoted as $J(\eta_1, \eta_0)$, is

$$J(\eta_1, \eta_0) = D(\eta_1||\eta_0) + D(\eta_0||\eta_1), \tag{3.19}$$

where $D(\eta_i||\eta_j)$ is the non-symmetric Kullback-Leibler (KL) distance between $\eta_i(x)$ and $\eta_j(x)$. The KL distance $D(\eta_i||\eta_j)$ is defined as

$$D(\eta_i||\eta_j) = \int_{-\infty}^{\infty} \log\left(\frac{\eta_i(x)}{\eta_j(x)}\right) \eta_i(x) dx. \tag{3.20}$$

Substituting (3.20) into (3.19) we obtain

$$J(\eta_1, \eta_0) = \int_{-\infty}^{\infty} [\eta_1(x) - \eta_0(x)] \log \left(\frac{\eta_1(x)}{\eta_0(x)} \right) dx. \tag{3.21}$$

In our problem setup, the two conditional pdfs $f(\boldsymbol{y}|h=1)$ and $f(\boldsymbol{y}|h=0)$ play the role of $\eta_1(x)$ and $\eta_0(x)$, respectively. Let J_{tot} denote the J-divergence between $f(\boldsymbol{y}|h=1)$ and $f(\boldsymbol{y}|h=0)$. The pdf of vector $\boldsymbol{y}$ given h is

$$f(\boldsymbol{y}|h) \overset{(a)}{=} \prod_{n=1}^{N} f(y_n|h) \overset{(b)}{=} \prod_{n=1}^{N} f(y_n|\alpha_n, h) \Pr(\alpha_n|h) \overset{(c)}{=} \prod_{n=1}^{N} \underbrace{f(y_n|\alpha_n) \Pr(\alpha_n|h)}_{=f(y_n|h)}, \qquad \text{for } h = 0, 1. \tag{3.22}$$

Equality (a) in (3.22) holds since the received signals from sensors at the FC, given h, are conditionally independent, equality (b) in (3.22) is obtained from Bayes' rule, and equality (c) in (3.22) is found noting that H, α_n, y_n satisfy the Markov property, i.e., $H \to \alpha_n \to y_n$ [18], [30] and hence y_n and H, given α_n, are conditionally independent. Let J_n represent the J-divergence between the two conditional pdfs $f(y_n|h=1)$ and $f(y_n|h=0)$. Using (3.21) we can express J_n as

$$J_n = \int_{-\infty}^{\infty} \Big[f(y_n|h=1) - f(y_n|h=0) \Big] \log \left(\frac{f(y_n|h=1)}{f(y_n|h=0)} \right) dy_n. \tag{3.23}$$

Based on (3.22) we have $J_{tot} = \sum_{n=1}^{N} J_n$. To calculate J_n, we need to find the conditional pdf $f(y_n|h)$. Considering (3.15) we realize that y_n, given α_n, is Gaussian. In particular, we have

$$f(y_n|\alpha_n = 0) = \mathcal{N}(0, \sigma_{w_n}^2), f(y_n|\alpha_n \neq 0) = \mathcal{N}(g_n \alpha_n, \sigma_{w_n}^2) \tag{3.24}$$

Also, considering (3.12) and noting that $\alpha_n = \sqrt{\mathcal{P}_n}$ we find

$$\Pr(\alpha_n \neq 0|h=0) = P_{\mathrm{f}_n}, \ \Pr(\alpha_n \neq 0|h=1) = P_{\mathrm{d}_n},$$

$$\Pr(\alpha_n = 0|h=0) = 1 - P_{\mathrm{f}_n}, \ \Pr(\alpha_n = 0|h=1) = 1 - P_{\mathrm{d}_n}.$$

Substituting (3.24) and (3.25) in (3.22), the conditional pdfs $f(y_n|h=0)$ and $f(y_n|h=1)$ become

$$f(y_n|h=0) = f(y_n|\alpha_n \neq 0)P_{\mathrm{f}_n} + f(y_n|\alpha_n = 0)(1-P_{\mathrm{f}_n}),$$
$$f(y_n|h=1) = f(y_n|\alpha_n \neq 0)P_{\mathrm{d}_n} + f(y_n|\alpha_n = 0)(1-P_{\mathrm{d}_n}).$$

Although $f(y_n|\alpha_n=0)$ and $f(y_n|\alpha_n\neq 0)$ in (3.25) are Gaussian, $f(y_n|h=0)$ and $f(y_n|h=1)$ are Gaussian mixtures, due to P_{d_n} and P_{f_n}. Unfortunately, the J-divergence between two Gaussian mixture densities does not have a general closed-form expression. Similar to [18], [30] we approximate the J-divergence between two Gaussian mixture densities by the J-divergence between two Gaussian densities $f^G(y_n|h) \sim \mathcal{N}(m_{n,h}, \Upsilon^2_{n,h})$, where the mean $m_{n,h}$ and the variance $\Upsilon^2_{n,h}$ of the approximate distributions are obtained from matching the first and second order moments of the actual and the approximate distributions. For our problem setup, one can verify that the parameters $m_{n,h}$ and $\Upsilon^2_{n,h}$ become

$$\begin{aligned} m_{n,0} &= g_n\alpha_n P_{\mathrm{f}_n},\ \Upsilon^2_{n,0} = g_n^2\alpha_n^2 P_{\mathrm{f}_n}(1-P_{\mathrm{f}_n}) + \sigma^2_{w_n}, \\ m_{n,1} &= g_n\alpha_n P_{\mathrm{d}_n},\ \Upsilon^2_{n,1} = g_n^2\alpha_n^2 P_{\mathrm{d}_n}(1-P_{\mathrm{d}_n}) + \sigma^2_{w_n}. \end{aligned} \tag{3.25}$$

The J-divergence between two Gaussian densities, represented as $J\big(f^G(y_n|h=1), f^G(y_n|h=0)\big)$, in terms of their means and variances is [18]

$$J\big(f^G(y_n|h=1), f^G(y_n|h=0)\big) = \frac{\Upsilon^2_{n,1} + (m_{n,1}-m_{n,0})^2}{\Upsilon^2_{n,0}} + \frac{\Upsilon^2_{n,0} + (m_{n,0}-m_{n,1})^2}{\Upsilon^2_{n,1}}. \tag{3.26}$$

Substituting $m_{n,h}$ and $\Upsilon^2_{n,h}$ into J_n in (3.26) we approximate J_n as the following

$$J_n = \frac{\sigma^2_{w_n} + A_n g_n^2\alpha_n^2}{\sigma^2_{w_n} + B_n g_n^2\alpha_n^2} + \frac{\sigma^2_{w_n} + C_n g_n^2\alpha_n^2}{\sigma^2_{w_n} + D_n g_n^2\alpha_n^2}, \tag{3.27}$$

where

$$A_n = P_{\mathrm{f}_n}(1-P_{\mathrm{d}_n}) + P_{\mathrm{d}_n}(P_{\mathrm{d}_n}-P_{\mathrm{f}_n}), \quad B_n = P_{\mathrm{d}_n}(1-P_{\mathrm{d}_n})$$
$$C_n = P_{\mathrm{d}_n}(1-P_{\mathrm{f}_n}) - P_{\mathrm{f}_n}(P_{\mathrm{d}_n}-P_{\mathrm{f}_n}), \quad D_n = P_{\mathrm{f}_n}(1-P_{\mathrm{f}_n}).$$

3.2.2 Error Probability Approximation

In this section, we provide a closed-form approximate expression for P_e in (3.18). To find the approximate expression for P_e, we approximate Δ in (3.17) using a similar Gaussian distribution approximation as we conducted in Section 3.2.1. In Section 3.2.1 we approximated the conditional pdf $f(y_n|h)$ with $f^G(y_n|h) = \mathcal{N}(m_{n,h}, \Upsilon^2_{n,h})$, where the mean $m_{n,h}$ and the variance $\Upsilon^2_{n,h}$ of the approximate distribution are provided in (3.25). Relying on this Gaussian distribution approximation, we can also approximate the conditional pdf $f(\boldsymbol{y}|h)$. In particular, since the received signals at the FC, conditioned on h, are independent across sensors (see (3.22-a)), we can approximate $f(\boldsymbol{y}|h)$ with $f^G(\boldsymbol{y}|h) = \mathcal{N}(\varphi_h, \Lambda_h)$, where φ_h and Λ_h are the mean vector and the *diagonal* covariance matrix with elements $m_{n,h}$ and $\Upsilon^2_{n,h}$, respectively. Using this Gaussian distribution approximation, we can approximate Δ in (3.17) as

$$\begin{aligned}\Delta \approx& \log\left(\frac{f^G(\boldsymbol{y}|h=1)}{f^G(\boldsymbol{y}|h=0)}\right) = \log\left(\frac{\sqrt{\det\Lambda_0}\exp\left(-\frac{1}{2}(\boldsymbol{y}-\varphi_1)^T\Lambda_1^{-1}(\boldsymbol{y}-\varphi_1)\right)}{\sqrt{\det\Lambda_1}\exp\left(-\frac{1}{2}(\boldsymbol{y}-\varphi_0)^T\Lambda_0^{-1}(\boldsymbol{y}-\varphi_0)\right)}\right)\\ =& R - \frac{1}{2}(\boldsymbol{y}-\varphi_1)^T\Lambda_1^{-1}(\boldsymbol{y}-\varphi_1) + \frac{1}{2}(\boldsymbol{y}-\varphi_0)^T\Lambda_0^{-1}(\boldsymbol{y}-\varphi_0),\end{aligned}$$

where $R = \log\left(\frac{\sqrt{\det\Lambda_0}}{\sqrt{\det\Lambda_1}}\right)$. Since the covariance matrices Λ_0 and Λ_1 are diagonal, the approximate expression for Δ in (3.28) can be rewritten as

$$\Delta \approx R + \frac{1}{2}\Delta'_N,\ \Delta'_N = \sum_{n=1}^{N} z_n,\ z_n = \frac{(y_n - m_{n,0})^2}{\Upsilon^2_{n,0}} - \frac{(y_n - m_{n,1})^2}{\Upsilon^2_{n,1}}, \tag{3.28}$$

With the Gaussian distribution approximation, the optimal fusion rule in (3.16) can be approximated with

$$u_0 = \begin{cases} 1, & \Delta'_N > \tau', \\ 0, & \Delta'_N < \tau', \end{cases} \tag{3.29}$$

where Δ'_N is given in (3.28) and $\tau' = 2(\tau - R)$. The error probability corresponding to the fusion rule in (3.29) is

$$P_e = \Pi_0 \Pr(\Delta'_N > \tau' | h = 0) + \Pi_1 \Pr(\Delta'_N < \tau' | h = 1). \tag{3.30}$$

To find P_e in (3.30) we need the pdf of Δ'_N given h. We note that z_n in (3.28) can be rewritten as a quadratic function of y_n

$$z_n = a y_n^2 + b y_n + c, \quad \text{where } a = \frac{1}{\Upsilon_{n,0}^2} - \frac{1}{\Upsilon_{n,1}^2},\ b = \frac{2m_{n,1}}{\Upsilon_{n,1}^2} - \frac{2m_{n,0}}{\Upsilon_{n,0}^2},\ c = \frac{m_{n,0}^2}{\Upsilon_{n,0}^2} - \frac{m_{n,1}^2}{\Upsilon_{n,1}^2}. \tag{3.31}$$

Let $\mu_{z_n|h}$ and $\sigma^2_{z_n|h}$, denote the mean and variance of z_n in (3.31) given h, respectively. To find $\mu_{z_n|h}, \sigma^2_{z_n,h}$ we recall the following fact.

Fact: Let $x \sim N(\mu, \sigma^2)$ be a Gaussian random variable with the mean $\mathbb{E}\{x\} = \mu$ and the variance $\sigma^2 = \mathbb{E}\{x^2\} - \mu^2$. Then we have [44]:

$$\mathbb{E}\{x^2\} = \mu^2 + \sigma^2, \quad \mathbb{E}\{x^3\} = \mu(\mu^2 + 3\sigma^2), \quad \mathbb{E}\{x^4\} = \mu^4 + 6\mu^2\sigma^2 + 3\sigma^4. \tag{3.32}$$

Using this fact, we find

$$\mu_{z_n|h} = a(m_{n,h}^2 + \Upsilon_{n,h}^2) + b\, m_{n,h} + c, \quad \sigma^2_{z_n|h} = 2a^2(2m_{n,h}^2 + \Upsilon_{n,h}^4) + b\Upsilon_{n,h}^2(b + 4\, a\, m_{n,h}), \tag{3.33}$$

where a, b, c are given in (3.31) and $m_{n,h}, \Upsilon_{n,h}^2$ are given in (3.25). Relying on the Gaussian distribution approximation of y_n given h, we can derive the pdf of z_n given h, where the pdf expression is provided in (3.34).

$$f(z_n|h) = \frac{1}{g(z_n)} \left\{ f^G_{y_n|h}\Big(\frac{\Upsilon^2_{n,0}\Upsilon^2_{n,1}}{2} g(z_n) + m_{n,0}\Upsilon^2_{n,1} - m_{n,1}\Upsilon^2_{n,0}\Big) + f^G_{y_n|h}\Big(\frac{-\Upsilon^2_{n,0}\Upsilon^2_{n,1}}{2} g(z_n) + m_{n,0}\Upsilon^2_{n,1} - m_{n,1}\Upsilon^2_{n,0}\Big) \right\},$$

$$g(z_n) = \frac{2}{\Upsilon_{n,1}\Upsilon_{n,1}} \sqrt{(m_{n,0} - m_{n,1})^2 + z_n(\Upsilon^2_{n,1} - \Upsilon^2_{n,0})}. \tag{3.34}$$

Since given h, z_n's are independent, the pdf of Δ'_N given h, is convolution of these N individual pdfs, which does not have a closed-form expression. This indicates that, even with the Gaussian distribution approximation, finding a closed-form expression of P_e in (3.30) for finite N remains *elusive*. Hence, we resort to the *asymptotic regime* when N grows very large and invoke the central limit theorem (CLT) to approximate P_e in (3.30).

Lindeberg CLT is a variant of CLT, where the random variables are independent, but not necessarily identically distributed [45]. Let $\mu_{\Delta'_N|h}$ and $\sigma^2_{\Delta'_N|h}$ indicate the mean and variance of Δ'_N in (3.28) given h. We have $\mu_{\Delta'_N|h} = \sum_{n=1}^N \mu_{z_n|h}$ and $\sigma^2_{\Delta'_N|h} = \sum_{n=1}^N \sigma^2_{z_n|h}$. Assuming Lindeberg's condition, given below, is satisfied

$$\lim_{N\to\infty} \frac{1}{\sigma^2_{\Delta'_N|h}} \sum_{n=1}^{N} \mathbb{E}\{(z_n - \mu_{z_n|h})^2\} = 0, \tag{3.35}$$

then, as N goes to infinity, the normalized sum $(1/\sigma^2_{\Delta'_N|h}) \sum_{n=1}^N (z_n - \mu_{z_n|h})$ converges in distribution toward the standard normal distribution

$$\frac{1}{\sigma^2_{\Delta'_N|h}} \sum_{n=1}^{N} (z_n - \mu_{z_n|h}) \xrightarrow{d} \mathcal{N}(0,1), \tag{3.36}$$

where $\xrightarrow{d}$ indicates convergence in distribution. Using (3.36) we can approximate P_e in (3.30) using Q-function

$$P_e = \Pi_0 Q\Big(\frac{\tau' - \mu_{\Delta'_N|0}}{\sigma^2_{\Delta'_N|0}}\Big) + \Pi_1\Big[1 - Q\Big(\frac{\tau' - \mu_{\Delta'_N|1}}{\sigma^2_{\Delta'_N|1}}\Big)\Big]. \tag{3.37}$$

3.3 Formulating Our Optimization Problem

As we stated before, our objective is to find the scale factors $\{c_{n,l}\}_{l=0}^{L-1}$ and the quantization thresholds $\{\mu_{n,l}\}_{l=1}^{L-1}$ in the transmit power control strategy (3.6) for all sensors such that the total J-divergence at the FC is maximized, subject to an average transmit power per sensor constraint. We formulate the optimization problem, via writing the cost function and the constraints in terms of the optimization variables. Recall total J-divergence at the FC is $J_{tot} = \sum_{n=1}^{N} J_n$, where J_n in given in (3.27), and transmit power per sensor $\mathcal{P}_n$ is given in (3.6). We note that J_n depends on g_n value, whereas $\mathcal{P}_n$ depends on the quantization interval to which g_n belongs. The dependency of J_n on g_n stems from the fact that the FC has full knowledge of all channel gains g_n's, and the optimal Bayesian fusion rule utilizes this full information. Hence, the error probability P_e and its bound J_{tot} depend on this full information. On the other hand, sensor n only knows the quantization interval to which g_n belongs, and adapts its transmit power $\mathcal{P}_n$ according to this *partial* knowledge as well as its battery state. We seek the best $\{c_{n,l}\}_{l=0}^{L-1}$ and $\{\mu_{n,l}\}_{l=1}^{L-1}$, such that the solutions we obtain that do not depend on the specific channel gain realizations. Hence, we take the average of J_n and $\mathcal{P}_n$ over g_n, conditioned that $g_n \in [\mu_{n,i}, \mu_{n,i+1})$. By taking such a conditional average over g_n, the solutions we obtain do not depend on the specific channel gain realizations and are valid, as long as the channel gain statistics remain unchanged. The problem can be solved *offline* and its solutions can become available a *a priori*at the FC and the sensors. Let $\bar{J}_n^{(i)} = \mathbb{E}\{J_n | g_n \in [\mu_{n,i}, \mu_{n,i+1})\}$ and $\bar{\mathcal{P}}_n^{(i)} = \mathbb{E}\{\mathcal{P}_n | g_n \in [\mu_{n,i}, \mu_{n,i+1})\}$, respectively, denote the expectations of J_n and $\mathcal{P}_n$ over g_n and, conditioned that $g_n \in [\mu_{n,i}, \mu_{n,i+1})$. In the following, we compute the two conditional expectations $\bar{J}_n^{(i)}$ and $\bar{\mathcal{P}}_n^{(i)}$, in terms of the optimization variables. To compute $\bar{J}_n^{(i)}$ we use the following fact.

Fact: Suppose random variable x has an exponential distribution with parameter λ, i.e., the pdf of x is $f(x) = \lambda e^{-\lambda x}$. Consider the function $h(x) = \frac{a+bx}{c+dx}$, with given constants a, b, c and d. Then, the average of $h(x)$, conditioned on x being in the interval $[\mu_i, \mu_{i+1})$ is

$$\begin{aligned}\mathbb{E}\{h(x)|x \in [\mu_i, \mu_{i+1})\} &= \int_{\mu_i}^{\mu_{i+1}} h(x)f(x)dx \\ &= \frac{1}{d}\Big[a\beta(\mu_{i+1}) - \frac{bc}{d}\beta(\mu_{i+1}) - be^{-\lambda\mu_{i+1}} - a\beta(\mu_i) - \frac{bc}{d}\beta(\mu_i) - be^{-\lambda\mu_i}\Big],\end{aligned}$$

where

$$\beta(x) = \lambda\exp(\frac{c\lambda}{d})\ \mathrm{Ei}\big(-\lambda x - \frac{c\lambda}{d}\big), \qquad \mathrm{Ei}(z) = \int_{-z}^{\infty}\frac{e^{-t}}{t}dt.$$

Using this fact and letting $a_1 = a_2 = c_1 = c_2 = \sigma^2_{w_n}$, $b_1 = A_n\alpha_n^2$, $b_2 = C_n\alpha_n^2$, $d_1 = B_n\alpha_n^2$ and $d_2 = D_n\alpha_n^2$, where A_n, B_n, C_n, D_n are given in (3.27), we reach at

$$\bar{J}_n^{(i)} = \sum_{k=0}^{K}\phi_{n,k}\pi_{n,i}\Big[\Omega(\lfloor c_{n,i}k\rfloor, \mu^2_{n,i+1}) - \Omega(\lfloor c_{n,i}k\rfloor, \mu^2_{n,i})\Big], \tag{3.38}$$

where the two dimensional function $\Omega(x, y)$ in (3.38) is

$$\begin{aligned}\Omega(x,y) \triangleq &\frac{1}{B_n x}\Big[\sigma^2_{w_n}\beta_1(x,y) - \frac{A_n}{B_n}\sigma^2_{w_n}\beta_1(x,y) - A_n x e^{(-y\gamma_{g_n})}\Big] \\ &+\frac{1}{D_n x}\Big[\sigma^2_{w_n}\beta_2(x,y) - \frac{C_n}{D_n}\sigma^2_{w_n}\beta_2(x,y) - C_n x e^{(-y\gamma_{g_n})}\Big],\end{aligned} \tag{3.39}$$

and the two dimensional functions $\beta_1(x, y)$ and $\beta_2(x, y)$ in (3.39) are

$$\beta_1(x,y) \triangleq \gamma_{g_n}\exp\big(\frac{\sigma^2_{w_n}\gamma_{g_n}}{xB_n}\big)\mathrm{Ei}\big(-\gamma_{g_n}y - \frac{\sigma^2_{w_n}\gamma_{g_n}}{xB_n}\big), \quad \beta_2(x,y) \triangleq \gamma_{g_n}\exp\big(\frac{\sigma^2_{w_n}\gamma_{g_n}}{xD_n}\big)\mathrm{Ei}\big(-\gamma_{g_n}y - \frac{\sigma^2_{w_n}\gamma_{g_n}}{xD_n}\big).$$

We can compute $\bar{\mathcal{P}}_n^{(i)}$ using (3.6) as the following

$$\bar{\mathcal{P}}_n^{(i)} = \widehat{\Pi}_{n,1}\sum_{k=0}^{K}\phi_{n,k}\pi_{n,i}\lfloor c_{n,i}k\rfloor \tag{3.40}$$

We formulate our problem, denoted as (3.P1), as the following

$$\text{(3.P1)} \qquad \max_{\{c_{n,l}\}_{l=0}^{L-1},\{\mu_{n,l}\}_{l=1}^{L-1},\forall n} \ \sum_{n=1}^{N}\sum_{i=0}^{L-1} \bar{J}_n^{(i)}$$

$$\text{s.t. } c_{n,l} \in [0,1],\ l=0,...,L-1,\forall n, \qquad 0<\mu_{n,l}<\infty,\ l=1,...,L-1,\forall n,$$

$$\sum_{i=0}^{L-1} \bar{\mathcal{P}}_n^{(i)} \leq \mathcal{P}_0,\ \forall n, \qquad \mathbf{\Phi}_n = -(\mathbf{\Psi}_n^T - \mathbf{I} - \mathbf{B})^{-1}\mathbf{1},\ \forall n$$

Regarding the implementation of (3.P1) a remark follows.

Remark: We note that cost function and the constraints in (3.P1) are *decoupled* across sensors. Hence, (3.P1) can be decomposed into n sub-problems, denoted as (3.P2), as the following

$$\text{(3.P2)} \qquad \max_{\{c_{n,l}\}_{l=0}^{L-1},\{\mu_{n,l}\}_{l=1}^{L-1}} \ \sum_{i=0}^{L-1} \bar{J}_n^{(i)}$$

$$\text{s.t. } c_{n,l} \in [0,1],\ l=0,...,L-1, \qquad 0<\mu_{n,l}<\infty,\ l=1,...,L-1,$$

$$\sum_{i=0}^{L-1} \bar{\mathcal{P}}_n^{(i)} \leq \mathcal{P}_0, \qquad \mathbf{\Phi}_n = -(\mathbf{\Psi}_n^T - \mathbf{I} - \mathbf{B})^{-1}\mathbf{1}.$$

This implies that solving (3.P1) is equivalent to solving (3.P2) N times for $n=1,...,N$. It also implies that solving 3.(P1) can lend itself to a *distributed* implementation, where sensor n solves its corresponding (3.P2) independent of the other sensors. For implementing our proposed power control strategy, we assume that the FC solves (3.P1) once. Based on the obtained solution, in each time slot t the FC quantizes $g_{n,t}$'s and informs sensor n of the quantization interval to which $g_{n,t}$ belongs, via a limited feedback channel. Sensor n solves its corresponding (3.P2) once, and based on the obtained solution it sets up its transmit power control strategy in (3.6) once. Then, in each time slot t sensor n chooses its transmit power

$\mathcal{P}_{n,t}$ according to (3.6), considering its battery state and the received feedback information. It is worth mentioning the difference between optimizing the total J-divergence and the approximate P_e expression in (3.37). Different from (3.P1), the approximate P_e expression in (3.37) *cannot be decoupled* across sensors. Therefore, constrained minimization of P_e does not render itself to a distributed implementation, i.e. each sensor needs to solve (3.P1), with P_e in (3.37) being the cost function, which ensues a much higher computational complexity.

Remark 2: With respect to the power allocation optimization problem in [18] for orthogonal channels, our (3.P1) has a different objective function, different constraints, and different optimization variables. In particular, our objective function and average transmit power per sensor constraint depend on (i) the battery size K and the number of quantization levels L, (ii) the stochastic energy arrival model, through the battery steady state probabilities $\phi_{n,k} = \lim_{t\to\infty} \Pr(B_{n,t} = k)$ for $k = 1, ..., K$, and (iii) the fading channel model through the probabilities $\pi_{n,i}$ for $i = 0, ..., L-1$.

3.4 Solving Problem (3.P1)

Since solving (3.P1) is equivalent to solving (3.P2) N times, in this section we focus on solving (3.P2). Let examine how the cost function and the constraints in (3.P2) depend on the optimization variables.

• Dependency of $\bar{J}_n^{(i)}$: Considering (3.38), its explicit dependency on $\{c_{n,l}, \mu_{n,l}\}$'s is clear. It also depends implicitly on $\{c_{n,l}, \mu_{n,l}\}$'s through the probabilities $\pi_{n,l}$'s and the vector entries $\phi_{n,k}$'s. Recall that $\phi_{n,k}$'s are the entries of vector $\mathbf{\Phi}_n$ given in (3.14). This vector depends on the matrix $\mathbf{\Psi}_n$, whose entries are given in (3.10) and depend on $\{c_{n,l}, \mu_{n,l}\}$'s.

• Dependency of $\bar{\mathcal{P}}_n^{(i)}$: Considering (3.40), its explicit dependency on $c_{n,l}$'s is clear. It also

depends implicitly on $\{c_{n,l}, \mu_{n,l}\}$'s through $\pi_{n,l}$'s and $\phi_{n,k}$'s.

• Dependency of $\mathbf{\Phi}_n$: It depends implicitly on $\{c_{n,l}, \mu_{n,l}\}$'s. We note that problem (3.P2) is *not concave* with respect to the optimization variables. Moreover, the objective function and the constraints in (3.P2) are *not differentiable* with respect to the optimization variables. Hence, existing gradient-based algorithms for solving non-convex optimization problems cannot be used to solve (3.P2).

3.4.1 Deterministic Search Method

We resort to a grid-based search method, which requires $(2L-1)$-dimensional search over the search (parameter) space $[0,1]^L \times (0,\infty)^{L-1}$. To curb the computational complexity of this grid-based search, we can limit $\mu_{n,l}$'s to a maximum value, denoted as μ_{max}. We refer to the solution obtained from solving (P2) using this method the *optimal* solution, in the sense that it is the *best* attainable solution for (P2). Clearly, the accuracy of this solution depends on the resolution of the grid-based search. Suppose the intervals $[0,1]$ and $(0,\mu_{\max}]$ are divided into N_c and N_μ sub-intervals, respectively. Therefore, the search space of (P2), denoted as $\mathcal{D}$, consists of $(N_c)^L (N_\mu)^{L-1}$ discrete points in the original $(2L-1)$-dimensional search space.

• Computational complexity of obtaining the *optimal* solution for (P2): We note that the solver unit (either FC or sensor n) needs to perform two tasks for each point in $\mathcal{D}$: task (i) forming $\mathbf{\Psi}_n$ and solving (3.14) to find $\mathbf{\Phi}_n$, task (ii) calculating $\bar{J}_n^{(i)}$ and $\bar{\mathcal{P}}_n^{(i)}$. Our numerical results show that for a fixed $\{c_{n,l}\}_{l=0}^{L-1}$ and $\{\mu_{n,l}\}_{l=1}^{L-1}$ the computational complexity of task (i) and task (ii) are $\mathcal{O}(K^{3.2})$ and $\mathcal{O}(K^{1.1})$, respectively. Hence, the computational complexity of finding the *optimal* solution for (P2) is $\mathcal{O}\left(N_c^L N_\mu^{L-1}(K^{3.2}+K^{1.1})\right)$.

3.4.2 Random Search Method

Finding the *optimal* solution of (P2) using the grid-based search, as described above, requires searching search space $\mathcal{D}$ *deterministically*. In contrast, in a *random* search algorithm, only a randomly chosen subset of the points in $\mathcal{D}$ is searched to find a solution. The size of this subset can be chosen to be smaller than $(N_c)^L(N_\mu)^{L-1}$, and hence, the computational complexity of finding a solution using a random search algorithm can be significantly lowered. We refer to the solution obtained from solving (P2) using a random search algorithm the *c-optimal* solution, in the sense that it is a close-to-optimal solution.

Among the random search algorithms in the literature, we choose the so-called "Recursive Random Search (RRS) algorithm" [46]. Our reason for this choice is that the authors in [46] showed that RRS algorithm outperforms significantly the traditional search algorithms (e.g., genetic algorithms, multi-start hill climbing algorithms, and simulated annealing algorithm) for most optimization problems. RRS algorithm consists of two phases: exploration (global) phase and exploitation (local) phase. In exploration phase, the algorithm performs random sampling from the entire sample space $\mathcal{D}$, to inspect the overall form of the objective function, and to identify "promising areas" in $\mathcal{D}$ [46]. In exploitation phase, the algorithm continues to search *only* within the identified "promising areas", using recursive random sampling. As the search continues, the sample space is shrunk gradually (according to the previously drawn samples), and the algorithm learns more details of the objective function, until it finally converges to a local optimum, which will be considered as the solution of the optimization problem in hand [46]. For our work to be self-contained, in the following we overview RRS algorithm, with reference to the lines in the pseudo-code of Algorithm 1.

• *Exploration Phase*: To describe this phase and to illustrate the efficiency of RRS algorithm in finding the solution of (3.P2), we need to first introduce the following notations

and concepts. Suppose $x=[c_{n,0},...,c_{n,L-1},\mu_{n,1},...\mu_{n,L-1}]$ denote a sample (point) in $\mathcal{D}$, and J_{min}, J_{max} indicate the minimum and the maximum values of the objective function, respectively. We define the distribution function of the objective function values as $r=\frac{m(A_{\mathcal{D}}(r))}{m(\mathcal{D})}$, for $r\in[0,1]$, where $m(.)$ denotes the cardinality of the set. Given r value, set $A_{\mathcal{D}}(r)\subset\mathcal{D}$ with the cardinality $m(A_{\mathcal{D}}(r))=r\times m(\mathcal{D})$ is the set of points in $\mathcal{D}$ whose values of the objective function exceed a threshold $J_{tr}\in[J_{min},J_{max}]$. $A_{\mathcal{D}}(r)=\Big\{x\in\mathcal{D}|\sum_{i=0}^{L-1}\bar{J}_n^{(i)}(x)\geq J_{tr}(r)\Big\}$, $m(A_{\mathcal{D}}(r))=r\times m(\mathcal{D})$. For this reason $A_{\mathcal{D}}(r)$ is called the *r-percentile* set in $\mathcal{D}$ [46]. We note that $A_{\mathcal{D}}(1)=\mathcal{D}$ and $\lim_{r\to 0}A_{\mathcal{D}}(r)$ converges to the global optimum of the problem [46]. Now, consider the *r-percentile* set $A_{\mathcal{D}}(r)$ in $\mathcal{D}$ and its corresponding $J_{tr}(r)$ value. The goal in exploration phase is to reach a point in $A_{\mathcal{D}}(r)$ with probability p, via random sampling. The question is: how many random samples of $\mathcal{D}$ should we draw, such that we reach a point in $A_{\mathcal{D}}(r)$ with probability p?

To answer this question, let $\boldsymbol{X}=\{x_j\}_{j=1}^{Q_1}$ be the set of randomly drawn samples from $\mathcal{D}$ that satisfy the average transmit power constraint in (P2), and $x_j^*\in\boldsymbol{X}$ provides the largest value of the objective function. We have $p=\Pr\left(x_j^*\in A_{\mathcal{D}}(r)\right)=1-\Pr\left(x_j^*\notin A_{\mathcal{D}}(r)\right)=1-(1-r)^{Q_1}$. Solving p for r we reach at $r=1-(1-p)^{1/Q_1}$. Solving p for Q_1 we obtain $Q_1=\frac{\ln(1-p)}{\ln(1-r)}$. For any probability value p, as Q_1 increases, r tends to 0 and $\lim_{r\to 0}A_{\mathcal{D}}(r)$ converges to the global maximum of (3.P2).

Lines 2,3,4 of the pseudo-code correspond to this phase. We take Q_1 random samples from $\mathcal{D}$, each denoted as x_{q_1}, and put them in $\boldsymbol{X}_t=\{x_{q_1}\}_{q_1=1}^{Q_1}$ and initialize $\boldsymbol{X}=\{\}$. For each sample $x_{q_1}\in\boldsymbol{X}_t$, we check whether the average transmit power constraint is held. If the constraint is satisfied, x_{q_1} is added to $\boldsymbol{X}$. If the constraint is not satisfied, we take another sample from the set $\mathcal{D}\backslash\boldsymbol{X}_t$ and add this new sample to $\boldsymbol{X}_t$. We repeat this procedure until $m(\boldsymbol{X})$ reaches Q_1. Using the samples in $\boldsymbol{X}=\{x_j\}_{j=1}^{Q_1}$, the algorithm computes the threshold J_{tr}.

Having the set $\boldsymbol{X}$, whose elements represent the "promising areas" in $\mathcal{D}$, the algorithm enters exploitation phase. Any future sample we encounter in the next phase that has a greater value of the objective function than J_{tr} belongs to $A_{\mathcal{D}}(r)$.

• *Exploitation Phase*: Consider $\boldsymbol{X} = \{x_j\}_{j=1}^{Q_1}$. For each sample $x_j \in \boldsymbol{X}$ we first determine several neighborhoods[6]

$N_\rho(x_j)$ for $\rho = 1, ..., \rho_0$, such that $m(N_\rho(x_j)) < m(N_{\rho+1}(x_j))$. Given the parameter[7] Q_2, the description of the recursive random search in these neighborhoods to find the solution of (3.P2) follows.

For each sample $x_j \in \boldsymbol{X}$, we start by letting the search space be $\mathcal{S} = N_{\rho_0}(x_j)$, and search $\mathcal{S}$ hoping to to find a *better* sample than x_j. In particular, we take Q_2 random samples from $N_{\rho_0}(x_j)$, each denoted as x_{q_2}, and put them in $\boldsymbol{Y}_t = \{x_{q_2}\}_{q_2=1}^{Q_2}$ and initialize $\boldsymbol{Y}_j = \{\}$. For each sample $x_{q_2} \in \boldsymbol{Y}_t$, we check two conditions: (i) whether the average transmit power constraint is held, (ii) whether the objective function evaluated at x_{q_2} provides a lager value than J_{tr}. If both constraints are satisfied, x_{q_2} is added to $\boldsymbol{Y}_j$. After checking all samples in $\boldsymbol{Y}_t$ we examine $\boldsymbol{Y}_j$. Depending on whether $\boldsymbol{Y}_j \neq \{\}$, meaning there exists at *least one better* sample than x_j in $\mathcal{S}$, or $\boldsymbol{Y}_j = \{\}$, meaning *no better* sample than x_j is found in $\mathcal{S}$, we take two different actions.

If $\boldsymbol{Y}_j \neq \{\}$ we select the sample in $\boldsymbol{Y}_j$ that provides the largest value of the objective function, denoted as x_i^*, and replace $x_j \in \boldsymbol{X}$ with x_i^*, and change $\mathcal{S}$ from $N_{\rho_0}(x_j)$ to $N_{\rho_0}(x_i^*)$, and continue with searching the new $\mathcal{S}$. This procedure of changing the center of $\mathcal{S}$ (without

[6]The neighborhood $N_\rho(x_j)$, for $\rho = 1, ..., \rho_0$, is the set of samples that are neighbors of x_j. Its size $m(N_\rho(x_j))$ depends on the dimensionality of search space $\mathcal{D}$ ($(2L-1)$ here) and the resolution of the grid (parameters N_c, N_μ here). To identify different neighborhoods of x_j, we have used MATLAB's function *neighbourND*. For instance, for $L = 2$ and $N_c = 10, N_\mu = 100$ we have $m(N_1(x_j)) = 17$, $m(N_2(x_j)) = 60$, $m(N_3(x_j)) = 139$.

[7]To enable efficient random search even in the smallest neighborhood we choose $Q_2 < m(N_1(.))$.

shrinking it) in exploitation phase is called "re-align sub-phase" [46]. However, if $\boldsymbol{Y}_j = \{\}$ we shrink $\mathcal{S}$ by changing $\mathcal{S}$ to $N_{\rho_0-1}(x_j)$. This procedure of shrinking $\mathcal{S}$ (without changing its center) in exploitation phase is called "shrink sub-phase" [46]. When searching $N_{\rho_0-1}(x_j)$, if we find a *better* sample than x_j, we replace $x_j \in \boldsymbol{X}$ with this *better* sample. Otherwise, we further shrink $\mathcal{S}$ by changing $\mathcal{S}$ to $N_{\rho_0-2}(x_j)$. We alternatively perform re-align and shrink sub-phases for x_j, until we get to search the smallest neighborhood $N_1(.)$ of a sample. Note that we limit the number of times we perform re-align sub-phase during the exploitation procedure for x_j to Q_1, relying on the fact that after drawing Q_1 samples from $\mathcal{D}$ we reach a point in $A_{\mathcal{D}}(r)$ with probability p. At this point, the exploitation procedure for x_j ends, and $x_j \in \boldsymbol{X}$ is either *kept unchanged* or *replaced with a better sample* that is found during its exploitation procedure. We repeat the exploitation procedure for all samples in $\boldsymbol{X}$, and at the end we obtain a refined and fully exploited $\boldsymbol{X}$. We let the solution of (P2) be $\arg\max_{x_j \in \boldsymbol{X}} (\sum_{i=0}^{L} \bar{J}_n^{(i)}(x_j))$.

• Computational complexity of obtaining the *c-optimal* solution for (3.P2): We note that during the exploitation phase the solver unit needs to perform *repeatedly* the same two tasks, task (i) and task (ii) in Section 3.4.1, with computational complexity $\mathcal{O}(K^{3.2})$ and $\mathcal{O}(K^{1.1})$, respectively. To find out the number of repetition of tasks, we focus on the exploitation procedure for $x_j \in \boldsymbol{X}$. After each performance of re-aligning $\mathcal{S}$ or shrinking $\mathcal{S}$, we randomly search $\mathcal{S}$. i.e., we evaluate the objective function Q_2 times. Hence, the number of repetition of tasks for each $x_j \in \boldsymbol{X}$ is equal to $Q_2 \times \#(\text{performing re-align}) \times \#(\text{performing shrink})$. Since $\#(\text{performing re-align}) \leq Q_1$ and $\#(\text{performing shrink}) \leq \rho_0$, the computational complexity corresponding to the exploitation procedure for $x_j \in \boldsymbol{X}$ is upper bounded by $\mathcal{O}(Q_2 Q_1 \rho_0 (K^{3.2} + K^{1.1}))$. Therefore, the computational complexity of finding the *c-optimal* solution for (P2) is upper bounded by $\mathcal{O}(Q_2 Q_1^2 \rho_0 (K^{3.2} + K^{1.1}))$.

Algorithm 1: pseudo-code of RRS algorithm

1: Initialization phase:

- Set parameter space $\mathcal{D}$ with $(N_c)^L \times (N_\mu)^{L-1}$ points;
- Initialize exploration parameters (p, r) and let $Q_1 = \ln(1-p)/\ln(1-r)$;
- Initialize exploitation parameter Q_2 based on (N_c, N_μ, L);

2: Start exploration phase, take Q_1 uniform random samples from $\mathcal{D}$ and put them in $\boldsymbol{X}_t = \{x_{q_1}\}_{q_1=1}^{Q_1}$, initialize $\boldsymbol{X} = \{\}$;

3: **repeat**
  for $x_{q_1} \in \boldsymbol{X}_t$ **do**
    if $\sum_{i=0}^{L-1} \bar{\mathcal{P}}_n^{(i)}(x_{q_1}) \leq \mathcal{P}_0$ **then**
      Put x_{q_1} in $\boldsymbol{X}$;
    else
      Take another sample from $\mathcal{D} \backslash \boldsymbol{X}_t$ and add it to $\boldsymbol{X}_t$;
    end
  end
until $m(\boldsymbol{X}) = Q_1$;

4: Calculate the threshold using the samples in $\boldsymbol{X} = \{x_j\}_{j=1}^{Q_1}$, $J_{tr} = 1/Q_1 \sum_{j=1}^{Q_1} \left(\sum_{i=0}^{L-1} \bar{J}_n^{(i)}(x_j) \right)$;

5: Start exploitation phase, determine the neighborhoods of sample x_j as $N_1(x_j), N_2(x_j), ..., N_{\rho_0}(x_j)$;

for $x_j \in \boldsymbol{X}$ **do**
  Initialize $\boldsymbol{Y}_j = \{\}$, $I = 0$, Take Q_2 uniform random samples from $N_\rho(x_j)$ and put them in $\boldsymbol{Y}_t = \{x_{q_2}\}_{q_2=1}^{Q_2}$;
  for $x_{q_2} \in \boldsymbol{Y}_t$ **do**
    if $\sum_{i=0}^{L-1} \bar{J}_n^{(i)}(x_{q_2}) \geq J_{tr}$ & $\sum_{i=0}^{L-1} \bar{\mathcal{P}}_n^{(i)}(x_{q_2}) \leq \mathcal{P}_0$ **then**
      Add x_{q_2} to $\boldsymbol{Y}_j$;
    end
  end
  if $\boldsymbol{Y}_j \neq \{\}$ & $I < Q_1$ **then**
    $x_i^* = \arg\max_{x_i \in \boldsymbol{Y}_j} (\sum_{i=0}^{L-1} \bar{J}_n^{(i)}(x_i))$, replace $x_j \in \boldsymbol{X}$ with x_i^*, change the search space from $N_\rho(x_j)$ to $N_\rho(x_i^*)$;
    $I = I + 1$;
  else
    change the search space from $N_\rho(x_j)$ to $N_{\rho-1}(x_j)$;
  end
end

6: $x_{opt} = \arg\max_{x_j \in \boldsymbol{X}} (\sum_{i=0}^{L-1} \bar{J}_n^{(i)}(x_j))$;

3.4.3 Hybrid Deterministic-Random Search Method

In this section we propose a *hybrid* method to find the optimization variable $\{c_{n,l}, \mu_{n,l}\}$'s. In particular, we first obtain the quantization thresholds $\{\mu_{n,l}\}$'s using a different objective function. Then given the optimized $\{\mu_{n,l}\}$'s, we solve (3.P3), given below, using RRS

algorithm.

$$\text{(3.P3)} \quad \max_{\{c_{n,l}\}_{l=0}^{L-1}} \sum_{i=0}^{L-1} \bar{J}_n^{(i)}$$

$$\text{s.t. } c_{n,l} \in [0,1],\ l = 0, ..., L-1, \qquad \sum_{i=0}^{L-1} \bar{\mathcal{P}}_n^{(i)} \leq \mathcal{P}_0, \qquad \mathbf{\Phi}_n = -(\mathbf{\Psi}_n^T - \mathbf{I} - \mathbf{B})^{-1}\mathbf{1}.$$

We refer to the solution we obtain using this hybrid method the *sub-optimal* solution, in the sense that it is worse than the optimal solution. The *sub-optimal* solution is also worse than *c-optimal* solution for two reasons: (i) we detangle optimizing $\{\mu_{n,l}\}$'s and $\{c_{n,l}\}$'s, (ii) we use a different objective function to optimize $\{\mu_{n,l}\}$'s. The main advantage of using this hybrid method is that finding the *sub-optimal* solution has a lower computational complexity than that of the *c-optimal* solution. Our numerical results in Section 3.5 show that the objective function values at the *c-optimal* and the *sub-optimal* solutions are very close to each other and also very close to that of the *optimal* solution.

In the following, we consider two different objective functions that we use to obtain the optimal $\{\mu_{n,l}\}$'s. To motivate these objective functions, we consider the input-output relationship of the quantizer in Section 3.1.2 $\bar{g}_n = Q(g_n)$. If the quantizer input g_n lies in the interval $\mathcal{I}_{n,l}$ then the quantizer output is $\bar{g}_n = \mu_{n,l}$. The quantization error is $e_n = g_n - \bar{g}_n$.

3.4.3.1 Finding $\{\mu_{n,l}\}$'s via Minimizing Mean Absolute Error (MMAE)

The first objective function we consider is mean of absolute quantization error (MAE), denoted as $\mathbb{E}\{|g_n - \bar{g}_n|\}$. We can express MAE as follows.

$$\mathbb{E}\{|g_n - \bar{g}_n|\} = \sum_{l=0}^{L-1} \int_{\mu_{n,l}}^{\mu_{n,l+1}} (x - \mu_{n,l}) f_{g_n}(x) dx \tag{3.41}$$

To find $\{\mu_{n,l}\}$'s that minimize MAE, we take the first derivative of MAE with respect to $\mu_{n,l}$ and set the derivative equal to zero. We reach at

$$F_{g_n}(\mu_{n,l+1}) = F_{g_n}(\mu_{n,l}) + (\mu_{n,l} - \mu_{n,l-1}) f_{g_n}(\mu_{n,l}) \tag{3.42}$$

Recall $\mu_{n,0}=0$ and $\mu_{n,L}=\infty$, and hence $F_{g_n}(0)=0$ and $F_{g_n}(\infty)=1$. We initiate $\mu_{n,1}$ and find $\mu_{n,2}$ using (3.42). Having $\mu_{n,1}, \mu_{n,2}$, we find $\mu_{n,3}$ using (3.42). We repeat this until we find all $\{\mu_{n,l}\}$'s. At this point, we check whether the condition $F_{g_n}(\infty)=1$ is met. If $F_{g_n}(\infty)$ is less (greater) than one, we increase (decrease) the initial value of $\mu_{n,1}$ and find a new set of values for $\{\mu_{n,l}\}$'s. We continue changing the initial value of $\mu_{n,1}$ and finding new values for $\{\mu_{n,l}\}$'s, until the condition $F_{g_n}(\infty)=1$ is satisfied.

3.4.3.2 Finding $\{\mu_{n,l}\}$'s via Maximizing output Entropy (MOE)

The second objective function we consider is the mutual information between g_n and $\bar{g}_n$, denoted as $I(g_n;\bar{g}_n)$. We have $I(g_n;\bar{g}_n)=H(\bar{g}_n)-H(\bar{g}_n|g_n)$, where $H(x)$ denotes the entropy of discrete random variable x. To find $\{\mu_{n,l}\}$'s that maximize $I(g_n;\bar{g}_n)$, we note that $H(\bar{g}_n|g_n)$ is zero, since $\bar{g}_n = Q(g_n)$ and hence, given g_n, $\bar{g}_n$ is also known. Furthermore, $H(\bar{g}_n)$ is maximized when $\bar{g}_n$ follows a uniform distribution, i.e., we set $\pi_{n,l}=\Pr(\mu_{n,l}\leq g_n<\mu_{n,l+1})=\frac{1}{L+1}$, and the threshold $\mu_{n,l}$ can be obtained as $\mu_{n,l}=\gamma_{g_n}\ln\left(1-\frac{l}{L+1}\right)$.

• Computational complexity of finding the *sub-optimal* solution for (3.P2): This computational complexity is the sum of two terms. The first term is the computational complexity of finding $\{c_{n,l}\}$'s using RRS algorithm in Section 3.4.2, and is upper bounded by $\mathcal{O}\left(Q_2Q_1^2\rho_0(K^{3.2}+K^{1.1})\right)$. We note that Q_2 in this section is chosen according to $m(N_1(.))$, which depends on (L, N_c), whereas Q_2 in Section 3.4.2 is chosen according to $m(N_1(.))$, which

depends[8] on (L, N_c, N_μ). Hence, Q_2 here is smaller than Q_2 in Section 3.4.2. The second term is the computational complexity of finding $\{\mu_{n,l}\}$'s via optimizing one of the two objective functions in this section. The computational complexity of finding $\{\mu_{n,l}\}$'s via MMAE is negligible, due to the simplicity of solving (3.42). Our simulations show that for different L values, solving (3.42) takes only several msec. The computational complexity of finding $\{\mu_{n,l}\}$'s via MOE is almost zero, due to the available closed-form solutions. Therefore, the computational complexity of finding the *sub-optimal* solution for (P2) is upper bounded by $\mathcal{O}\left(Q_2 Q_1^2 \rho_0 (K^{3.2} + K^{1.1})\right)$, where Q_2 here is smaller than Q_2 in Section 3.4.2.

3.5 Simulation results and discussion

We corroborate our analysis with MATLAB simulations and investigate: (i) the effect of the optimization variables on the objective function and the entries of $\mathbf{\Phi}$ in (3.13), (ii) the accuracy of different search methods in Section 3.4 in solving (P2) as well as the existing trade-off between detection performance and average transmit power, , (iii) the behavior of the optimized scale factors $\{c_l\}$'s with respect to the fading channel gain g_n,

(iv) the accuracy of the P_e approximate in (3.37).

(v) the dependency of the system error probability P_e (achieved with the optimized variables) on K, ρ, L, and the SNR corresponding to observation channel defined as $\text{SNR}_s = 20\log(\mathcal{A}/\sigma_v)$.

• **Effect of optimization variables**: Considering one sensor and $L=2$, the optimization variables are $\{c_{1,0}, c_{1,1}, \mu_{1,1}\}$. Fig. 3.3a illustrates the objective function $\sum_{i=0}^{L-1} \bar{J}_1^{(i)}$ versus

[8]For instance, for $L=2$ and $N_c=10, N_\mu=100$, we choose $Q_2 < 17$ in Section 3.4.2 and we choose $Q_2 < 5$ here.

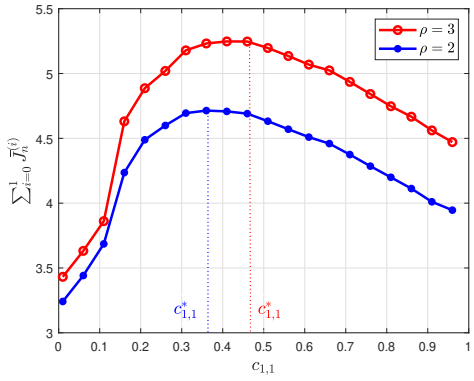

(a) $\mu_{1,1} = 1.1$

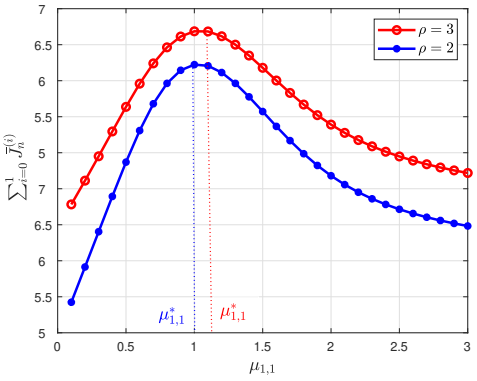

(b) $c_{1,1} = 0.5$

Figure 3.3: $K = 5,\ c_{1,0} = 0.3,\ \gamma_{g_1} = 1.$

Table 3.1: The values of $\Pr(B_1 = 0), \Pr(B_1 = 50), \overline{B}_1,\ \sum_{i=0}^{2} \bar{J}_1^{(i)}$ for $K = 50,\ \rho = 10,\ \gamma_{g_1} = 1.$

		$\Pr(B_1 = 0)$	$\Pr(B_1 = 50)$	$\bar{B}_1$	$\sum_{i=0}^{2} \bar{J}_1^{(i)}$
(a)	$\mu_{1,l} = [0, 0.8, 1.2, \infty]$ $c_{1,l} = [0.3, 0.4, 0.2]$	≈ 0	0.0451	31.97	5.1
(b)	$\mu_{1,l} = [0, 0.8, 1.2, \infty]$ $c_{1,l} = [0.5, 0.7, 0.9]$	0.0318	0.0023	14.33	3.2
(c)	$\mu_{1,l} = [0, 0.1, 2, \infty]$ $c_{1,l} = [0.4, 0.6, 0.3]$	0.0265	0.0039	15.32	3.6
(d)	$\mu_{1,l} = [0, 0.01, 0.1, \infty]$ $c_{1,l} = [0.4, 0.6, 0.3]$	≈ 0	0.0357	28.32	4.5
(e)	$\mu^*_{1,l} = [0, 0.3, 1.1, \infty]$ $c^*_{1,l} = [0.2, 0.5, 0.4]$	0.0014	0.0236	20.52	6.7

the scale factor $c_{1,1}$. We observe that the objective function is not a concave function of $c_{1,1}$. Still there exists a point, denoted as $c^*_{1,1}$, at which the function attains its maximum. Starting from small values of $c_{1,1}$, as $c_{1,1}$ increases (until it reaches $c^*_{1,1}$), the function value increases, because the harvested energy can recharge the battery and can yield more power for data transmission. However, when $c_{1,1}$ exceeds $c^*_{1,1}$, the harvested and stored energy cannot support the data transmission and the function value decreases. Fig. 3.3b shows the objective function versus the quantization threshold $\mu_{1,1}$. We observe that the objective function is not a concave function of $\mu_{1,1}$. Still there exists a point, denoted as $\mu^*_{1,1}$, at which the function achieves its maximum. To accentuate the effect of the optimization

variables on the entries of $\mathbf{\Phi}$ we define the average energy stored at the battery of sensor n as $\overline{B}_n = \mathbb{E}\{B_n\} = \sum_{k=0}^{K} k\ \phi_{n,k}$, where the largest possible value for $\overline{B}_n$ is K. Considering one sensor and $L = 3$, the optimization variables are $\{c_{1,0}, c_{1,1}, c_{1,2}, \mu_{1,1}, \mu_{1,2}\}$. Table 3.1 shows $\Pr(B_1 = 0)$, $\Pr(B_1 = 50)$, $\overline{B}_1$ for four sets of arbitrary chosen values for the optimization variables in (a), (b), (c), (d). Going from (a) to (b), we note that given μ_l's, as c_l's increase data transmit power in (3.6) increases. Due to large energy energy consumption for data transmission $\overline{B}_1$ decreases and the chance of energy outage increases. Going from (c) to (d), we note that given c_l's, as μ_l's decrease, $\Pr(B_1 = 50)$ increases and $\Pr(B_1 = 0)$ decreases, and $\overline{B}_1$ increases. Due to small energy consumption for data transmission, the chance of having near full battery increases, indicating that sensor has failed to utilize the excess energy. Both energy outage and energy overflow inevitably impact transmission and detection performance, leading to a reduction in the objective function. The *optimized* variables are listed in (e). Also, Table 3.1 tabulates the objective function value, showing that the objective function attains its maximum when the variables are optimized. This table shows that the optimization variables play a key role in balancing the rates of energy harvesting and energy consumption for data transmission, such that the objective function is maximized.

• **Accuracy of different search methods in solving (3.P2) and detection performance-transmit power trade-off**:

Table 3.2: The exploitation parameter $Q_2' < Q_2$, and $Q_2 Q_1^2 \rho_0 \ll N_c^L N_\mu^{L-1}$.

Features / Method	computational complexity	detection performance
deterministic	$\mathcal{O}\left(N_c^L N_\mu^{L-1}(K^{3.2} + K^{1.1})\right)$	lowest P_e
random	$\mathcal{O}\left(Q_2 Q_1^2 \rho_0 (K^{3.2} + K^{1.1})\right)$	P_e(deterministic) < P_e(random) < P_e(hybrid)
MMAE & MOE	$\mathcal{O}\left(Q_2' Q_1^2 \rho_0 (K^{3.2} + K^{1.1})\right)$	P_e(random) < P_e(hybrid MOE) < P_e(hybrid MMAE)

First, we compare the accuracy of deterministic, random, and hybrid search methods in

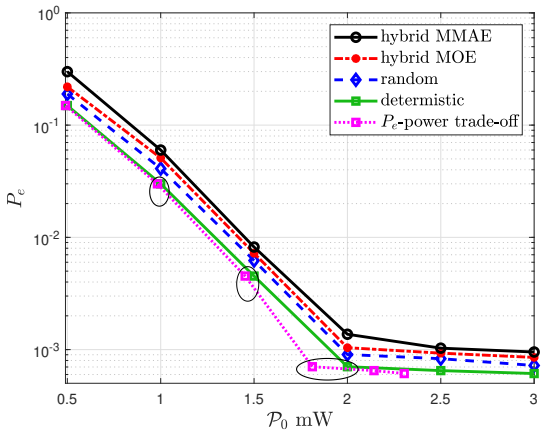

Figure 3.4: P_e vs. $\mathcal{P}_0$ for $N=3,\ K=5,\ L=2, \rho=2,\ \sigma^2_{w_n}=1,\ \gamma_{g_n}=2,\ P_{\mathrm{d}_n}=0.9, \forall n$, $\mathrm{SNR}_s=3$dB.

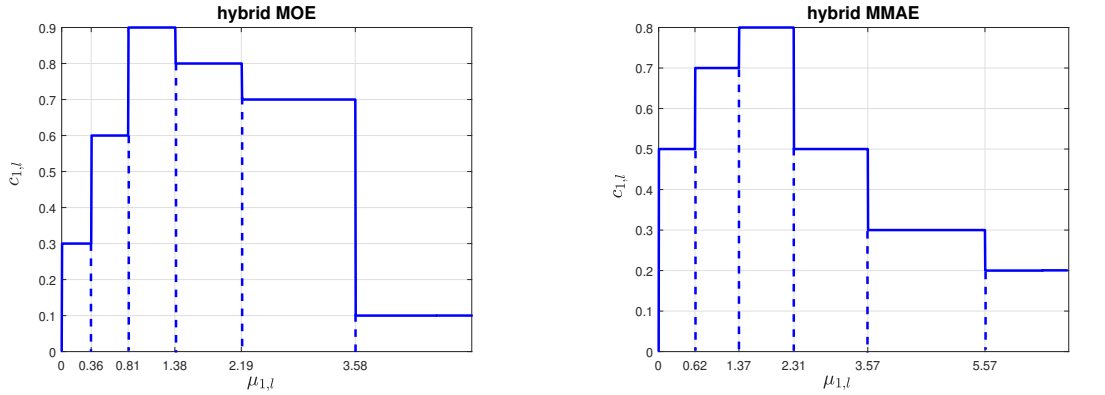

(a) sub-optimal solution corresponding to hybrid MOE

(b) sub-optimal solution corresponding to hybrid MMAE

Figure 3.5: $K=5,\ L=6,\ \rho=2,\ \sigma^2_{w_1}=1,\ \gamma_{g_1}=2,\ P_{\mathrm{d}_1}=0.9$, $\mathcal{P}_0=2$ mW, $\mathrm{SNR}_s=2$ dB.

Section 3.4 for solving (3.P2). Fig. 3.4 shows P_e versus $\mathcal{P}_0$ for $L=2$. To plot the curve labeled as "deterministic" first we obtain the *optimal* solution, set transmit power control strategy in (3.6) accordingly, and run Monte-Carlo simulation to find P_e. For Monte-Carlo we consider 10000 independent Monte Carlo runs, i.e., we generate 10000 realizations of random noises and fading channels and count the errors, P_e is the number of errors occurred divided by 10000. Similarly, we plot the curves labeled as "random", "hybrid MMAE", "hybrid MOE" using the *c-optimal* solution, the *sub-optimal* solution corresponding to MMAE, and the *sub-*

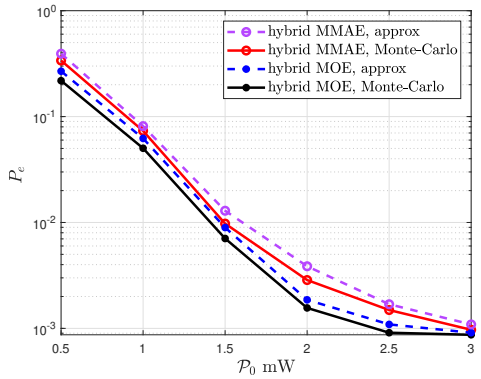

Figure 3.6: P_e vs. $\mathcal{P}_0$ for $N=5,\ K=5,\ L=3, \rho=2,\ \sigma^2_{w_n}=1\ \gamma_{g_n}=2,\ P_{d_n}=0.9, \forall n$, $\text{SNR}_s=3$ dB.

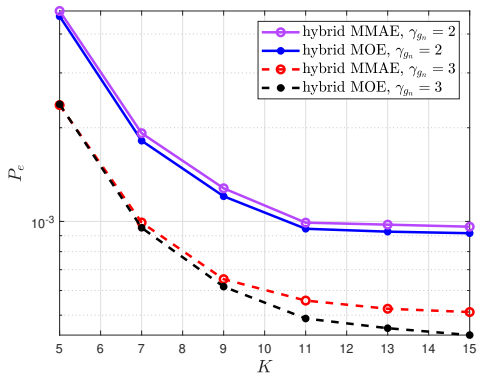

Figure 3.7: P_e vs. K for $N=5,\ L=3,\ \rho=5,\ \sigma^2_{w_n}=1,\ P_{\text{d}_n}=0.9, \forall n, \mathcal{P}_0=3\text{mW}$, $\text{SNR}_s=5\text{dB}$.

optimal solution corresponding to MOE, respectively. When using RRS algorithm we choose the parameters of exploration phase $p=0.99, r=0.1$, leading to $Q_1=44$. For exploitation phase, we choose $Q_2=10$ for "random" and $Q_2=3$ for "hybrid MMAE" and "hybrid MOE". Note that for all curves, as $\mathcal{P}_0$ increases P_e decreases, which is expected. Fig. 3.4 shows (i) "determistic" has the lowest P_e, followed by "random", followed by "hybrid MOE", followed by "hybrid MMAE", (ii) "random", "hybrid MMAE" and "hybrid MOE" perform very close to "determistic". Fig. 3.4 also allows us to examine the existing trade-off between the average transmit power and the detection performance. Consider the curve labeled "P_e-power trade-off" in Fig. 3.4, which shows how much average transmit power is required to provide a certain P_e value. This curve is obtained from examining the points on "deterministic" and checking whether the power constraint in (3.P2) is active or inactive. At a given point, when this constraint is active (inactive), the average transmit power is equal to (less than) $\mathcal{P}_0$. Note that as $\mathcal{P}_0$ increases and P_e reaches an error floor, the average transmit power is less than $\mathcal{P}_0$. Table 3.2 compares the computational complexity and detection performance of these methods. Since finding the *sub-optimal* solution has the lowest computational complexity, and its performance is very close to the *optimal* solution, from this point forward, we focus on "hybrid MMAE" and "hybrid MOE".

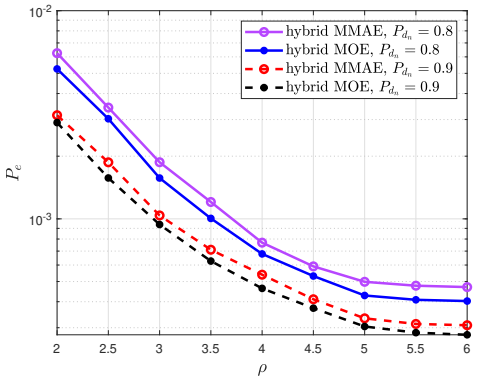

Figure 3.8: P_e vs. ρ for $N=5$, $K=5$, $L=3$, $\sigma^2_{w_n}=1$, $\gamma_{g_n}=3, \forall n, \mathcal{P}_0=3$ mW, $\text{SNR}_s=3$ dB.

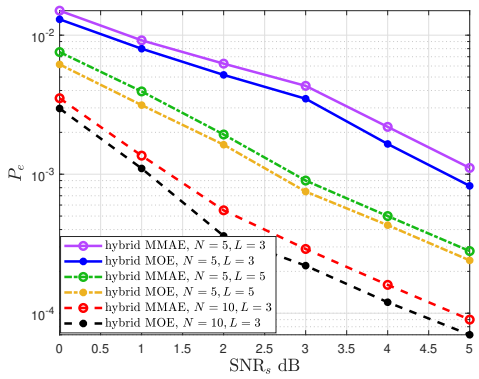

Figure 3.9: P_e vs. SNR_s for $K=5$, $\rho=2$, $\sigma^2_{w_n}=1$, $\gamma_{g_n}=2$, $P_{\text{d}_n}=0.9, \forall n, \mathcal{P}_0=2$ mW.

• **Behavior of the optimized scale factors**: Considering one sensor and $L=6$, the optimization variables are $\{c_{1,l}\}_{l=0}^{5}, \{\mu_{1,l}\}_{l=1}^{5}$. Fig. 3.5a and Fig. 3.5b depict the optimized $\{c_{1,l}, \mu_{1,l}\}$'s corresponding to "hybrid MMAE" and "hybrid MOE". We note that, as l increases (i.e., channel gain $g_{n,t}$ increases), the length of quantization interval $(\mu_{1,l+1} - \mu_{1,l})$ becomes larger. Also, $c_{1,l}$ first increases and then decreases. Considering (3.6) this implies that, given the battery state k, as $g_{n,t}$ increases $\mathcal{P}_{n,t}$ first increases and then decreases.

• **Accuracy of P_e approximate in** (3.37): To examine the accuracy of P_e approximate in (3.37), we focus on "hybrid MMAE" and "hybrid MOE". Fig. 3.6 plots P_e versus $\mathcal{P}_0$, in which P_e values obtained from Monte-Carlo simulations are denoted as "Monte-Carlo", and P_e values obtained from (3.37) are denoted as "approx".

• **Dependency of P_e on different parameters**: Fig. 3.7- 3.10 plot P_e corresponding to "hybrid MMAE" and "hybrid MOE" in terms of different system parameters.

Fig. 3.7 depicts P_e versus K as γ_{g_n} changes. As K increases P_e decreases, until it reaches an error floor. This is because for large K, power $\mathcal{P}_{n,t}$ in (3.6) is no longer restricted by K, and instead it is restricted by ρ. Also, the communication channel noise $\sigma^2_{w_n}$ becomes dominant and leads to an error floor. Clearly, the error floor becomes smaller when γ_{g_n} increases. Also,

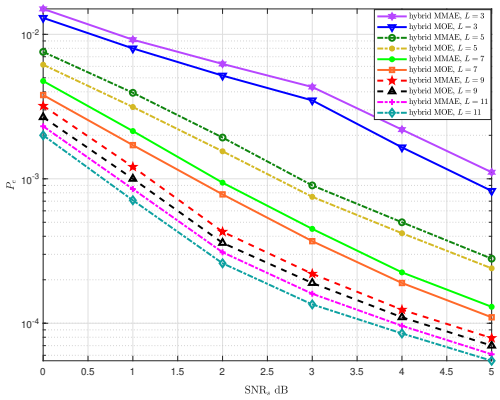

Figure 3.10: P_e vs. SNR_s for $K=5,\ N=5,\ \rho=2,\ \sigma^2_{w_n}=1,\ \gamma_{g_n}=2,\ P_{\mathrm{d}_n}=0.9, \forall n, \mathcal{P}_0=2\mathrm{mW}$.

"hybrid MOE" outperforms "hybrid MMAE". Fig. 3.8 shows P_e versus ρ as $\overline{P}_{\mathrm{d}}$ changes. As ρ increases P_e decreases, until it reaches an error floor. This is because for large ρ, power $\mathcal{P}_{n,t}$ is no longer limited by the amount of harvested energy. Instead, $\sigma^2_{w_n}$ becomes the dominant factor and leads to an error floor. Also, increasing $\overline{P}_{\mathrm{d}}$ lowers the error floor. Fig. 3.9 shows P_e versus SNR_s as N, L vary. Fig. 3.9 indicates that P_e reduces when (i) given the pair (N, L), SNR_s increases; (ii) given the pair (SNR_s, N), L increases; (iii) given the pair (SNR_s, L), N increases. To highlight the effect of increasing L, Fig. 3.10 shows P_e versus SNR_s for $N=5$ as L varies. We note that as L increases, the performance gap between "hybrid MMAE" and "hybrid MOE" decreases. Also, the performance improvement due to increasing L reduces (i.e., the P_e difference between $L=11$ and $L=9$ is much smaller than the P_e difference between $L=5$ and $L=3$). This is expected, since as L increases P_e approaches to the clairvoyant scenario where perfect CSI is available at the sensors.

3.6 Conclusions

We developed a power control strategy for an EH-enabled WSN, that is tasked with solving a binary distributed detection problem. Our proposed strategy is parameterized in terms

of the channel gain quantization thresholds and the scale factors, which play key roles in balancing the rates of energy harvesting and energy consumption for transmission. We explored the optimal and sub-optimal strategies such that the J-divergence based detection metric is maximized, subject to an average transmit power per sensor constraint. These optimization problems can be solved offline and allow each sensor to adapt its power based on its battery state and its quantized CSI (acquired via limited feedback from the FC). Since our non-convex optimization problem is not differentiable with respect to the optimization variables, we explored deterministic, random, and hybrid grid-based search methods, and showed that our proposed hybrid search methods have a low-computational complexity and near-optimal performance. The structure of the optimized scale factors reveals that, given the battery state, the optimized power level is not a monotonic function of the channel gain. We examined the existing trade-off between the average transmit power and the detection performance. We also demonstrated that increasing K or ρ do not necessarily lower the detection error, and it depends on the communication channel noise. We plan to extend our work to multiple access channels, where sensors transmit over a channel simultaneously. Further, we note that the widely adopted signal model in (3.1) relies on the assumption that the distances between the signal source to be detected and the sensors in the field are known [4–7], i.e., the signal model applies to an arbitrary, but fixed sensor deployment. We plan to study how our work can be expanded to incorporate random deployment of sensors. Finally, we note that having CSI at the FC requires channel estimation, which is possible when sensors send training symbols. We plan to study channel-dependent power control strategies that consider the combined effects of channel estimation and channel quantization.

CHAPTER 4: LEARNING-BASED DISTRIBUTED DETECTION WITH ENERGY HARVESTING [1]

We consider a wireless network, consisting of several sensors and a fusion center (FC), that is tasked with solving a binary distributed detection problem. Each sensor is capable of harvesting randomly arrived energy and storing it in a finite-size battery. Modeling the channel fading process as a time-homogeneous finite-state Markov chain and assuming that each sensor knows its current battery state and its quantized channel state information (CSI) obtained by a limited feedback from the FC, our goal is to find the optimal transmit power control policy such that the detection performance metric of interest is maximized. We formulate the problem at hand as a finite-horizon Markov decision process (MDP) problem and obtain the optimal policy via finite-horizon dynamic programming. Our simulations demonstrate that the proposed policy outperforms Greedy-based policy, in which each sensor uses all its available energy for transmission.

4.1 System Model

4.1.1 Observation Model at Sensors

Our system model consists of N spatially distributed sensors and a FC that is tasked with solving a binary hypothesis testing problem. Each sensor is capable of harvesting energy from the ambient environment and is equipped with a battery of finite size to store the harvested energy. We divide time horizon into slots of equal length T_s. Each time slot is indexed by an integer t for $t = 1, 2, ..., T$. We model the underlying binary hypothesis H_t in time slot

[1] © 2021 IEEE. Part of this chapter is reprinted, with permission, from [47].

t as a binary random variable $H_t \in \{0,1\}$ with a-priori probabilities $\Pi_0 = \Pr(H_t = 0)$ and $\Pi_1 = \Pr(H_t = 1) = 1 - \Pi_0$. Let $x_{n,t}$ denote the local observation at sensor t during an observation period. We assume the following signal model

$$\begin{aligned} H_t = 1: \quad & x_{n,t} = \mathcal{A} + v_{n,t}, \\ H_t = 0: \quad & x_{n,t} = v_{n,t}, \quad \text{for } n = 1, \ldots, N \end{aligned} \tag{4.1}$$

where Gaussian observation noises $v_{n,t} \sim \mathcal{N}(0, \sigma^2_{v_n})$ are independent over time slots and across sensors. Given observation $x_{n,t}$ sensor n finds local log-likelihood ratio (LLR) and uses its value to choose its non-negative transmission symbol $\alpha_{n,t}$ (to be optimized) to be sent to the FC. When LLR is below a given local threshold θ_n, sensor n does not transmit and let $\alpha_{n,t} = 0$. When LLR exceeds the given local threshold θ_n, sensor n chooses $\alpha_{n,t}$. In particular, we have

$$\begin{aligned} \widehat{\Pi}_{n,0} &= \Pr(\alpha_{n,t} = 0) = \Pi_0(1 - P_{\mathrm{f}_n}) + \Pi_1(1 - P_{\mathrm{d}_n}), \\ \widehat{\Pi}_{n,1} &= \Pr(\alpha_{n,t} \neq 0) = \Pi_0 P_{\mathrm{f}_n} + \Pi_1 P_{\mathrm{d}_n}, \end{aligned} \tag{4.2}$$

where the probabilities P_{f_n} and P_{d_n} denote, respectively, the false alarm and detection probabilities at sensor n can be determined as

$$\begin{aligned} P_{\mathrm{f}_n} &= \Pr(\alpha_{n,t} \neq 0 | h_t = 0) = Q\Big(\frac{\theta_n + \mathcal{A}^2/2\sigma^2_{v_n}}{\sqrt{\mathcal{A}^2/\sigma^2_{v_n}}}\Big), \\ P_{\mathrm{d}_n} &= \Pr(\alpha_{n,t} \neq 0 | h_t = 1) = Q\Big(\frac{\theta_n - \mathcal{A}^2/2\sigma^2_{v_n}}{\sqrt{\mathcal{A}^2/\sigma^2_{v_n}}}\Big). \end{aligned} \tag{4.3}$$

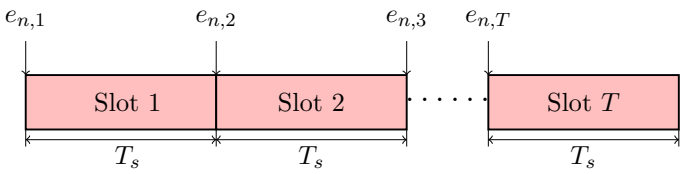

Figure 4.1: Our adopted time frame structure for harvesting and transmission.

4.1.2 Battery State, Harvesting and Transmission Models

We assume sensors are equipped with identical batteries of finite size K cells (units), where each cell corresponds to b_u Joules of stored energy. Therefore, each battery is capable of storing at most Kb_u Joules of harvested energy. Let $b_{n,t} \in \{0, 1, ..., K\}$ denote the discrete random process indicating the battery state of sensor n. Let $e_{n,t}$ be the state of stored and harvested energy units in the battery at sensor n during time slot t (see Fig. 4.1). Note that the harvested energy $e_{n,t}$ cannot be used during slot t. We assume, $e_{n,t}$ is a stationary first-order Markov process. This assumption is justified by empirical measurements in the case of solar energy [48], [49]. For each time slot t we assume that the random variable $e_{n,t}$ takes values from a finite set $\mathcal{E} = \{E_1, E_2, \dots E_M\}$ where $E_m \in Z^+$, $E_m < E_{m+1}$. This Markov chain is characterized with the transition probability denoted as $\Pr(e_{n,t}|e_{n,t-1})$. Let $g_{n,t}$ indicate the narrow-band (flat) fading channel gain between sensor n and the FC during time slot t. We assume $g_{n,t}$'s are independent across sensors. We consider a coherent FC with the knowledge of all channel gains and assume that the FC quantizes the $g_{n,t}$'s using a quantizer with L quantization thresholds $\{\mu_{n,l}\}_{l=0}^{L}$, where $0 = \mu_{n,0} < \mu_{n,1} < \ldots < \mu_{n,L} = \infty$. Let $\mathcal{I}_{n,l} = [\mu_{n,l}, \mu_{n,l+1})$ for $l = 1, \ldots, L$ denote L intervals obtained from partitioning the positive real line with this quantizer. A bandwidth-limited feedback channel from the FC to sensor n conveys the information about which interval $g_{n,t}$ belongs to. The channel gain quantization rule at the FC for sensor n follows: if $g_{n,t} \in \mathcal{I}_{n,l}$ then $g_{n,t}$ is quantized to $\mu_{n,l}$. We define $\mathcal{G} = \{0, \mu_{n,l}, ..., \mu_{n,L}\}$ and the probability $\pi_{n,l} = \Pr(g_{n,t} \in \mathcal{I}_{n,l})$, which can be found

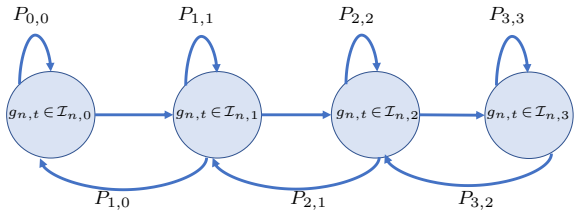

Figure 4.2: Our adopted FSMC model for channel fading process.

based on the distribution of fading model in terms of the two quantization thresholds $\mu_{n,l}$ and $\mu_{n,l+1}$. For instance, for Rayleigh fading model $g_{n,t}^2$ has exponential distribution with the mean $\mathbb{E}\{g_{n,t}^2\} = \gamma_{g_n}$ and we have

$$\pi_{n,l} = \Pr\left(g_{n,t}^2 \in [\mu_{n,l}^2, \mu_{n,l+1}^2)\right) = e^{\frac{-\mu_{n,l}^2}{\gamma_{g_n}}} - e^{\frac{-\mu_{n,l+1}^2}{\gamma_{g_n}}}. \tag{4.4}$$

Further, we assume the channel fading process is a time-homogeneous finite-state Markov chain (FSMC) [50], the channel state remains unchanged in each time slot [51], and the channel fluctuation is slow. Thus, the transition only happens between adjacent states [48] (see Fig. 4.2). For Rayleigh fading channel model, the state transition probability becomes [52]

$$\Pr\left(g_{n,t+1} \in \mathcal{I}_{n,k} | g_{n,t} \in \mathcal{I}_{n,l}\right) = P_{k,l} = \begin{cases} \frac{G(\mu_{n,l+1}^2)}{\pi_{n,l}}, & k = l+1,\ l = 1, ..., L-1 \\ \frac{G(\mu_{n,l}^2)}{\pi_{n,l}}, & k = l-1,\ l = 2, ..., L \\ 1 - \frac{G(\mu_{n,l}^2)}{\pi_{n,l}} - \frac{G(\mu_{n,l+1}^2)}{\pi_{n,l}}, & k = l,\ l = 2, ..., L-1 \\ 1 - \frac{G(\mu_{n,2}^2)}{\pi_{n,1}}, & k = 1,\ l = 1 \\ 1 - \frac{G(\mu_{n,L}^2)}{\pi_{n,L}}, & k = L,\ l = L \end{cases}$$

where $G(x) = \sqrt{2\pi x/\gamma_{g_n}} f_D \exp\left(-x/\gamma_{g_n}\right)$ is the level crossing rate, and f_D (in Hz) is the maximum Doppler frequency.

Adaptive transmission is particularly important for efficient transmission of data in wireless networks. As the name suggests, in the adaptive scheme the transmitter adapts its transmission strategy based on some side information about the quality of the fading channel [53]. The objective is often to devise an efficient adaptive scheme that maximizes the probability of successful data transfer at a tolerable cost, such as power. The side information for adaptive transmission is often provided by the receiver via a feedback link. For example, side information can be the fading level, which is obtained at the receiver by doing extra processing/measurements such as channel estimation. The treatment of the fading channel as an FSMC is attractive from a practical viewpoint. First, the receiver may need to estimate few states for the fading level and send them back to the transmitter. This can greatly reduce the bandwidth required for the feedback link. Second, only a finite number of transmission strategies need to be devised. This simplifies the implementation of the adaptive transmitter.

The main characteristic of the fading channel under consideration is that it is a correlated and time-varying random process. In other words, the communication channel is a dynamic system with the fading channel gain being a random process that changes over time in a correlated manner due to relative movements in the environment.

We formulate our problem of finding the optimal transmit power control strategy (i.e., optimizing $\alpha_{n,t}$) as a finite-horizon Markov decision process (MDP) problem by specifying the system state, the action set, the state transition probability, and the reward functions. At the beginning of time slot t, the system state of sensor n, denoted as $s_{n,t}$, consists of $b_{n,t}, g_{n,t}, e_{n,t-1}$, that is

$$s_{n,t} = (b_{n,t}, g_{n,t}, e_{n,t-1}) \tag{4.5}$$

Based on the current state $s_{n,t}$ at time slot t, sensor n chooses its transmission symbol $\alpha_{n,t}$, i.e., for data transmission an action $a(s_{n,t}) = \alpha_{n,t}$ is taken from its feasible set $\mathcal{U}_{s_{n,t}} =$

$\left\{0, \sqrt{b_u/T_s}, ..., \sqrt{b_{n,t}b_u/T_s}\right\}$ which is discrete and finite. The state transition probability $\Pr(s_{n,t+1}|s_{n,t}, \alpha_{n,t})$ is the probability that the system enters state $s_{n,t+1}$ if action $a(s_{n,t})$ is taken at state $s_{n,t}$. We can simplify the state transition probability as the product of three conditional probabilities

$$\begin{aligned}\Pr(s_{n,t+1}|s_{n,t}, \alpha_{n,t}) &= \Pr(b_{n,t+1}, g_{n,t+1}, e_{n,t}|b_{n,t}, g_{n,t}, e_{n,t-1}, \alpha_{n,t}) \\ &= \Pr(b_{n,t+1}|b_{n,t}, g_{n,t+1}, e_{n,t}, \alpha_{n,t}) \Pr(e_{n,t}|e_{n,t-1}) \Pr(g_{n,t+1}|g_{n,t}),\end{aligned} \tag{4.6}$$

where the second and the third conditional probabilities in (4.6) are the transition probabilities of $e_{n,t}$ and $g_{n,t}$ Markov chains, respectively. Assuming the consumed energy for sensing is negligible, the battery state at the beginning of slot $t+1$ depends on the battery state at the beginning of slot t, the harvested energy during slot t, and the transmission symbol $\alpha_{n,t}$, i.e.,

$$b_{n,t+1} = \min\left\{[b_{n,t} + e_{n,t} - \alpha_{n,t}^2 T_s/b_u]^+, K\right\}, \tag{4.7}$$

where $[x]^+ = \max\{0, x\}$. Considering the dynamic battery state model in (4.7) we note that, conditioned on $e_{n,t}$ and $\alpha_{n,t}$ the value of $b_{n,t+1}$ only depends on the value of $b_{n,t}$. Hence, the process $b_{n,t}$ can be modeled as a Markov chain. Therefore, the first conditional probability in (4.6) becomes

$$\Pr(b_{n,t+1}|b_{n,t}, g_{n,t+1}, e_{n,t}, \alpha_{n,t}) = \begin{cases} 1 & \text{if } b_{n,t+1} = \min\left\{[b_{n,t} + e_{n,t} - \alpha_{n,t}^2 T_s/b_u]^+, K\right\}, \\ 0 & \text{otherwise.} \end{cases}$$

4.1.3 Received Signals at FC and Optimal Bayesian Fusion Rule

The received signal at the FC from sensor n corresponding to time slot t is

$$y_{n,t} = g_{n,t}\,\alpha_{n,t} + w_{n,t}, \qquad \text{for } n = 1, \ldots, N \tag{4.8}$$

where $w_{n,t} \sim \mathcal{N}(0, \sigma^2_{w_n})$ is the additive Gaussian noise. We assume $w_{n,t}$'s are i.i.d. over time slots and independent across sensors. Let $\boldsymbol{y}_t = [y_{1,t}, y_{2,t}, \ldots, y_{N,t}]$ denote the vector that includes the received signals at the FC from all sensors in time slot t. The FC applies the optimal binary Bayesian fusion rule to the received vector $\boldsymbol{y}_t$ and obtains a global decision, $u_{0,t}$, about the underlying hypothesis [16]. From Bayesian perspective, the natural choice to measure the detection performance corresponding to the $u_{0,t}$ at the FC is the error probability, defined as

$$P_e = \Pi_0 \Pr(u_{0,t} = 1 | h_t = 0) + \Pi_1 \Pr(u_{0,t} = 0 | h_t = 1).$$

However, finding a closed form expression for P_e is often intractable. Instead, we choose the total J-divergence between the distributions of the detection statistics at the FC under different hypotheses, as our detection performance metric. This choice allows us to provide a more tractable analysis.

4.2 Total J-Divergence Derivation

We define the total J-divergence and derive a closed-form expression for it, using Gaussian approximation. For sensor n the J-divergence between $f(y_{n,t}|h_t=1)$ and $f(y_{n,t}|h_t=0)$ is

$$J_{n,t}=\int_{-\infty}^{\infty}\Big[f(y_{n,t}|h_t=1)-f(y_{n,t}|h_t=0)\Big]\log\left(\frac{f(y_{n,t}|h_t=1)}{f(y_{n,t}|h_t=0)}\right)dy_{n,t}. \tag{4.9}$$

Note that $f(y_{n,t}|h_t=0)=f(y_{n,t}|\alpha_{n,t}\neq 0)P_{\mathrm{f}_n}+f(y_{n,t}|\alpha_{n,t}=0)(1-P_{\mathrm{f}_n})$ and $f(y_{n,t}|h_t=1)=f(y_{n,t}|\alpha_{n,t}\neq 0)P_{\mathrm{d}_n}+f(y_{n,t}|\alpha_{n,t}=0)(1-P_{\mathrm{d}_n})$ are Gaussian mixtures and the J-divergence between two Gaussian mixture densities does not have a closed-form expression [18]. Similar to [2,3,18], we approximate the J-divergence between two Gaussian mixture densities by the J-divergence between two Gaussian densities $f^G(y_{n,t}|h_t)\sim\mathcal{N}(m_{n,h},\Upsilon^2_{n,h})$, where $m_{n,h}$ and $\Upsilon^2_{n,h}$ are obtained from matching the first and second order moments of the actual and the approximate distributions [3]. For our problem setup, $m_{n,h}$ and $\Upsilon^2_{n,h}$ are

$$\begin{aligned} m_{n,0}&=g_n\alpha_nP_{\mathrm{f}_n}, \quad \Upsilon^2_{n,0}=g_n^2\alpha_n^2P_{\mathrm{f}_n}(1-P_{\mathrm{f}_n})+\sigma^2_{w_n},\\ m_{n,1}&=g_n\alpha_nP_{\mathrm{d}_n}, \quad \Upsilon^2_{n,1}=g_n^2\alpha_n^2P_{\mathrm{d}_n}(1-P_{\mathrm{d}_n})+\sigma^2_{w_n}. \end{aligned} \tag{4.10}$$

The J-divergence between two Gaussian densities, represented as $J\big(f^G(y_{n,t}|h_t=1),f^G(y_{n,t}|h_t=0)\big)$, in terms of their means and variances is [18]

$$J\big(f^G(y_{n,t}|h_t=1),f^G(y_{n,t}|h_t=0)\big)=\frac{\Upsilon^2_{n,1}+(m_{n,1}-m_{n,0})^2}{\Upsilon^2_{n,0}}+\frac{\Upsilon^2_{n,0}+(m_{n,0}-m_{n,1})^2}{\Upsilon^2_{n,1}}. \tag{4.11}$$

Substituting $m_{n,h}$ and $\Upsilon^2_{n,h}$ into $J_{n,t}$ in (4.11) we approximate $J_{n,t}$ as the following

$$J(g_{n,t},\alpha_{n,t})=\frac{\sigma^2_{w_n}+A_ng^2_{n,t}\alpha^2_{n,t}}{\sigma^2_{w_n}+B_ng^2_{n,t}\alpha^2_{n,t}}+\frac{\sigma^2_{w_n}+C_ng^2_{n,t}\alpha^2_{n,t}}{\sigma^2_{w_n}+D_ng^2_{n,t}\alpha^2_{n,t}}, \tag{4.12}$$

where

$$A_n = P_{\mathrm{f}_n}(1-P_{\mathrm{d}_n}) + P_{\mathrm{d}_n}(P_{\mathrm{d}_n}-P_{\mathrm{f}_n}),\ \ C_n = \ P_{\mathrm{d}_n}(1-P_{\mathrm{f}_n}) - P_{\mathrm{f}_n}(P_{\mathrm{d}_n}-P_{\mathrm{f}_n}),$$
$$B_n = P_{\mathrm{d}_n}(1-P_{\mathrm{d}_n}),\ \ D_n = P_{\mathrm{f}_n}(1-P_{\mathrm{f}_n}).$$

The notation $J(g_{n,t}, \alpha_{n,t})$ in (4.12) is to emphasize that J-divergence depends on both $\alpha_{n,t}$ and $g_{n,t}$.

4.3 Finite-Time Horizon Optimal Power Control Policy with causal Quantized CSI information

The problem of finding the optimal power control policy, such that the average total J-divergence is maximized (averaged over the channel gains), can be formulated as below

$$\text{(4.P1)} \qquad \max_{\{a(s_{n,t});\ 1\le t\le T\}} \ \sum_{t=1}^{T}\sum_{n=1}^{N} \mathbb{E}_{g_{n,t}}\Big\{ J\big(g_{n,t}, a(s_{n,t})\big)|g_{n,t-1}\Big\}$$
$$\text{s.t.} \quad a(s_{n,t}) \in \mathcal{U}_{s_{n,t}},\ \forall n,\ 1 \le t \le T$$

in which the average total J-divergence value in each time slot is adopted as the reward function. For time slot t, given the current state $s_{n,t}$ and the corresponding action $a(s_{n,t})$ the reward is

$$r\big(s_{n,t}, a(s_{n,t})\big) = \Pr(\alpha_{n,t}\neq 0)\mathbb{E}_{g_{n,t}}\Big[J\big(g_{n,t}, a(s_{n,t})\big)|g_{n,t-1}\Big] = \widehat{\Pi}_{n,1}\sum_{g_{n,t}\in\mathcal{G}} \Pr(g_{n,t}|g_{n,t-1}) J\big(g_{n,t}, a(s_{n,t})\big).$$

Let $\omega = \Big\{a(s_{n,t}) \in \mathcal{U}_{s_{n,t}}, t \in \{1,2,\ldots,T\}\Big\}$ be a feasible policy and Ω be the set of all feasible policies. Our goal is to find the optimal policy ω^*, i.e., the policy that maximizes the expected total reward summed over a finite horizon by choosing a suitable sequence of

actions. Suppose for a given initial system state $s_{n,1} = \{b_{n,1}, g_{n,1}, e_{n,0} : n = 1, \ldots, N\}$, sensor n solves the following optimization problem

$$V^* = \max_{\omega \in \Omega} \sum_{t=1}^{T} \mathbb{E}\Big[r\big(s_{n,t}, a(s_{n,t})\big) | s_{n,1}, \omega\Big], a(s_{n,t}) \in \mathcal{U}_{s_{n,t}}, \tag{4.13}$$

where V^* denotes the maximum total expected reward accrued starting from current time slot with an initial state $s_{n,1}$ and continuing with the policy ω from then on until T time slots. The expectation is taken over all relevant random variables given initial state $s_{n,1}$ and the policy ω. In general, the optimization problem in (4.13) cannot be solved independently for each time slot, because there is a temporal correlation between different variables. Therefore, we use **finite horizon dynamic programming** to solve the sequential decision problem in (4.13). We use $V(s_{n,t})$ to denote the maximum expected reward from time slot t to $T-1$, given that the system state is $s_{n,t}$ at time slot t. Based on the Bellman's equations, the optimization problem V^* in (4.13) can be recursively computed from $t = T-1$ to $t = 1$ as follows

$$\begin{aligned} V(s_{n,t}) = \max_{a(s_{n,t}) \in \mathcal{U}_{s_{n,t}}} \Big\{ & r\big(s_{n,t}, a(s_{n,t})\big) + \sum_{i=0,1} \widehat{\Pi}_{n,i} \\ & \sum_{\forall s_{n,t+1}} \Pr(s_{n,t+1} | s_{n,t}, \alpha_{n,t}) V(s_{n,t+1}) \Big\}, \ \forall s, \ 1 \le t \le T-1 \end{aligned} \tag{4.14}$$

The first term on the right hand side of (4.14) represents the expected immediate reward for time slot t, while the second term indicates the total expected future reward from $t+1$ to $T-1$ in the case where action $a(s_{n,t})$ is chosen. The terminal condition is given by

$$V(s_{n,T}) := \max_{a(s_{n,t}) \in \mathcal{U}_{s_{n,T}}} \Big\{ r\big(s_{n,t}, a(s_{n,t})\big) \Big\} \tag{4.15}$$

Algorithm 2: Optimal transmit power control policy

1: Calculate $V(s_{n,T})$ according to (4.15);
2: Set $t = T - 1$
3: **while** $t \geq 1$ **do**
  Calculate $V(s_{n,t})$ according to (4.14);
  Find the optimal action $a_{\text{opt}}(s_{n,t})$, using (4.16);
  Set $t := t - 1$;
end
4: Obtain the optimal policy $\omega^* = \Big\{ a_{\text{opt}}(s_{n,t}) \in \mathcal{U}_{s_{n,t}}, t \in \{1, 2, \ldots, T\} \Big\}$.

where all available energy is used for data transmission in the final time slot T. The solution to (4.P1) is then given by

$$a_{\text{opt}}(s_{n,t}) = \arg \max_{a(s_{n,t}) \in \mathcal{U}_{s_{n,t}}} V(s_{n,t}), \text{ for } t = 1, 2, ..., T \tag{4.16}$$

Algorithm 2 shows how we find the optimal transmit power control policy.

4.4 Simulation Results and Conclusions

In our simulations, we consider $T = 20$, $\mathcal{E} = \{2b_u, 4b_u, 6b_u\}$ and the transition probability matrix of $e_{n,t}$ is $P_{\mathcal{E}} = \begin{pmatrix} 0.5 & 0.5 & 0 \\ 0.25 & 0.5 & 0.25 \\ 0 & 0.5 & 0.5 \end{pmatrix}$. For $f_D T_s = 0.04$, $\mathcal{G} = \{0, 0.5, 1.5, 2.5\}$ and the transition probability matrices of $g_{n,t}$ for $\gamma_{g_n} = 2$ and $\gamma_{g_n} = 2.5$, respectively, are $P_{\mathcal{G}} = \begin{pmatrix} 0.87 & 0.13 & 0 & 0 \\ 0.13 & 0.56 & 0.31 & 0 \\ 0 & 0.27 & 0.52 & 0.21 \\ 0 & 0 & 0.28 & 0.72 \end{pmatrix}$ and $P_{\mathcal{G}} = \begin{pmatrix} 0.85 & 0.15 & 0 & 0 \\ 0.16 & 0.52 & 0.32 & 0 \\ 0 & 0.38 & 0.40 & 0.22 \\ 0 & 0 & 0.31 & 0.69 \end{pmatrix}$. We obtain the average total J-divergence corresponding to the optimal power control policy from averaging the results over 5000 independent Monte Carlo runs. Fig. 4.3 illustrates the average J-divergence versus b_u for $K = 10,\ 20,\ 30$. We observe that, given a K value, the average J-divergence increases

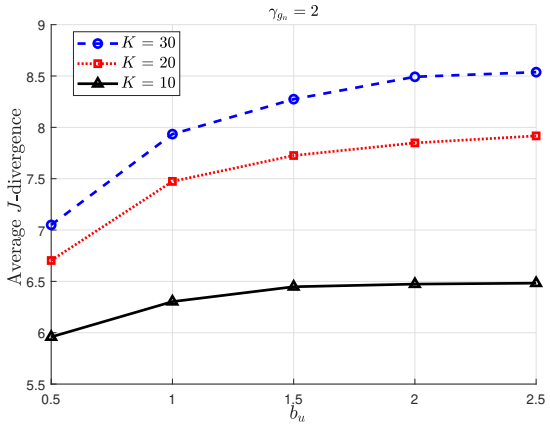

Figure 4.3: The average J-divergence versus b_u for $K = 10,\ 20,\ 30$.

in b_u, however, it remains almost the same after b_u reaches and exceeds a certain value. This is due to the fact that, for larger b_u values transmit power is not limited by energy harvesting. Instead, it is limited by the communication channel noise. As K increases, the saturation of the average J-divergence occurs at a larger value of b_u. Fig. 4.4 shows the average J-divergence versus K for $b_u = 0.5,\ 1,\ 2$. The average J-divergence can be enhanced by enlarging the battery capacity to store more energy units. Given a b_u value as K increases, transmit power is no longer restricted by K, and instead it is restricted by energy harvesting. To demonstrate the effectiveness of our proposed power control policy in striking a balance between energy harvesting and energy consumption for data transmission, Fig. 4.5 compares its P_e performance against that of a Greedy-based policy, in which sensor n in time slot t uses all its available energy for transmission, i.e., $\alpha_{n,t} = \sqrt{b_{n,t} b_u / T_s}$. Fig. 4.5 depicts P_e versus K for $\gamma_{g_n} = 2,\ 2.5$. Clearly, our proposed policy outperforms the Greedy-based policy. As K increases P_e decreases, until it reaches an error floor. This is because for large K, transmit power no longer restricted by K, and instead the communication channel noise $\sigma^2_{w_n}$ becomes dominant and leads to an error floor. Clearly, the error floor becomes smaller when γ_{g_n} increases.

In summary, we considered a binary distributed detection system where each sensor is ca-

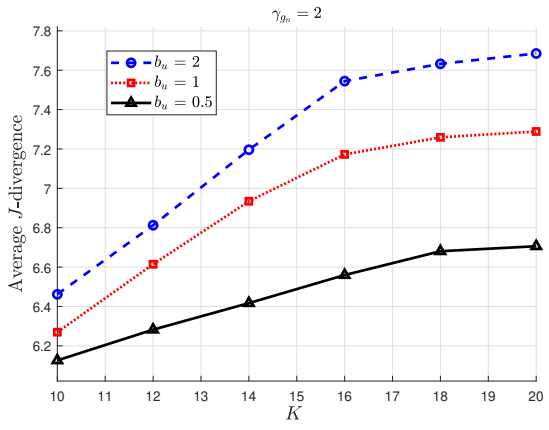

Figure 4.4: The average J-divergence versus K for $b_u = [0.5,\ 1,\ 2]$.

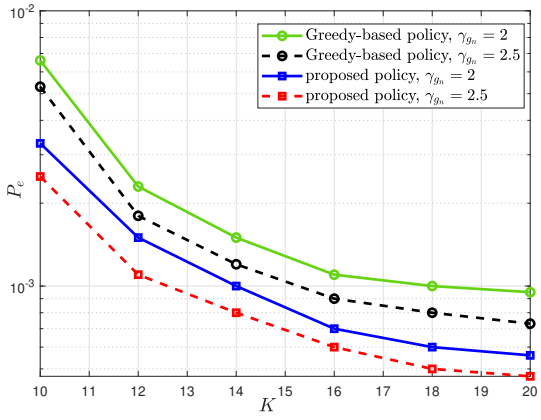

Figure 4.5: P_e versus K for $b_u = 1,\ \gamma_{g_n} = 2,\ 2.5$.

pable of harvesting and storing randomly arrived energy in its battery. We formulated the problem of finding the optimal power control policy that optimizes the detection performance as a finite-horizon MDP problem, and solved the problem via finite horizon dynamic programming. The optimal policy allows each sensor to adapt its transmission symbol based on its current quantized CSI and battery state.

CHAPTER 5: ON DISTRIBUTED DETECTION IN EH-WSNS WITH FINITE-STATE MARKOV CHANNEL AND LIMITED FEEDBACK

We consider a network, tasked with solving binary distributed detection, consisting of N sensors, a fusion center (FC), and a feedback channel from the FC to sensors. Each sensor is capable of harvesting energy and is equipped with a finite size battery to store randomly arrived energy. Sensors process their observations and transmit their symbols to the FC over orthogonal fading channels. The FC fuses the received symbols and makes a global binary decision. We aim at developing adaptive channel-dependent transmit power control policies such that J-divergence based detection metric is maximized at the FC, subject to total transmit power constraint. Modeling the quantized fading channel, the energy arrival, and the battery dynamics as time-homogeneous finite-state Markov chains, and the network lifetime as a geometric random variable, we formulate our power control optimization problem as a discounted infinite-horizon constrained Markov decision process (MDP) problem, where sensors' transmit powers are functions of the battery states, quantized channel gains, and the arrived energies. We utilize stochastic dynamic programming and Lagrangian approach to find the optimal and sub-optimal power control policies. We demonstrate that our sub-optimal policy provides a close-to-optimal performance with a reduced computational complexity and without imposing signaling overhead on sensors.

5.1 System Model

5.1.1 Observation Model at Sensors

We consider a WSN tasked with solving a binary distributed detection problem (see Fig. 5.1). To describe our signal processing blocks at sensors and the FC as well as energy harvesting model, we divide time horizon into slots of equal length T_s. Each time slot is indexed by an integer t for $t = 1, 2, ..., T$ (see Fig. 5.2). We model the underlying binary hypothesis H_t in time slot t as a binary random variable $H_t \in \{0, 1\}$ with a-priori probabilities $\zeta_0 = \Pr(H_t = 0)$ and $\zeta_1 = \Pr(H_t = 1) = 1 - \zeta_0$. We assume that the hypothesis H_t varies over time slots in an independent and identically distributed (i.i.d.) manner. Let $x_{n,t}$ denote the local observation at sensor n in time slot t. We assume that sensors' observations given each hypothesis with conditional distribution $f(x_{n,t}|H_t = h_t)$ for $h_t \in \{0, 1\}$ are independent across sensors. This model is relevant for WSNs that are tasked with detection of a known signal in uncorrelated Gaussian noises with the following signal model

$$H_t = 1: \quad x_{n,t} = \mathcal{A} + v_{n,t}, \;\; H_t = 0: \quad x_{n,t} = v_{n,t}, \quad \text{for } n = 1, \ldots, N, \tag{5.1}$$

where Gaussian observation noises $v_{n,t} \sim \mathcal{N}(0, \sigma_{v_n}^2)$ are independent over time slots and across sensors. Given observation $x_{n,t}$ sensor n forms local log-likelihood ratio (LLR)

$$\Gamma_n(x_{n,t}) \triangleq \log\left(\frac{f(x_{n,t}|h_t = 1)}{f(x_{n,t}|h_t = 0)}\right), \tag{5.2}$$

and uses its value to choose its non-negative transmission symbol $\alpha_{n,t}$ to be sent to the FC. In particular, when LLR is below a given local threshold θ_n, sensor n does not transmit and let $\alpha_{n,t} = 0$. When LLR exceeds the given local threshold θ_n, sensor n chooses $\alpha_{n,t}$ according

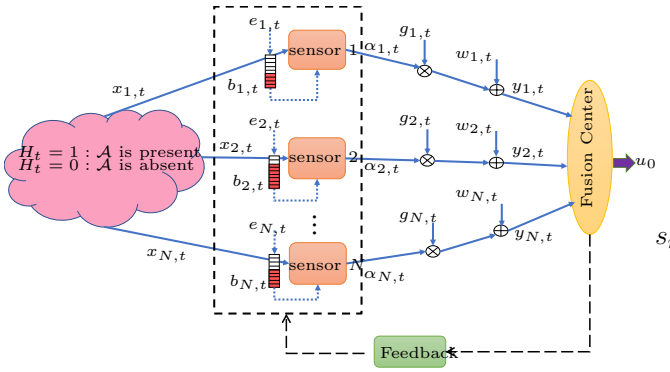

Figure 5.1: Our system model and the schematic of battery state in time slot t.

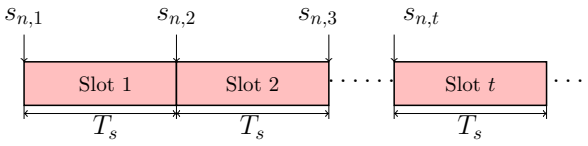

Figure 5.2: Our adopted time frame structure for harvesting and transmission.

to the available information (will be explained later). In particular, we have

$$\widehat{\zeta}_{n,0} = \Pr(\alpha_{n,t}=0) = \zeta_0(1-P_{\mathrm{f}_n}) + \zeta_1(1-P_{\mathrm{d}_n}),\ \widehat{\zeta}_{n,1} = \Pr(\alpha_{n,t}\neq 0) = \zeta_0 P_{\mathrm{f}_n} + \zeta_1 P_{\mathrm{d}_n}, \quad (5.3)$$

where the probabilities P_{f_n} and P_{d_n} can be determined using our signal model in (5.1) and given the local threshold θ_n

$$P_{\mathrm{f}_n} = \Pr(\mathcal{P}_{n,t}\neq 0|h_t=0) = Q\Big(\frac{\theta_n + \mathcal{A}^2/2\sigma_{v_n}^2}{\sqrt{\mathcal{A}^2/\sigma_{v_n}^2}}\Big),\ P_{\mathrm{d}_n} = \Pr(\mathcal{P}_{n,t}\neq 0|h_t=1) = Q\Big(\frac{\theta_n - \mathcal{A}^2/2\sigma_{v_n}^2}{\sqrt{\mathcal{A}^2/\sigma_{v_n}^2}}\Big). \quad (5.4)$$

Instead of fixing θ_n, one can fix P_{d_n} and let $P_{\mathrm{d}_n} = \overline{P}_{\mathrm{d}}, \forall n$. Then the false alarm probability in (5.4) can be written as $P_{\mathrm{f}_n} = Q\left(Q^{-1}(\overline{P}_{\mathrm{d}}) + \sqrt{\mathcal{A}^2/\sigma_{v_n}^2}\right)$.

Note that sensors are typically deployed in hostile outdoor environments (e.g., for forestry fire and volcano monitoring and detection, and battlefield surveillance) in an unattended and distributed manner. Therefore, they are highly susceptible to physical destruction. We include this factor into our modeling by letting $\eta \in [0, 1)$ be the probability that a sensor can survive physical destruction or hardware failure and continue to function in time slot t. Defining the network lifetime T as the time until the first sensor fails, we find that T

becomes a geometrically distributed random variable with mean $\mathbb{E}\{T\}=1/(1-\eta)$ [54].

5.1.2 Battery State, Energy Harvesting and Transmission Models

We assume sensors are equipped with identical batteries of finite size K cells (units), where each cell corresponds to b_u Joules of stored energy. Therefore, each battery is capable of storing at most Kb_u Joules of harvested energy. Let $b_{n,t} \in \mathcal{B}=\{0,1,...,K\}$ denote the energy state of battery of sensor n at the beginning time slot t (also referred to as the battery state). Note that $b_{n,t}=0$ and $b_{n,t}=K$ represent energy states of empty battery and full battery, respectively.

Let $e_{n,t}$ be the number of energy units that are harvested and stored at sensor n during time slot t, i.e., at the beginning of time slot t, sensor n knows the value of $e_{n,t-1}$ but not $e_{n,t}$, and hence the harvested energy $e_{n,t}$ cannot be used during slot t. We assume $e_{n,t}$'s are independent across sensors, and model $e_{n,t}$ as a set of independent stationary first-order homogeneous Markov process with transition probability matrix $\Phi_{\mathcal{E}}$. For each time slot t we assume that the random variable $e_{n,t}$ takes values from a finite set $\mathcal{E}=\{E_1,E_2,\dots E_M\}$ where $E_m \in Z^+$, $E_m < E_{m+1}$. Therefore, matrix $\Phi_{\mathcal{E}}$ is $M \times M$ and its (i,j)-th entry is $[\Phi_{\mathcal{E}}]_{i,j} = \Pr(e_{n,t}=E_i|e_{n,t-1}=E_j)$. This modelling for the harvested energy processes is justified by empirical measurements in the case of solar energy [48].

Let $g_{n,t}$ indicate the narrow-band (flat) fading channel gain between sensor n and the FC during time slot t. We assume $g_{n,t}$'s are independent across sensors. We consider a coherent FC with the knowledge of all channel gains. The FC quantizes $g_{n,t}$ to $\bar{g}_{n,t}$ and informs sensor n of $\bar{g}_{n,t}$, through a bandwidth-limited feedback channel from the FC to sensor n. Suppose the quantizer has L quantization thresholds $\bar{\mathcal{G}}=\{\mu_1,\mu_2,...,\mu_L\}$, where $0=\mu_1<\mu_2<\ldots<\mu_L=\infty$, and $\mathcal{I}_l=[\mu_l,\mu_{l+1})$ for $l=1,\ldots,L$ denote the corresponding quantization intervals.

Suppose $\bar{g}_{n,t} = Q(g_{n,t})$ indicates the input-output relationship of the quantizer. If $g_{n,t} \in \mathcal{I}_l$ then $\bar{g}_{n,t} = \mu_l$. We define the probability $\phi_{n,l} = \Pr(\bar{g}_{n,t} = \mu_l)$, which can be found based on the distribution of fading model in terms of the two quantization thresholds μ_l and μ_{l+1}. We assume $\bar{g}_{n,t}$ is a homogeneous finite-state Markov chain (FSMC) [50] with an $L \times L$ transition probability matrix $\Psi_{\bar{\mathcal{G}}}^{(n)}$ and its (k,l)-th entry is $[\Psi_{\bar{\mathcal{G}}}^{(n)}]_{k,l} = \Pr(\bar{g}_{n,t} = \mu_k | \bar{g}_{n,t-1} = \mu_l)$. Fig. 5.3 is the schematic representation of this L-state Markov chain. Suppose that the channel fluctuation due to Doppler is slow enough such that the transition in $\bar{g}$ only happens between adjacent channel states [48]. For Rayleigh fading model, $g_{n,t}^2$ is modeled as an exponential random variable with the mean $\mathbb{E}\{g_{n,t}^2\} = \gamma_{g_n}$ and we have

$$\phi_{n,l} = \Pr(\bar{g}_{n,t} = \mu_l) = e^{\frac{-\mu_l^2}{\gamma_{g_n}}} - e^{\frac{-\mu_{l+1}^2}{\gamma_{g_n}}}. \tag{5.5}$$

Furthermore

$$[\Psi_{\bar{\mathcal{G}}}^{(n)}]_{k,l} = \begin{cases} \frac{G(\mu_{l+1}^2)}{\phi_{n,l}}, & k = l+1,\ l = 1, ..., L-1 \\ \frac{G(\mu_l^2)}{\phi_{n,l}}, & k = l-1,\ l = 2, ..., L \\ 1 - \frac{G(\mu_l^2)+G(\mu_{l+1}^2)}{\phi_{n,l}}, & k = l,\ l = 2, ..., L-1 \\ 1 - \frac{G(\mu_2^2)}{\phi_{n,1}}, & k = 1,\ l = 1 \\ 1 - \frac{G(\mu_L^2)}{\phi_{n,L}}, & k = L,\ l = L \\ 0, & \text{O.W.} \end{cases} \tag{5.6}$$

where $G(x) = \sqrt{2\pi x/\gamma_{g_n}} f_D T_s \exp(-x/\gamma_{g_n})$ is the level crossing rate, and f_D is the maximum Doppler frequency. We assume the feedback channel from the FC to sensor n has a delay, i.e., at the beginning of time slot t, sensor n only knows $\bar{g}_{n,t-1}$ but not $\bar{g}_{n,t}$.

Let $s_{n,t}$ denote the state of sensor n during time slot t. We characterize $s_{n,t}$ by a three-tuple

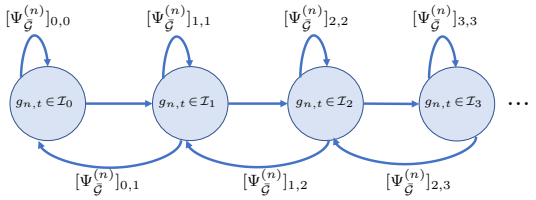

Figure 5.3: Our adopted FSMC model for channel fading process.

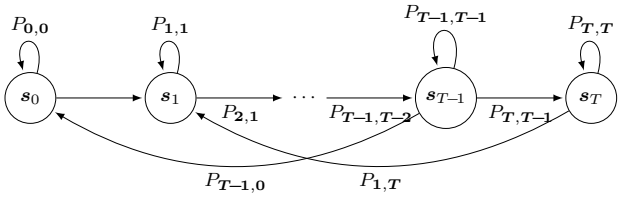

Figure 5.4: Schematics of Markov chain corresponding to the global state $\boldsymbol{s}_t$. In this figure we have $P_{\boldsymbol{t,t+1}} = \Pr\left(\boldsymbol{s}_{t+1}|\boldsymbol{s}_t, \boldsymbol{\alpha}_t\right)$.

$s_{n,t} = (b_{n,t}, \bar{g}_{n,t-1}, e_{n,t-1})$. We denote the state space as $\mathcal{S} = \mathcal{B} \times \bar{\mathcal{G}} \times \mathcal{E}$, where $\mathcal{B}$ is the set of battery energy states, $\bar{\mathcal{G}}$ is the set of communication channel states and $\mathcal{E}$ is the set of energy harvesting states. Let $\boldsymbol{s}_t = (s_{1,t}, s_{2,t}, ..., s_{N,t})$ denote the network state during time slot t and $\bar{\mathcal{S}} = \mathcal{S} \times \mathcal{S} \times \ldots \mathcal{S}$ denote the network state space, where $\mathcal{S} = \mathcal{B} \times \bar{\mathcal{G}} \times \mathcal{E}$. We refer to $s_{n,t} \in \mathcal{S}$ and $\boldsymbol{s}_t \in \bar{\mathcal{S}}$ as the *local state* and the *global (network) state*, respectively. Clearly, $\mathcal{S}, \bar{\mathcal{S}}$ are discrete and finite. Let the dimensions of $\mathcal{S}, \bar{\mathcal{S}}$ be denoted as $|\mathcal{S}|, |\bar{\mathcal{S}}|$. We have $|\bar{\mathcal{S}}| = |\mathcal{S}|^N = ((K+1)LM)^N$.

In time slot t, if LLR exceeds a given local threshold θ_n, sensor n chooses its non-negative transmission symbol $\alpha_{n,t}$ according to the *available information* (either the local state $s_{n,t}$ or the global state $\boldsymbol{s}_t$). Note that the amount of energy consumed for transmitting non-negative symbol $\alpha_{n,t}$ cannot be more than the energy stored in the battery, i.e., $\alpha_{n,t}$ must satisfy the inequality $\alpha_{n,t}^2 T_s / b_u \leq b_{n,t}$. This implies that $\alpha_{n,t} \in \mathcal{U}_{n,t}$ where the feasible set $\mathcal{U}_{n,t} = \left\{0, \sqrt{b_u/T_s}, ..., \sqrt{b_{n,t} b_u / T_s}\right\}$ is discrete and finite. Let $\boldsymbol{\alpha}_t = \left(\alpha_{1,t}, \alpha_{2,t}, ..., \alpha_{N,t}\right)$ contains transmission symbols by all sensors. We have $\boldsymbol{\alpha}_t \in \bar{\mathcal{U}}_t = \mathcal{U}_{1,t} \times \mathcal{U}_{2,t} \times \ldots \mathcal{U}_{N,t}$. Further, we assume that the nodes in the network must satisfy a total transmit power constraint. Such power constraint can be translated into $\sum_{n=1}^{N} \alpha_{n,t}^2 \leq \mathcal{P}_{tot}$. *Our goal is to develop (sub-)optimal adaptive power control strategy such that the detection performance at the FC is optimized.*

In Section 5.2 we formulate the constrained optimization of transmission symbol $\alpha_{n,t}$ as a

discounted infinite-horizon constrained MDP problem. In this problem formulation, $\alpha_{n,t}$ is the action taken by sensor n, and $\boldsymbol{\alpha}_t$ is the collection of actions taken by all sensors, during time slot t. We refer to $\alpha_{n,t}$ as the *local action* and $\boldsymbol{\alpha}_t$ as the *global (network) action*, respectively. We use dynamic programming to solve the problem and provide two types of solutions: (i) *the optimal policy*, in which local action $\alpha_{n,t}$ depends on the global state $\boldsymbol{s}_t = (s_{1,t}, s_{2,t}, ..., s_{N,t})$ where $s_{n,t} = (b_{n,t}, \bar{g}_{n,t-1}, e_{n,t-1})$, i.e., during time slot t sensor n has access to the global state $\boldsymbol{s}_t$ and determines its action $\alpha_{n,t}$ according to $\boldsymbol{s}_t$, and (ii) *the sub-optimal policy*, in which local action $\alpha_{n,t}$ depends on the local state $s_{n,t}$ only, i.e., during time slot t sensor n has access to the local state $s_{n,t}$ only and determines its action $\alpha_{n,t}$ according to $s_{n,t}$.

Let the global state transition probability $\Pr\left(\boldsymbol{s}_{t+1}|\boldsymbol{s}_t, \boldsymbol{\alpha}_t\right)$ denote the probability of entering network state $\boldsymbol{s}_{t+1}$ if network action $\boldsymbol{\alpha}_t$ is taken at network state $\boldsymbol{s}_t$. Define $\boldsymbol{b}_t = (b_{1,t}, b_{2,t}, ..., b_{N,t})$, $\bar{\boldsymbol{g}}_t = (\bar{g}_{1,t}, \bar{g}_{2,t}, ..., \bar{g}_{N,t})$, $\boldsymbol{e}_t = (e_{1,t}, e_{2,t}, ..., e_{N,t})$. We can simplify the global state transition probability as the product of three conditional probabilities (see Fig. 5.4)

$$\Pr\big(\boldsymbol{s}_{t+1}|\boldsymbol{s}_t, \boldsymbol{\alpha}_t\big)=\Pr\big(\boldsymbol{b}_{t+1}, \bar{\boldsymbol{g}}_t, \boldsymbol{e}_t|\boldsymbol{b}_t, \bar{\boldsymbol{g}}_{t-1}, \boldsymbol{e}_{t-1}, \boldsymbol{\alpha}_t\big)=\Pr\big(\boldsymbol{b}_{t+1}|\boldsymbol{b}_t, \bar{\boldsymbol{g}}_t, \boldsymbol{e}_t, \boldsymbol{\alpha}_t\big)\Pr(\boldsymbol{e}_t|\boldsymbol{e}_{t-1})\Pr(\bar{\boldsymbol{g}}_t|\bar{\boldsymbol{g}}_{t-1}). \tag{5.7}$$

The second and third conditional probabilities in (5.7) can be decomposed across sensors, since $\bar{g}_{n,t}$'s and $e_{n,t}$'s are independent across sensors. In other words, we have

$$\Pr(\boldsymbol{e}_t|\boldsymbol{e}_{t-1})=\prod_{n=1}^{N}\Pr(e_{n,t}|e_{n,t-1}),\ \ \Pr(\bar{\boldsymbol{g}}_t|\bar{\boldsymbol{g}}_{t-1})=\prod_{n=1}^{N}\Pr(\bar{g}_{n,t}|\bar{g}_{n,t-1}) \tag{5.8}$$

in which $\Pr(e_{n,t}|e_{n,t-1}), \Pr(\bar{g}_{n,t}|\bar{g}_{n,t-1})$ are the transition probabilities of $e_{n,t}$ and $\bar{g}_{n,t}$ Markov chains, respectively. To find the first conditional probability in (5.7), we need to know the dynamic battery state model. The battery state at the beginning of time slot $t+1$ depends on the battery state at the beginning of time slot t, the harvested energy during time slot t,

and the transmission symbol $\alpha_{n,t}$, i.e.,

$$b_{n,t+1} = \min\left\{[b_{n,t} + e_{n,t} - \alpha_{n,t}^2 T_s/b_u]^+, K\right\}, \tag{5.9}$$

where $[x]^+ = \max\{0, x\}$. Considering the dynamic battery state model in (5.9) we notice that, conditioned on $e_{n,t}$ and $\alpha_{n,t}$ the value of $b_{n,t+1}$ only depends on the value of $b_{n,t}$ (and not the battery states before time slot t). Hence, the process $\boldsymbol{b}_t$ can be modeled as a Markov chain and the first conditional probability in (5.7) becomes

$$\Pr\left(\boldsymbol{b}_{t+1}|\boldsymbol{b}_t, \bar{\boldsymbol{g}}_t, \boldsymbol{e}_t, \boldsymbol{\alpha}_t\right) = \begin{cases} 1 & \text{if (5.9) is satisfied } \forall n \\ 0 & \text{otherwise,} \end{cases} \tag{5.10}$$

We define the reward function in Section 5.1.4.

5.1.3 Received Signals at FC and Optimal Bayesian Fusion Rule

In each time slot, sensors send their data symbols to the FC over orthogonal fading channels. The received signal at the FC from sensor n corresponding to time slot t is

$$y_{n,t} = g_{n,t}\,\alpha_{n,t} + w_{n,t}, \quad \text{for } n = 1, \ldots, N \tag{5.11}$$

where $w_{n,t} \sim \mathcal{N}(0, \sigma_{w_n}^2)$ is the additive Gaussian noise. We assume $w_{n,t}$'s are i.i.d. over time slots and independent across sensors. Let $\boldsymbol{y}_t = [y_{1,t}, y_{2,t}, \ldots, y_{N,t}]$ denote the vector that includes the received signals at the FC from all sensors in time slot t. The FC applies the optimal Bayesian fusion rule $\Gamma_0(.)$ to the received vector $\boldsymbol{y}_t$ and obtains a global decision $u_{0,t} = \Gamma_0(\boldsymbol{y}_t)$, where $u_{0,t} \in \{0, 1\}$. In particular, we have

$$u_{0,t} = \Gamma_0(\boldsymbol{y}_t) = \begin{cases} 1, & \Delta_t > \tau, \\ 0, & \Delta_t < \tau, \end{cases} \tag{5.12}$$

where the decision threshold is $\tau = \log(\frac{\zeta_0}{\zeta_1})$ and

$$\Delta_t = \log\left(\frac{f(\boldsymbol{y}_t|h_t=1)}{f(\boldsymbol{y}_t|h_t=0)}\right), \tag{5.13}$$

and $f(\boldsymbol{y}_t|h_t)$ is the conditional probability density function (pdf) of the received vector $\boldsymbol{y}_t$ at the FC. From Bayesian perspective, the natural choice to measure the detection performance corresponding to the global decision $u_{0,t}$ at the FC is the error probability, defined as

$$P_e = \zeta_0 \Pr(u_{0,t}=1|h_t=0) + \zeta_1 \Pr(u_{0,t}=0|h_t=1) = \zeta_0 \Pr(\Delta_t > \tau|h_t=0) + \zeta_1 \Pr(\Delta_t < \tau|h_t=1). \tag{5.14}$$

However, finding a closed form expression for P_e is mathematically intractable. Instead, we choose the total J-divergence between the distributions of the detection statistics at the FC under different hypotheses, as our detection performance metric. This choice allows us to provide a tractable analysis. Next, we define the total J-divergence and derive a closed-form expression for it, using Gaussian approximation.

5.1.4 Total J-Divergence Derivation and Reward Function

Consider two pdfs of a continuous random variable x, denoted as $\eta_1(x)$ and $\eta_2(x)$. By definition [18], the J-divergence between $\eta_1(x)$ and $\eta_0(x)$, denoted as $J(\eta_1, \eta_0)$, is $J(\eta_1, \eta_0) = D(\eta_1||\eta_0) + D(\eta_0||\eta_1)$, where $D(\eta_i||\eta_j)$ is the non-symmetric Kullback-Leibler (KL) distance between $\eta_i(x)$ and $\eta_j(x)$. The KL distance $D(\eta_i||\eta_j)$ is defined as

$$D(\eta_i||\eta_j) = \int_{-\infty}^{\infty} \log\left(\frac{\eta_i(x)}{\eta_j(x)}\right) \eta_i(x) dx. \tag{5.15}$$

Therefore, we obtain

$$J(\eta_1, \eta_0) = \int_{-\infty}^{\infty} [\eta_1(x) - \eta_0(x)] \log\left(\frac{\eta_1(x)}{\eta_0(x)}\right) dx. \tag{5.16}$$

In our problem setup, the two conditional pdfs $f(\boldsymbol{y}_t|h_t=1)$ and $f(\boldsymbol{y}_t|h_t=0)$ in (5.13) play the role of $\eta_1(x)$ and $\eta_0(x)$, respectively. Let $J_{tot,t}$ denote the J-divergence between $f(\boldsymbol{y}_t|h_t=1)$ and $f(\boldsymbol{y}_t|h_t=0)$. The pdf of vector $\boldsymbol{y}_t$ given h_t is

$$f(\boldsymbol{y}_t|h_t) = \prod_{n=1}^{N} f(y_{n,t}|h_t) \quad \text{for } h_t = 0, 1. \tag{5.17}$$

where the equality in (5.17) holds since the received signals from sensors at the FC, given h_t, are conditionally independent. Let $J_{n,t}$ represent the J-divergence between the two conditional pdfs $f(y_{n,t}|h_t=1)$ and $f(y_{n,t}|h_t=0)$. We have

$$J_{n,t} = \int_{-\infty}^{\infty} \Big[f(y_{n,t}|h_t=1) - f(y_{n,t}|h_t=0) \Big] \log\left(\frac{f(y_{n,t}|h_t=1)}{f(y_{n,t}|h_t=0)} \right) dy_{n,t}. \tag{5.18}$$

Based on (5.17), the total J-divergence, denoted as $J_{tot,t}$, is $J_{tot,t} = \sum_{n=1}^{N} J_{n,t}$. Note that $f(y_{n,t}|h_t=0) = f(y_{n,t}|\alpha_{n,t} \neq 0) P_{\mathrm{f}_n} + f(y_{n,t}|\alpha_{n,t}=0)(1-P_{\mathrm{f}_n})$ and $f(y_{n,t}|h_t=1) = f(y_{n,t}|\alpha_{n,t} \neq 0) P_{\mathrm{d}_n} + f(y_{n,t}|\alpha_{n,t}=0)(1-P_{\mathrm{d}_n})$ are Gaussian mixtures and the J-divergence between two Gaussian mixture densities does not have a closed-form expression [3, 18]. We approximate $J_{n,t}$ in (5.18) using the Gaussian densities $f^G(y_{n,t}|h_t) \sim \mathcal{N}(m_{n,h}, \Upsilon_{n,h}^2)$, where $m_{n,h}$ and $\Upsilon_{n,h}^2$ are obtained from matching the first and second order moments of the actual and the approximate distributions. For our problem setup, $m_{n,h}$ and $\Upsilon_{n,h}^2$ are

$$\begin{aligned} m_{n,0} &= g_{n,t}\alpha_{n,t}P_{\mathrm{f}_n}, \quad & \Upsilon_{n,0}^2 &= g_{n,t}^2\alpha_{n,t}^2 P_{\mathrm{f}_n}(1-P_{\mathrm{f}_n}) + \sigma_{w_n}^2, \\ m_{n,1} &= g_{n,t}\alpha_{n,t}P_{\mathrm{d}_n}, \quad & \Upsilon_{n,1}^2 &= g_{n,t}^2\alpha_{n,t}^2 P_{\mathrm{d}_n}(1-P_{\mathrm{d}_n}) + \sigma_{w_n}^2. \end{aligned}$$

The J-divergence between two Gaussian densities, represented as $J\big(f^G(y_{n,t}|h_t=1), f^G(y_{n,t}|h_t=0)\big)$, in terms of their means and variances is [3, 18]

$$J\big(f^G(y_n|h=1), f^G(y_n|h=0)\big) = \frac{\Upsilon_{n,1}^2 + (m_{n,1}-m_{n,0})^2}{\Upsilon_{n,0}^2} + \frac{\Upsilon_{n,0}^2 + (m_{n,0}-m_{n,1})^2}{\Upsilon_{n,1}^2}. \tag{5.19}$$

Substituting $m_{n,h}$ and $\Upsilon^2_{n,h}$ of (5.19) into (5.19) we approximate $J_{n,t}$ in (5.18) as the following

$$J_{n,t}(g_{n,t},\alpha_{n,t})=\frac{\sigma^2_{w_n}+A_n g^2_{n,t}\alpha^2_{n,t}}{\sigma^2_{w_n}+B_n g^2_{n,t}\alpha^2_{n,t}}+\frac{\sigma^2_{w_n}+C_n g^2_{n,t}\alpha^2_{n,t}}{\sigma^2_{w_n}+D_n g^2_{n,t}\alpha^2_{n,t}}, \tag{5.20}$$

where

$$\begin{aligned} A_n &= P_{\mathrm{f}_n}(1-P_{\mathrm{d}_n})+P_{\mathrm{d}_n}(P_{\mathrm{d}_n}-P_{\mathrm{f}_n}), \quad B_n = P_{\mathrm{d}_n}(1-P_{\mathrm{d}_n}) \\ C_n &= P_{\mathrm{d}_n}(1-P_{\mathrm{f}_n})-P_{\mathrm{f}_n}(P_{\mathrm{d}_n}-P_{\mathrm{f}_n}), \quad D_n = P_{\mathrm{f}_n}(1-P_{\mathrm{f}_n}). \end{aligned} \tag{5.21}$$

The notation $J_{n,t}(g_{n,t},\alpha_{n,t})$ in (5.20) is to emphasize that J-divergence depends on both transmission symbol $\alpha_{n,t}$ and fading channel gain $g_{n,t}$. The dependency on $g_{n,t}$ stems from the fact that the FC has full knowledge of all channel gains $g_{n,t}$'s, and the optimal Bayesian fusion rule utilizes this full information to make the binary decision. On the other hand, sensor n only knows $\bar{g}_{n,t-1}=Q(g_{n,t-1})$. Hence, $\alpha_{n,t}$ can only depend on $\bar{g}_{n,t-1}$. To resolve this issue, we take the average of $J_{n,t}$ over $g_{n,t}$, conditioned on $\bar{g}_{n,t-1}$. Let $\mathbb{E}_{g_{n,t}|\bar{g}_{n,t-1}}\{J_{n,t}(g_{n,t},\alpha_{n,t})|\bar{g}_{n,t-1}\}$ denote the average of J-divergence over $g_{n,t}$ when action $\alpha_{n,t}$ is taken according to the available information at sensor n, conditioned on $\bar{g}_{n,t-1}$. Let $r\big(\alpha_{n,t}\big)$ indicate the immediate reward function of sensor n at time slot t. We define the immediate reward function of sensor n as the average of J-divergence over $g_{n,t}$ when action $\alpha_{n,t}\neq 0$ is taken according to the available information at sensor n, conditioned on $\bar{g}_{n,t-1}$, i.e.,

$$r(\alpha_{n,t})=\widehat{\zeta}_{n,1}\mathbb{E}_{g_{n,t}|\bar{g}_{n,t-1}}\{J(g_{n,t},\alpha_{n,t})|\bar{g}_{n,t-1}\} \tag{5.22}$$

where $\widehat{\zeta}_{n,1}=\Pr(\alpha_{n,t}\neq 0)$ is given in (5.3). Note that when action $\alpha_{n,t}=0$ is taken from (3.27) we find $J_{n,t}(g_{n,t},0)=2$. By defining the immediate reward as (5.22) we neglect the constant term $\widehat{\zeta}_{n,0}\mathbb{E}_{g_{n,t}|\bar{g}_{n,t-1}}\{J(g_{n,t},0)|\bar{g}_{n,t-1}\}=2\widehat{\zeta}_{n,0}$ and do not count it toward the immediate reward

function. To compute the immediate reward function in (5.22), first we define the following

$$\begin{aligned} \hat{J}_{n,t}^{(l)} &= \mathbb{E}_{g_{n,t}|\bar{g}_{n,t}=\mu_l}\{J_{n,t}\big(g_{n,t},\alpha_{n,t}\big)|\bar{g}_{n,t}=\mu_l\} \\ \bar{J}_{n,t}^{(l)} &= \mathbb{E}_{g_{n,t}|\bar{g}_{n,t-1}=\mu_l}\{J_{n,t}\big(g_{n,t},\alpha_{n,t}\big)|\bar{g}_{n,t-1}=\mu_l\} \end{aligned} \tag{5.23}$$

Hence, the immediate reward function in (5.22) can be rewritten in terms of $\bar{J}_{n,t}^{(l)}$ for $l = 1, ..., L$ as

$$r(\alpha_{n,t}) = \widehat{\zeta}_{n,1}\Big(\sum_{l=2}^{L-1}\underbrace{\Pr(\bar{g}_{n,t-1}=\mu_l)}_{=\phi_{n,l}}\bar{J}_{n,t}^{(l)} + \underbrace{\Pr(\bar{g}_{n,t-1}=\mu_1)}_{=\phi_{n,1}}\bar{J}_{n,t}^{(1)} + \underbrace{\Pr(\bar{g}_{n,t-1}=\mu_L)}_{=\phi_{n,L}}\bar{J}_{n,t}^{(L)}\Big) \tag{5.24}$$

To fully characterize the reward function in (5.24) we need to find $\bar{J}_{n,t}^{(l)}$ defined in (5.23) for $l = 1, ..., L$. When $\bar{g}_{n,t-1}=\mu_l$ for $l = 2, .., L-1$, from (5.6) we have

$$\bar{g}_{n,t} = \begin{cases} \mu_{l-1} & \text{with probability } [\Psi_{\bar{\mathcal{G}}}^{(n)}]_{l-1,l} \\ \mu_l & \text{with probability } [\Psi_{\bar{\mathcal{G}}}^{(n)}]_{l,l} \\ \mu_{l+1} & \text{with probability } [\Psi_{\bar{\mathcal{G}}}^{(n)}]_{l+1,l} \end{cases} \tag{5.25}$$

When $\bar{g}_{n,t-1}=\mu_1$, from (5.6) we have

$$\bar{g}_{n,t} = \begin{cases} \mu_1 & \text{with probability } [\Psi_{\bar{\mathcal{G}}}^{(n)}]_{1,1} \\ \mu_2 & \text{with probability } [\Psi_{\bar{\mathcal{G}}}^{(n)}]_{2,1} \end{cases} \tag{5.26}$$

and when $\bar{g}_{n,t-1}=\mu_L$, from (5.6) we have

$$\bar{g}_{n,t} = \begin{cases} \mu_{L-1} & \text{with probability } [\Psi_{\bar{\mathcal{G}}}^{(n)}]_{L-1,L} \\ \mu_L & \text{with probability } [\Psi_{\bar{\mathcal{G}}}^{(n)}]_{L,L-1} \end{cases} \tag{5.27}$$

Therefore, $\bar{J}_{n,t}^{(l)}$ and $\hat{J}_{n,t}^{(l)}$ in (5.23) become related as the following

$$\bar{J}_{n,t}^{(l)} = \begin{cases} [\Psi_{\bar{\mathcal{G}}}^{(n)}]_{l-1,l}\hat{J}_{n,t}^{(l-1)} + [\Psi_{\bar{\mathcal{G}}}^{(n)}]_{l,l}\hat{J}_{n,t}^{(l)} + [\Psi_{\bar{\mathcal{G}}}^{(n)}]_{l+1,l}\hat{J}_{n,t}^{(l+1)} & l \neq 1, L \\ [\Psi_{\bar{\mathcal{G}}}^{(n)}]_{1,1}\hat{J}_{n,t}^{(1)} + [\Psi_{\bar{\mathcal{G}}}^{(n)}]_{2,1}\hat{J}_{n,t}^{(2)} & l = 1 \\ [\Psi_{\bar{\mathcal{G}}}^{(n)}]_{L-1,L}\hat{J}_{n,t}^{(L-1)} + [\Psi_{\bar{\mathcal{G}}}^{(n)}]_{L,L}\hat{J}_{n,t}^{(L)} & l = L \end{cases} \tag{5.28}$$

Note that $\hat{J}_{n,t}^{(l)}$ in (5.23) can be obtained based on the distribution of fading model. For Rayleigh fading model, we have [3]

$$\hat{J}_{n,t}^{(l)} = \phi_{n,l}\Big[\Omega(\alpha_{n,t}^2, \mu_{n,l+1}^2) - \Omega(\alpha_{n,t}^2, \mu_{n,l}^2)\Big], \tag{5.29}$$

where the two dimensional function $\Omega(x, y)$ in (5.29) is

$$\begin{aligned} \Omega(x,y) \triangleq & \frac{1}{B_n x}\Big[\sigma_{w_n}^2\beta_1(x,y) - \frac{A_n}{B_n}\sigma_{w_n}^2\beta_1(x,y) - A_n x e^{(-y\gamma_{g_n})}\Big] \\ & + \frac{1}{D_n x}\Big[\sigma_{w_n}^2\beta_2(x,y) - \frac{C_n}{D_n}\sigma_{w_n}^2\beta_2(x,y) - C_n x e^{(-y\gamma_{g_n})}\Big], \end{aligned} \tag{5.30}$$

Also, $A_n,\ B_n,\ C_n$ and D_n are given in (5.21) and the two dimensional functions $\beta_1(x, y)$ and $\beta_2(x, y)$ in (5.30) are

$$\beta_1(x,y) \triangleq \gamma_{g_n}\exp\big(\frac{\sigma_{w_n}^2\gamma_{g_n}}{xB_n}\big)\mathrm{Ei}\big(-\gamma_{g_n}y - \frac{\sigma_{w_n}^2\gamma_{g_n}}{xB_n}\big), \quad \beta_2(x,y) \triangleq \gamma_{g_n}\exp\big(\frac{\sigma_{w_n}^2\gamma_{g_n}}{xD_n}\big)\mathrm{Ei}\big(-\gamma_{g_n}y - \frac{\sigma_{w_n}^2\gamma_{g_n}}{xD_n}\big).$$

In summary, the reward function in (5.24) can be written as

$$r(\alpha_{n,t}) = \widehat{\zeta}_{n,1}\Big(\sum_{l=2}^{L-1}\phi_{n,l}\bar{J}_{n,t}^{(l)} + \phi_{n,1}\bar{J}_{n,t}^{(1)} + \phi_{n,L}\bar{J}_{n,t}^{(L)}\Big) \tag{5.31}$$

in which $\bar{J}_{n,t}^{(l)}$ is given in (5.28). The immediate network reward function at time slot t, denoted as $r(\boldsymbol{\alpha}_t)$, is the sum of the reward functions of all sensors

$$r(\boldsymbol{\alpha}_t) = \sum_{n=1}^{N} r\big(\alpha_{n,t}\big). \tag{5.32}$$

where $r\big(\alpha_{n,t}\big)$ is given in (5.31).

At every time slot t, sensor n decides the transmission symbol $\alpha_{n,t}$ according to the available information (either the local state $s_{n,t}$ or the global state $\boldsymbol{s}_t$) such that the discounted sum of reward is maximized, subject to two constraints: (i) the amount of energy consumed for transmission symbol $\alpha_{n,t}$ cannot be more than the energy stored in the battery $b_{n,t}$, i.e., $\alpha_{n,t}^2 T_s/b_u \leq b_{n,t}$, or equivalently, $\alpha_{n,t} \in \mathcal{U}_{n,t},\ \forall n,t$, (ii) the nodes in the network must satisfy a total transmit power constraint, i.e., $\sum_{n=1}^{N} \alpha_{n,t}^2 \ \leq \mathcal{P}_{tot},\ \forall t$. In the next section we formulate the constrained optimization of $\alpha_{n,t}$ as a discounted infinite-horizon constrained MDP problem. We use dynamic programming to solve the problem and provide two types of solutions: (i) the optimal policy, in which the local action $\alpha_{n,t}$ depends on the global state $\boldsymbol{s}_t$, and (ii) the sub-optimal policy, in which the local action $\alpha_{n,t}$ depends on the local state $s_{n,t}$ only.

5.2 Problem Formulation

We start our problem formulation by defining the set of feasible policies. Let δ_t denote a general decision rule that describes how a network action $\boldsymbol{\alpha}_t$ is selected according to the global state $\boldsymbol{s}_t$ in time slot t, i.e., $\boldsymbol{\alpha}_t = \delta_t(\boldsymbol{s}_t)$, and $\pi = (\delta_1, \delta_2, ...\delta_T)$ be the corresponding policy for $t = 1, ..., T$, i.e., π is the sequence of decision rules to be employed for time slots $t = 1, ..., T$ [55, pp.21]. We say that a policy π is feasible if it satisfies the two constraints:

(i) $\boldsymbol{\alpha}_t \in \bar{\mathcal{U}}_t,\ \forall t$, (ii) $\sum_{n=1}^{N} \alpha_{n,t}^2 \leq \mathcal{P}_{tot},\ \forall t$. Let Π be the set of feasible policies π. Then, for any given global state $\boldsymbol{s}_1$ at the first time slot $t = 1$, the expected network reward between the first time slot until a sensor stops functioning with policy $\pi \in \Pi$ is given by

$$V_\pi(\boldsymbol{s}_1) = \mathbb{E}\left\{ \mathbb{E}_T\left\{ \sum_{t=1}^{T} r(\boldsymbol{\alpha}_t) \right\} \Big| \boldsymbol{s}_1, \pi \right\}, \quad \text{s.t. } \boldsymbol{\alpha}_t \in \bar{\mathcal{U}}_t,\ \sum_{n=1}^{N} \alpha_{n,t}^2 \leq \mathcal{P}_{tot},\ \forall t \tag{5.33}$$

where the outer expectation $\mathbb{E}\{.\}$ in (5.33) denotes the statistical expectation taken over all relevant random variables given initial global state $\boldsymbol{s}_1$ and policy π. The inner expectation $\mathbb{E}_T\{.\}$ in (5.33) denotes the expectation with respect to the random variable T. Note that with a different initial global state $\boldsymbol{s}_1$ and a different policy π, a different network action $\boldsymbol{\alpha}_t$ will be selected in time slot t, which results in a different state transition probability $\Pr\left(\boldsymbol{s}_{t+1} | \boldsymbol{s}_t, \boldsymbol{\alpha}_t\right)$ when the outer expectation $\mathbb{E}\{.\}$ in (5.33) is computed. Since T is a geometric random variable with mean $\mathbb{E}\{T\} = 1/(1-\eta)$, (5.33) is equivalent to the objective function of an infinite-horizon MDP with discounted reward given by [55, Proposition 5.3.1]

$$V_\pi(\boldsymbol{s}_1) = \mathbb{E}\left\{ \sum_{t=1}^{\infty} \eta^t r(\boldsymbol{\alpha}_t) | \boldsymbol{s}_1, \pi \right\}, \quad \text{s.t. } \boldsymbol{\alpha}_t \in \bar{\mathcal{U}}_t,\ \sum_{n=1}^{N} \alpha_{n,t}^2 \leq \mathcal{P}_{tot},\ \forall t \tag{5.34}$$

where η in (5.34) can be interpreted as the discount factor of the model and $V_\pi(\boldsymbol{s}_1)$ in (5.34) can be interpreted as the long-term expected network reward starting from an initial global state $\boldsymbol{s}_1$ and continuing with the policy π from then on [55]. Since the network will stop functioning at some time in the future, the network reward at time slot t is discounted by factor η^t. The problem in (5.34) is our discounted infinite-horizon constrained MDP problem. One can easily show that that the objective function $V_\pi(\boldsymbol{s}_1)$ in (5.34) converges to a finite value [55, pp. 121]. The proof follows. First, we note

$$\sup_{\boldsymbol{s}_t \in \bar{\mathcal{S}},\ \boldsymbol{\alpha}_t \in \bar{\mathcal{U}}_t} |r(\boldsymbol{\alpha}_t)| \leq \sup_{\boldsymbol{s}_t \in \bar{\mathcal{S}},\ \boldsymbol{\alpha}_t \in \bar{\mathcal{U}}_t} \sum_{n=1}^{N} |r(\alpha_{n,t})| \tag{5.35}$$

Next, we examine $r(\alpha_{n,t})$ in (5.31) and we note that $\widehat{\zeta}_{n,1}, \{\phi_{n,l}\}_{l=1}^{L}$ are probabilities and $\{\bar{J}_{n,t}^{(l)}\}_{l=1}^{L}$ depend on the two dimensional $\Omega(.,.), \beta_1(.,.), \beta_2(.,.)$ functions, which all take finite values $\forall \boldsymbol{s}_t \in \bar{\mathcal{S}},\ \boldsymbol{\alpha}_t \in \bar{\mathcal{U}}_t$. Hence the right-hand side of (5.35) is finite. This completes the proof. Due to Markovian property of MDP problems, it suffices to consider only *Markovian policies*. Hence, our aim is finding an optimal Markovian policy $\pi \in \Pi$ that maximizes $V_\pi(\boldsymbol{s}_1)$ in (5.34). That is, given the initial global state $\boldsymbol{s}_1$, our goal is to obtain the optimal expected total discounted network reward $V^*(\boldsymbol{s}_1)$ and the optimal Markovian policy $\pi^* \in \Pi$ defined as follows:

$$V^*(\boldsymbol{s}_1) = \max_{\pi \in \Pi}\ V_\pi(\boldsymbol{s}_1), \quad \pi^* = \arg\max_{\pi \in \Pi} V_\pi(\boldsymbol{s}_1), \quad \text{s.t. } \boldsymbol{\alpha}_t \in \bar{\mathcal{U}}_t,\ \sum_{n=1}^{N} \alpha_{n,t}^2 \leq \mathcal{P}_{tot},\ \forall t \tag{5.36}$$

A Markovian policy $\pi = (\delta_1, \delta_2, ...\delta_T)$ is said to be stationary deterministic if $\delta_t = \delta$ for all time slots such that $\pi = (\delta, \delta, \ldots, \delta)$ and δ is deterministic [55, pp. 21]. The existence of a stationary deterministic optimal policy is guaranteed when the network state space $\bar{\mathcal{S}}$ is discrete and finite [55]. Thus, *our objective is to find an optimal stationary deterministic policy* $\pi \in \Pi$ that maximizes $V_\pi(\boldsymbol{s}_1)$ in (5.34).

5.2.1 Finding the Optimal Policy

To maximize $V_\pi(\boldsymbol{s}_1)$ in (5.34), we first utilize the Lagrangian approach [56, 57] to transform the constrained MDP optimization problem into an equivalent unconstrained MDP optimization problem. For each global state $\boldsymbol{s}_t$ we introduce a Lagrangian multiplier $\lambda_{\boldsymbol{s}_t}$ associated with the constraint $\left(\sum_{n=1}^{N} \alpha_{n,t}^2 - \mathcal{P}_{tot}\right)$. We define the Lagrangian value function $\mathcal{L}(\boldsymbol{s}_t, \lambda_{\boldsymbol{s}_t})$

$$\mathcal{L}(\boldsymbol{s}_t, \lambda_{\boldsymbol{s}_t}) = \max_{\pi \in \Pi} \Big\{ \underbrace{L(\boldsymbol{s}_t, \boldsymbol{\alpha}_t, \lambda_{\boldsymbol{s}_t})}_{=\text{ term 1}} + \underbrace{\eta \Big(\Pr(\boldsymbol{\alpha}_t = 0) \sum_{\boldsymbol{s}_{t+1}} \Pr\left(\boldsymbol{s}_{t+1} | \boldsymbol{s}_t, 0\right) \mathcal{L}(\boldsymbol{s}_{t+1}, \lambda_{\boldsymbol{s}_{t+1}}) + \Pr(\boldsymbol{\alpha}_t \neq 0) \sum_{\boldsymbol{s}_{t+1}} \Pr\left(\boldsymbol{s}_{t+1} | \boldsymbol{s}_t, \boldsymbol{\alpha}_t\right) \mathcal{L}(\boldsymbol{s}_{t+1}, \lambda_{\boldsymbol{s}_{t+1}}) \Big)}_{=\text{ term 2}} \Big\}. \quad (5.39)$$

---

using the dynamic programming [57]

$$\mathcal{L}(\boldsymbol{s}_t, \lambda_{\boldsymbol{s}_t}) = \max_{\pi \in \Pi} \Big\{ \underbrace{L(\boldsymbol{s}_t, \boldsymbol{\alpha}_t, \lambda_{\boldsymbol{s}_t})}_{=\text{ term 1}} + \underbrace{\eta \sum_{\boldsymbol{s}_{t+1}} \Pr\left(\boldsymbol{s}_{t+1} | \boldsymbol{s}_t, \boldsymbol{\alpha}_t\right) \mathcal{L}(\boldsymbol{s}_{t+1}, \lambda_{\boldsymbol{s}_{t+1}})}_{=\text{ term 2}} \Big\}, \quad (5.37)$$

where $L(\boldsymbol{s}_t, \boldsymbol{\alpha}_t, \lambda_{\boldsymbol{s}_t})$ is defined as

$$L(\boldsymbol{s}_t, \boldsymbol{\alpha}_t, \lambda_{\boldsymbol{s}_t}) = r(\boldsymbol{\alpha}_t) - \lambda_{\boldsymbol{s}_t} \left(\sum_{n=1}^{N} \alpha_{n,t}^2 - \mathcal{P}_{tot} \right). \quad (5.38)$$

In fact, $L(\boldsymbol{s}_t, \boldsymbol{\alpha}_t, \lambda_{\boldsymbol{s}_t})$ in (5.38) can be interpreted as the modified network reward function at time slot t, where the cost of violating the constraint is subtracted from the immediate reward $r(\boldsymbol{\alpha}_t)$ earned in time slot t. On the other hand, term 2 in $\mathcal{L}(\boldsymbol{s}_t, \lambda_{\boldsymbol{s}_t})$ is the expected total discounted future network reward if network action $\boldsymbol{\alpha}_t$ is chosen. Since $\boldsymbol{\alpha}_t$ can be zero or non-zero, term 2 can be expanded as (5.39). Note that $\boldsymbol{\alpha}_t = 0$ only if $\alpha_{n,t} = 0, \forall n$, i.e., when LLR is below the local threshold $\theta_n, \forall n$. Using (5.3) we find $\Pr(\boldsymbol{\alpha}_t = 0) = \prod_{n=1}^{N} \Pr(\alpha_{n,t} = 0) = \prod_{n=1}^{N} \widehat{\zeta}_{n,0}$ and $\Pr(\boldsymbol{\alpha}_t \neq 0) = 1 - \Pr(\boldsymbol{\alpha}_t = 0)$. With fixed $\lambda_{\boldsymbol{s}_t}$, the constrained MDP problem in (5.34) can be viewed as a non-constrained MDP problem in (5.39) with the modified network reward function $L(\boldsymbol{s}_t, \boldsymbol{\alpha}_t, \lambda_{\boldsymbol{s}_t})$ at time slot t given in (5.38). Let $U(\lambda_{\boldsymbol{s}_t})$ denote the Lagrangian dual function, where

$$U(\lambda_{\boldsymbol{s}_t}) = \max_{\pi} \mathcal{L}(\boldsymbol{s}_t, \lambda_{\boldsymbol{s}_t}) \quad (5.40)$$

Then the Lagrangian dual problem can be written as

$$\min_{\lambda_{\boldsymbol{s}_t} \geq 0} U(\lambda_{\boldsymbol{s}_t}) \tag{5.41}$$

The resulting dual solution has zero duality gap compared to the primary problem in (5.37) [57, pp.2]. To solve the dual problem in (5.41), we iteratively solve the following two sub-problems until a pre-specified convergence criterion is reached. The outer minimization sub-problem (the outer loop in Algorithm 3 with iteration index i) updates $\lambda^i_{\boldsymbol{s}_t}$. The inner maximization sub-problem (the inner loop in Algorithm 3 with iteration index j) finds the optimal π_i given $\lambda^i_{\boldsymbol{s}_t}$. The pseudo code of the algorithm is given in Algorithm 3.

1. **the inner maximization sub-problem:** Given $\lambda^i_{\boldsymbol{s}_t}$ we adopt the value iteration algorithm [58] to find the optimal policy π_i. The convergence criterion is $|\mathcal{L}^j(\boldsymbol{s}_t, \lambda^i_{\boldsymbol{s}_t}) - \mathcal{L}^{j-1}(\boldsymbol{s}_t, \lambda^i_{\boldsymbol{s}_t})| < \epsilon_1(1-\eta)/2\eta$, for a given ϵ_1, where $\mathcal{L}^j(\boldsymbol{s}_t, \lambda^i_{\boldsymbol{s}_t})$ indicates the long-term expected reward in the j-th iteration from (5.39).

2. **the outer minimization sub-problem:** The outer minimization over the Lagrangian multiplier $\lambda_{\boldsymbol{s}_t}$ is a linear programming problem. We use the sub-gradient method to update $\lambda^i_{\boldsymbol{s}_t}$ as the following.

$$\lambda^{i+1}_{\boldsymbol{s}_t} = \left[\lambda^i_{\boldsymbol{s}_t} + \beta^i \left(\sum_{n=1}^{N} \alpha^2_{n,t} - \mathcal{P}_{tot} \right) \right]^+, \tag{5.42}$$

   where β is a positive scalar step size satisfying the conditions $\sum_{i=1}^{\infty} \beta^i = \infty$ and $\sum_{i=1}^{\infty} (\beta^i)^2 < \infty$. The update rule is such that if $\sum_{n=1}^{N} \alpha^2_{n,t}$ is larger (smaller) than $\mathcal{P}_{tot}$ then $\lambda_{\boldsymbol{s}_t}$ should increase (decrease). Unless the convergence criterion $\frac{|\lambda^{i+1}_{\boldsymbol{s}_t} - \lambda^i_{\boldsymbol{s}_t}|}{\lambda^i_{\boldsymbol{s}_t}} < \epsilon_2$ is met, for a given ϵ_2, we increase i and solve the inner maximization sub-problem again.

Algorithm 3: optimal power control algorithm

1: Specify $\epsilon_1 > 0$, $\epsilon_2 > 0$ set $\mathcal{L}(\boldsymbol{s}_1, \lambda_{\boldsymbol{s}_1}) = 0,\ \boldsymbol{s}_t \in \bar{\mathcal{S}}$ set $i = 1$;

2: **for** fixed $\lambda^i_{\boldsymbol{s}_t}$ **do**

  3: Set $j = 1$, **for** each $\boldsymbol{s}_t \in \bar{\mathcal{S}}$ **do**

    for each $\boldsymbol{\alpha}_t \in \mathcal{U}_{\boldsymbol{s}_t}$ **do**

      calculate

$$\mathcal{F}(\boldsymbol{s}_t, \boldsymbol{\alpha}_t, \lambda^i_{\boldsymbol{s}_t}) = L(\boldsymbol{s}_t, \boldsymbol{\alpha}_t, \lambda^i_{\boldsymbol{s}_t}) + \eta \sum_{\boldsymbol{s}_{t+1}} \Pr\left(\boldsymbol{s}_{t+1} | \boldsymbol{s}_t, \boldsymbol{\alpha}_t\right) \mathcal{L}^{j-1}(\boldsymbol{s}_{t+1}, \lambda^i_{\boldsymbol{s}_{t+1}})$$

    end

    calculate $\mathcal{L}^j(\boldsymbol{s}_t, \lambda^i_{\boldsymbol{s}_t}) = \max_{\pi_i \in \Pi} \{\mathcal{F}(\boldsymbol{s}_t, \boldsymbol{\alpha}_t, \lambda^i_{\boldsymbol{s}_t})\}$;

  end

  4: If $\max_{\boldsymbol{s}_t \in \bar{\mathcal{S}}} |\mathcal{L}^j(\boldsymbol{s}_t, \lambda^i_{\boldsymbol{s}_t}) - \mathcal{L}^{j-1}(\boldsymbol{s}_t, \lambda^i_{\boldsymbol{s}_t})| < \epsilon_1(1-\eta)/2\eta$,

  go to Step 5. Otherwise, increase j and go back to Step 3.

  5: We obtain the optimal policy

$$\pi^*_i = \arg \max_{\pi_i \in \Pi} \left\{ \mathcal{L}^j(\boldsymbol{s}_t, \lambda^i_{\boldsymbol{s}_t}) \right\}.$$

end

6: Update $\lambda^i_{\boldsymbol{s}_t}$ using the rule in (5.42) and π^*_i;

7: If $\frac{|\lambda^{i+1}_{\boldsymbol{s}_t} - \lambda^i_{\boldsymbol{s}_t}|}{\lambda^i_{\boldsymbol{s}_t}} < \epsilon_2$. then $\pi^* = \pi^*_i$. Otherwise, increase i and go back to Step 2.

Note that the above sub-gradient method is guaranteed to converge to the optimum $\lambda_{\boldsymbol{s}_t}$, as long as β satisfies the conditions stated above, due to the convexity of the dual problem (5.41) over $\lambda_{\boldsymbol{s}_t}$.

Remark on the computational complexity of Algorithm 3: We switch between solving two sub-problems until the convergence criterion for updating the Lagrangian multiplier is met. Given $\lambda_{\boldsymbol{s}_t}$ we solve the inner maximization sub-problem, i.e., we solve (5.39) for each $\boldsymbol{s}_t \in \bar{\mathcal{S}}$ (refer to Step 3 of Algorithm 3), where $|\bar{\mathcal{S}}| = |\mathcal{S}|^N$. Our numerical results show that the computational complexity of calculating π^*_i (Step 5 of Algorithm 3) is $\mathcal{O}(|\mathcal{S}|^N K^{1.2N})$. On the other hand, the complexity order of the gradient-descent algorithm to find the local minimum of function $U(\lambda_{\boldsymbol{s}_t})$ and converge to an ϵ_2-accurate solution is $\bar{\epsilon} = 1/\epsilon_2$ [59, p. 232]. Hence, the overall the computational complexity of finding the optimal solution using Algorithm 3 is $\mathcal{O}(\bar{\epsilon}|\mathcal{S}|^N K^{1.2N})$. Note that the complexity order scales *exponentially* in N.

Remark on implementing the optimal policy: The optimal policy, a.k.a. centralized solution in the dynamic control literature, requires the knowledge of the global state $\boldsymbol{s}_t$ to determine the network action $\boldsymbol{\alpha}_t = \delta(\boldsymbol{s}_t)$. This implies that sensor n in the network cannot find its local action $\alpha_{n,t}$ at time slot t, unless it knows the global state $\boldsymbol{s}_t$. Hence, implementing this solution requires all N sensors to report their local states $s_{n,t}, \forall n$ to the FC. The FC concatenates all the received local states and forms the global state $\boldsymbol{s}_t$. Then based on $\boldsymbol{s}_t$, the FC determines and broadcasts the network action $\boldsymbol{\alpha}_t$. This process, however, consumes significant signaling overhead.

To reduce the signaling overhead, we consider finding a sub-optimal policy, a.k.a. decentralized solution in the literature, where sensor n in the network finds its local action $\alpha_{n,t}$ at time slot t, only based on its own local state $s_{n,t}$.

5.2.2 Finding the Sub-Optimal Policy

Let δ' denote a deterministic decision rule that describes how a local action $\alpha_{n,t}$ is selected according to the local state $s_{n,t}$ in time slot t, i.e., $\alpha_{n,t} = \delta'(s_{n,t})$, and $\omega = (\delta', \delta', ..., \delta')$ is the corresponding stationary deterministic policy for $t = 1, ..., T$ [55, pp.21].

We say that a policy ω is feasible if it satisfies the two constraints: (i) $\alpha_{n,t} \in \mathcal{U}_{n,t},\ \forall t, n$, (ii) $\sum_{n=1}^{N} \alpha_{n,t}^2 \leq \mathcal{P}_{tot},\ \forall t$. Let Ω be the set of feasible policies ω. Our objective is to find a stationary deterministic policy $\omega \in \Omega$ that maximizes $V_\omega(\boldsymbol{s}_1)$ in (5.43). We refer to this solution as the sub-optimal policy.

$$V_\omega(\boldsymbol{s}_1) = \mathbb{E}\left\{ \sum_{t=1}^{\infty} \eta^t \sum_{n=1}^{N} r\big(\alpha_{n,t}\big) | \boldsymbol{s}_1, \pi \right\}, \quad \text{s.t. } \alpha_{n,t} \in \mathcal{U}_{n,t},\ \forall t, n,\ \sum_{n=1}^{N} \alpha_{n,t}^2 \leq \mathcal{P}_{tot},\ \forall t \tag{5.43}$$

We note that maximizing $V_\omega(\boldsymbol{s}_1)$ in (5.43) with respect to ω is significantly simpler than

maximizing $V_\pi(\boldsymbol{s}_1)$ in (5.34) with respect to π, i.e., finding the sub-optimal policy is much easier than finding the optimal policy. This is due to the fact that, when the local action $\alpha_{n,t}$ is selected according to the local state $s_{n,t}$ only in time slot t, the global state transition probability $\Pr\left(\boldsymbol{s}_{t+1}|\boldsymbol{s}_t,\boldsymbol{\alpha}_t\right)$ in (5.7) can be completely decomposed across sensors. In other words, we have

$$\begin{aligned}\Pr\left(\boldsymbol{s}_{t+1}|\boldsymbol{s}_t,\boldsymbol{\alpha}_t\right)&=\prod_{n=1}^{N}\Pr\left(s_{n,t+1}|s_{n,t},\alpha_{n,t}\right)\\&=\prod_{n=1}^{N}\Pr\big(b_{n,t+1}|b_{n,t},\bar{g}_{n,t},e_{n,t},\alpha_{n,t}\big)\Pr(e_{n,t}|e_{n,t-1})\Pr(\bar{g}_{n,t}|\bar{g}_{n,t-1}).\end{aligned}$$

where

$$\Pr\left(b_{n,t+1}|b_{n,t},\bar{g}_{n,t},e_{n,t},\alpha_{n,t}\right)=\begin{cases}1 & \text{if (5.9) is satisfied}\\ 0 & \text{otherwise,}\end{cases}$$

The decomposition of the global state transition probability into the product of the local state transition probabilities directly impacts how the outer expectation $\mathbb{E}\{.\}$ in (5.43) is computed and allows the objective function in (5.43) to be decoupled across sensors. If there were no total transmit power constraint in (5.43), the MDP problem in (5.43) would have become completely decoupled across sensors. The challenge imposed by the total transmit power constraint can be addressed via adopting a uniform Lagrangian multiplier. Similar to [57] we let a uniform Lagrangian multiplier $\lambda_{\boldsymbol{s}_t}=\lambda,\forall\boldsymbol{s}_t$ be associated with the constraint $\left(\sum_{n=1}^{N}\alpha_{n,t}^2-\mathcal{P}_{tot}\right)$. This uniform Lagrangian multiplier allows us to decouple the MDP problem in (5.43) across sensors and reduces solving (5.43) into solving N smaller MDP problems. While the computational complexity of finding the optimal policy scales exponentially in N, we will show that the computational complexity of finding the sub-optimal policy scales *linearly* in N.

$$\mathcal{X}(s_{n,t},\lambda)=\max_{\omega\in\Omega}\Big\{\underbrace{X(s_{n,t},\alpha_{n,t},\lambda)}_{=\text{ term 1}}+\underbrace{\eta\big(\Pr(\alpha_{n,t}=0)\sum_{s_{n,t+1}}\Pr\big(s_{n,t+1}|s_{n,t},0\big)\mathcal{X}(s_{n,t+1},\lambda)+\Pr(\alpha_{n,t}\neq 0)\sum_{s_{n,t+1}}\Pr\big(s_{n,t+1}|s_{n,t},\alpha_{n,t}\big)\mathcal{X}(s_{n,t+1},\lambda)\big)}_{=\text{ term 2}}\Big\},\quad(5.46)$$

We define the Lagrangian value function $\mathcal{X}(s_{n,t},\lambda)$ using the dynamic programming

$$\mathcal{X}(s_{n,t},\lambda)=\max_{\omega\in\Omega}\Big\{\underbrace{X(s_{n,t},\alpha_{n,t},\lambda)}_{=\text{ term 1}}+\underbrace{\eta\sum_{s_{n,t+1}}\Pr\big(s_{n,t+1}|s_{n,t},\alpha_{n,t}\big)\mathcal{X}(s_{n,t+1},\lambda)}_{=\text{ term 2}}\Big\},\qquad(5.44)$$

where the modified reward function $X(s_{n,t},\alpha_{n,t},\lambda)$ is defined as

$$X(s_{n,t},\alpha_{n,t},\lambda)=r\big(\alpha_{n,t}\big)-\lambda\left(\alpha_{n,t}^2-\frac{\mathcal{P}_{tot}}{N}\right)\qquad(5.45)$$

With fixed λ, the constrained MDP problem in (5.43) can be viewed as N non-constrained MDP problems in (5.46) with the modified network reward function $X(s_{n,t},\alpha_{n,t},\lambda)$ at time slot t given in (5.45). Let $\widehat{U}(\lambda)$ denote the Lagrangian dual function, where

$$\widehat{U}(\lambda)=\max_{\omega\in\Omega}\mathcal{X}(s_{n,t},\lambda)\qquad(5.47)$$

Then the Lagrangian dual problem can be written as

$$\min_{\lambda\geq 0}\widehat{U}(\lambda)\qquad(5.48)$$

To solve the dual problem in (5.48), we iteratively solve the following two sub-problems until a pre-specified convergence criterion is reached. The outer minimization sub-problem updates λ^i. The inner maximization sub-problem finds the optimal ω_i given λ^i. The pseudo code of the algorithm is given in Algorithm 4.

1. **the inner maximization problem:** Given λ^i we adopt the value iteration algo-

rithm [58] to find the optimal policy ω_i. The convergence criterion is $|\mathcal{X}^j(s_{n,t},\lambda) - \mathcal{X}^{j-1}(s_{n,t},\lambda)| < \epsilon_1(1-\eta)/2\eta$, for a given ϵ_1, where $\mathcal{X}^j(s_{n,t},\lambda)$ indicates the long-term expected reward in the j-th iteration from (5.46).

2. **the outer minimization problem:**

   The outer minimization over the Lagrangian multiplier λ is a linear programming problem. We use the sub-gradient method to update λ^i as the following

$$\lambda^{i+1} = \left[\lambda^i + \beta^i \left(\sum_{n=1}^{N} \alpha_{n,t}^2 - \mathcal{P}_{tot}\right)\right]^+, \tag{5.49}$$

   where β is a positive scalar step size satisfying the conditions $\sum_{i=1}^{\infty} \beta^i = \infty$ and $\sum_{i=1}^{\infty} (\beta^i)^2 < \infty$. The update rule is such that if $\sum_{n=1}^{N} \alpha_{n,t}^2$ is larger (smaller) than $\mathcal{P}_{tot}$ then λ should increase (decrease). Unless the convergence criterion $\frac{|\lambda^{i+1}-\lambda^i|}{\lambda^i} < \epsilon_2$ is met, for a given ϵ_2, we increase i and solve the inner maximization sub-problem again.

Note that the above sub-gradient method is guaranteed to converge to the optimum λ, as long as β satisfies the conditions stated above.

Remark on the computational complexity of Algorithm 4: We switch between solving two sub-problems until the convergence criterion for updating the Lagrangian multiplier is met. Given λ we solve the inner maximization sub-problem, i.e., we solve (5.46) for each $s_{n,t} \in \mathcal{S}$ (refer to Step 3 of Algorithm 4), where the dimension of $\mathcal{S}$, denoted as $|\mathcal{S}|$. Our numerical results show that the computational complexity of calculating ω_i^* (Step 5 of Algorithm 4) is $\mathcal{O}(|\mathcal{S}|K^{1.5})$. On the other hand, the complexity order of the gradient-descent algorithm to find the local minimum of function $\widehat{U}(\lambda)$ and converge to an ϵ_2-accurate solution is $\bar{\epsilon} = 1/\epsilon_2$ [59, p. 232]. Hence, the overall the computational complexity of finding the

Algorithm 4: sub-optimal power control algorithm

1: Specify $\epsilon_1 > 0$, $\epsilon_2 > 0$ set $\mathcal{X}(s_{n,0}, \lambda) = 0,\ s_{n,t} \in \mathcal{S}$ set $i = 1$;
2: **for** fixed λ^i **do**
  3: Set $j = 1$, **for** each sensor **do**
    for each $\alpha_{n,t} \in \mathcal{U}_{s_{n,t}}$ **do**
      calculate

$$\mathcal{F}(s_{n,t}, \alpha_{n,t}, \lambda^i) = X(s_{n,t}, \alpha_{n,t}\lambda) + \eta\Big(\sum_{s_{t+1}} \Pr(s_{n,t+1}|s_{n,t}, \alpha_{n,t})\mathcal{X}^{j-1}(s_{n,t+1}, \lambda^i)\Big)$$

    end
    calculate

$$\mathcal{X}^j(s_{n,t}, \lambda^i) = \max_{\omega_i \in \Omega}\{\mathcal{F}(s_{n,t}, \alpha_{n,t}, \lambda^i)\}$$

  end
  4: If

$$\max_{s_{n,t} \in \mathcal{S}} |\mathcal{X}^j(s_{n,t}, \lambda^i) - \mathcal{X}^{j-1}(s_{n,t}, \lambda^i)| < \epsilon_1(1-\eta)/2\eta$$

  go to step 5. Otherwise, increase j and go back to Step 3.
  5: We obtain policy

$$\omega_i^* = \arg\max_{\omega_i \in \Omega} \Big\{\mathcal{X}^j(s_{n,t})\Big\}.$$

end
6: Update λ^i by using (5.49) and ω_i^*;
7: If $\frac{|\lambda^{i+1} - \lambda^i|}{\lambda^i} < \epsilon_2$ then $\omega = \omega_i^*$. Otherwise, increase i and go back to Step 2.

optimal solution using Algorithm 4 is $\mathcal{O}(N|\mathcal{S}|\bar{\epsilon}K^{1.5})$. Note that the complexity order scales *linearly* in N.

Remark on implementing the sub-optimal policy: The sub-optimal policy, a.k.a. decentralized solution in the dynamic control literature, requires the knowledge of the local state $s_{n,t}$ only to determine the local action $\alpha_{n,t} = \delta'(s_{n,t}), \forall n$. This implies that sensor n in the network can find its local action $a_{n,t}$ at time slot t with the knowledge of its local state $s_{n,t}$. Hence, implementing this solution, different from the optimal solution, does not require sensors to report to the FC and does not impose signaling overhead to the sensors.

5.3 Effect of random deployment of sensors

Our signal model in (5.1) is a widely adopted model in the literature of signal (target) detection [17, 18, 60], in which the signal source is typically modeled as an isotropic radiator and the emitted power of the signal source at a reference distance d_0 is known [61]. Suppose P_0 is the emitted power of the signal source at the reference distance d_0, and d_n is the Euclidean distance between the source and sensor n. For a general intensity decay model, the signal intensity at sensor n, denoted as $z_{n,t}$, is [61]

$$z_{n,t} = \frac{P_0}{(d_n/d_0)^\gamma}, \tag{5.50}$$

where γ is the path-loss exponent, e.g., for free-space wave propagation $\gamma = 2$. With this model, the problem of noisy signal detection is equivalent to the following binary hypothesis testing problem

$$H_t = 1 : x_{n,t} = z_{n,t} + v_{n,t}, \qquad H_t = 0 : x_{n,t} = v_{n,t}, \tag{5.51}$$

in which $z_{n,t}$ and variance of $v_{n,t}$, denoted as $\sigma^2_{v_n}$, are assumed to be known [18], [17], [60]. Note that the binary hypothesis testing problem in (5.51) can be recast as the problem in (5.1), by scaling the sensor observation $x_{n,t}$ with $(d_n/d_0)^\gamma$. This signal model applies to an arbitrary, but fixed (given) deployment of sensors. For applications where the sensors are deployed randomly in a field, the sensors' locations are not known a prior. This implies that $\mathcal{A}$ in (5.1) is unknown, and consequently, P_{f_n} in (5.4) cannot be determined before deployment. To expand our optimization method beyond fixed deployment of sensors, we assume that sensors are randomly deployed in a circle field, the signal source is located at the center of this field, and it is at least r_0 meters away from any sensor within the field. Let $r_{n,t}$ be the distance of sensor n from the center. We assume $r_{n,t}$ is uniformly distributed

in the interval (r_0, r_1), i.e.,

$$f(r_{n,t}) = \begin{cases} \frac{1}{r_1 - r_0}, & r_0 < r_{n,t} \leq r_1, \\ 0, & \text{o.w.} \end{cases} \tag{5.52}$$

Suppose the emitted power of the signal source at radius r_0 is P_0. Then the signal intensity at sensor n is $z_{n,t} = \frac{P_0}{(r_{n,t}/r_0)^2}$. Given the pdf of $r_{n,t}$ in (5.52), we obtain the pdf of $z_{n,t}$ as follows

$$f(z_{n,t}) = \begin{cases} \frac{\sqrt{P_0}}{2z_{n,t}\sqrt{z_{n,t}}(r_1 - r_0)}, & \frac{P_0}{r_1^2} < z_{n,t} \leq \frac{P_0}{r_0^2}, \\ 0, & \text{o.w.} \end{cases} \tag{5.53}$$

Based on the pdf of $z_{n,t}$ in (5.53) we can recompute P_{f_n} in (5.4)

$$P_{\mathrm{f}_n} = \int_{\frac{P_0}{r_1^2}}^{\frac{P_0}{r_0^2}} \left[Q\Big(\frac{\theta_n + \frac{z_{n,t}^2}{2\sigma_{v_n}^2}}{\sqrt{z_{n,t}^2/\sigma_{v_n}^2}} \Big) \right] f(z_{n,t}) dz_{n,t}, \;\; P_{\mathrm{d}_n} = \int_{\frac{P_0}{r_1^2}}^{\frac{P_0}{r_0^2}} \left[Q\Big(\frac{\theta_n - \frac{z_{n,t}^2}{2\sigma_{v_n}^2}}{\sqrt{z_{n,t}^2/\sigma_{v_n}^2}} \Big) \right] f(z_{n,t}) dz_{n,t}, \tag{5.54}$$

$$P_{\mathrm{f}_n} = \int_{\frac{P_0}{r_1^2}}^{\frac{P_0}{r_0^2}} Q\left(Q^{-1}(\overline{P}_{\mathrm{d}}) + \sqrt{z_{n,t}^2/\sigma_{v_n}^2} \right) f(z_{n,t}) dz_{n,t}. \tag{5.55}$$

With random deployment of sensors, problem (P1) is still valid, with the difference that, for $J_{n,t}$ in (3.27), P_{f_n} expression should be replaced with the ones in (5.54)-(5.55).

5.4 simulation Results

We corroborate our analysis with MATLAB simulations and investigate: (i) the effect of policy (optimal versus sub-optimal) on transmit powers of sensors, (ii) the achievable J-divergence when we adopt the optimal, and sub-optimal, and random policies to set transmit

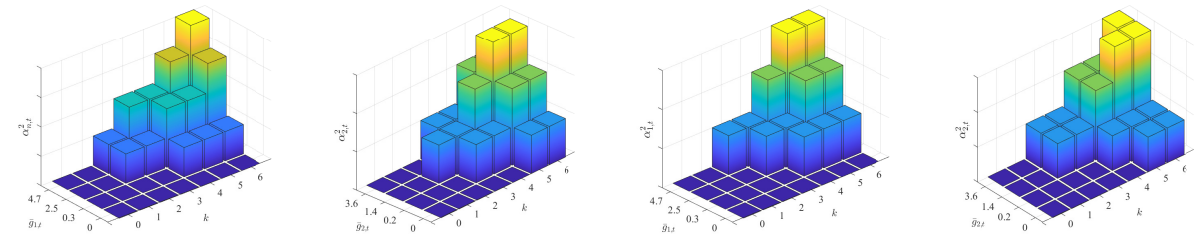

(a) Optimal policy, sensor 1 (b) Optimal policy, sensor 2 (c) Sub-optimal policy, sensor1 (d) Sub-optimal policy, sensor 2

Figure 5.5: Transmit powers $(\alpha_{1,t}^2, \alpha_{2,t}^2)$ in optimal and sub-optimal policies for $N=2$, $\text{SNR}_s=3\text{dB}, \mathcal{P}_{tot}=5\text{mW}, K=6, b_u=0.5\text{mJ}, (\gamma_{g_1}, \gamma_{g_2})=(1,1.5), f_D T_s=0.04, L=4, \bar{\mathcal{G}}_1=\{0,0.3,2.5,4.7\}, \bar{\mathcal{G}}_2=\{0,0.2,1.4,3.6\}$, $(\rho_1,\rho_2)=(0.4,0.5), (e_{1,t}, e_{2,t})=(2b_u, 2b_u)$.

powers of sensors, (iii) error probability P_e when we adopt the optimal and sub-optimal policies to set transmit powers of sensors, and the trade-off between P_e and consumed transmit power, (iv) the behavior of P_e as different system parameters vary, (v) the effect of random deployment of sensors on P_e. In all our simulations, we let $\sigma_{w_n}^2=\sigma_w^2=1, \forall n$ and $P_{d_n}=P_d, \forall n$. Also, $\gamma_{g_n}^2=\gamma_g^2, \forall n$ except for Fig. 4.5. We let $P_d=0.9$ except for Fig. 3.4, the discount factor $\eta=0.9$ except for Fig. 3.7, and $f_D T_s=0.05$ except for Fig. 3.4. We assume the Gaussian observation noise variance $\sigma_{v_n}^2=\sigma_v^2, \forall n$ and we define the SNR corresponding to observation channel as $\text{SNR}_s=20\log(\mathcal{A}/\sigma_v)$. We adopt a solar-power energy harvesting model similar to [48], in which the harvesting condition is classified to $M=4$ states as "Poor", "Fair", "Good", and "Excellent". We assume $\mathcal{E}=\{0, 2b_u, 4b_u, 6b_u\}$ and the transition probability matrix $\Phi_{\mathcal{E}}$ is characterized in terms of an energy harvesting parameter ρ as the following

$$\Phi_{\mathcal{E}}=\begin{pmatrix} \rho & 1-\rho & 0 & 0 \\ \frac{1-\rho}{2} & \rho & \frac{1-\rho}{2} & 0 \\ 0 & \frac{1-\rho}{2} & \rho & \frac{1-\rho}{2} \\ 0 & 0 & 1-\rho & \rho \end{pmatrix}.$$

We let $\rho=0.5$ except for Figs. 5.5 and 5.14. Our battery-related parameters are (K, b_u). Our system setup is based on a given set of L channel gain quantization thresholds $\bar{\mathcal{G}}=\{\mu_1, \mu_2, ..., \mu_L\}$. To explore the effect of quantization thresholds we consider two different

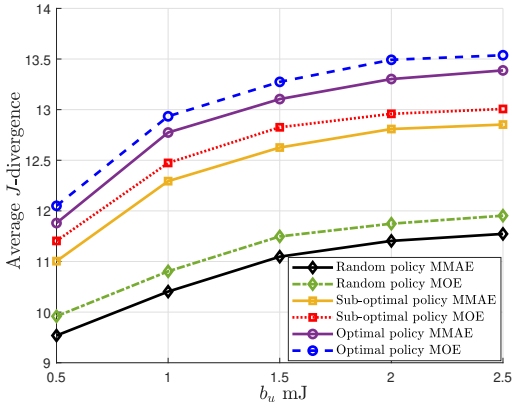

Figure 5.6: The average J-divergence versus b_u for $K=5, N=3, \mathcal{P}_{tot}=5\text{mW}, \gamma_g=2, L=3$, $\text{SNR}_s=3\text{dB}$.

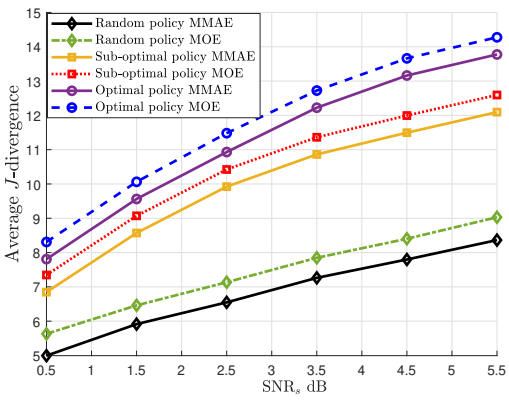

Figure 5.7: The average J-divergence versus SNR_s dB for $K=5,\ N=3, \mathcal{P}_{tot}=5\text{mW}, b_u=1\text{mJ}, \gamma_g=2, L=3$.

objective functions to obtain the quantization thresholds $\{\mu_l\}_{l=1}^{L}$.

• *Finding* $\{\mu_l\}_{l=1}^{L}$ *via Minimizing Mean Absolute Error (MMAE)*: We consider mean of absolute quantization error (MAE), denoted as $\mathbb{E}\{|g_{n,t}-\bar{g}_{n,t}|\}$, as the objective function

$$\mathbb{E}\{|g_{n,t}-\bar{g}_{n,t}|\}=\sum_{l=0}^{L-1}\int_{\mu_l}^{\mu_{l+1}}(x-\mu_l)f_{g_{n,t}}(x)dx. \tag{5.56}$$

To find $\{\mu_l\}_{l=1}^{L}$ that minimize MAE, we take the derivative of MAE with respect to μ_l and set the derivative equal to zero.

• *Finding* $\{\mu_l\}_{l=1}^{L}$ *via Maximizing output Entropy (MOE)*: We consider the mutual information between $g_{n,t}$ and $\bar{g}_{n,t}$, denoted as $I(g_{n,t};\bar{g}_{n,t})$, as the objective function, where $I(g_n;\bar{g}_{n,t})=H(\bar{g}_{n,t})-H(\bar{g}_{n,t}|g_{n,t})$, and $H(x)$ denotes the entropy of discrete random variable x. To find $\{\mu_l\}_{l=1}^{L}$ that maximize $I(g_{n,t};\bar{g}_{n,t})$, we note that $H(\bar{g}_{n,t}|g_{n,t})$ is zero, since given $g_{n,t}$, $\bar{g}_{n,t}$ is known. Furthermore, $H(\bar{g}_{n,t})$ is maximized when $\bar{g}_{n,t}$ follows a uniform distribution, i.e., we set $\phi_{n,l}=\Pr(\bar{g}_{n,t}=\mu_l)=\Pr(\mu_l\leq g_{n,t}<\mu_{l+1})=\frac{1}{L+1}$, and the threshold μ_l can be obtained as $\mu_l=\left(-\gamma_{g_n}\ln\left(1-\frac{l-1}{L+1}\right)\right)^{\frac{1}{2}}$.

Overall, our channel-related parameters are $(\gamma_{g_n}, f_D T_s, L, \bar{\mathcal{G}})$, where $\bar{\mathcal{G}}$ depends on (γ_{g_n}, L) and the choice of objective function to obtain the quantization thresholds. The state probabilities and the entries of the transition probability matrix $\Psi_{\bar{\mathcal{G}}}^{(n)}$ can be obtained via (5.5)-(5.6) given $(\gamma_{g_n}, f_D T_s, L, \bar{\mathcal{G}})$.

• **Effect of policy on transmit powers of sensors**: To show how transmit power $\alpha_{n,t}^2$ of sensor n changes based on the adopted policy, we consider $N = 2$ sensors. Recall for the sub-optimal policy $\alpha_{n,t}$ depends on the local state $s_{n,t} = (b_{n,t}, \bar{g}_{n,t-1}, e_{n,t-1})$, whereas for the optimal policy the local action $\alpha_{n,t}$ depends on the global state $\boldsymbol{s}_t = (s_{1,t}, s_{2,t})$. We use Algorithm 3 and Algorithm 4, to find and set transmit power $\alpha_{n,t}^2$ corresponding to the optimal and the sub-optimal policies, respectively. Fig. 4.5 illustrates $(\alpha_{1,t}^2, \alpha_{2,t}^2)$ when optimal and sub-optimal policies are adopted, given a set of energy harvesting, battery-related, and channel-related parameters, and assuming the quantization thresholds are obtained via MMAE. To enable the illustration, we assume the state of energy harvesting for both sensors is "Fair", i.e., $(e_{1,t-1}, e_{2,t-1}) = (2b_u, 2b_u)$, and the states of battery $(b_{1,t}, b_{2,t})$ and the states of quantized channel gains $(\bar{g}_{1,t-1}, \bar{g}_{2,t-1})$ are variable. For example, this figure shows that when the local states are $s_{1,t} = (7, 3, 2)$, $s_{2,t} = (7, 3, 2)$, then transmit powers of sensors corresponding to the optimal policy is $(\alpha_{1,t}, \alpha_{2,t}) = (1.5\text{mW}, 2\text{mW})$, whereas transmit powers of sensors corresponding to the sub-optimal policy is $(\alpha_{1,t}, \alpha_{2,t}) = (1\text{mW}, 3\text{mW})$. The Achievable J_{tot} corresponding to optimal and sub-optimal policies are 11.58 and 10.43, respectively. These figures also show that, $\alpha_{n,t}^2(b_{n,t}, \bar{g}_{n,t-1}, e_{n,t-1})$ is monotonically increasing in $b_{n,t}$, given $\bar{g}_{n,t-1}$ and $e_{n,t-1}$.

• **Achievable J-divergence corresponding to optimal, sub-optimal, and random policies**: Fig. 5.6 and Fig. 5.7 show average J-divergence versus b_u and SNR_s respectfully. To plot the curves we set transmit power $\alpha_{n,t}^2$ corresponding to the optimal, the sub-optimal, and random policies, and then we average $J_{tot,t} = \sum_{n=1}^{N} J_{n,t}$ over 10^4 independent Monte Carlo

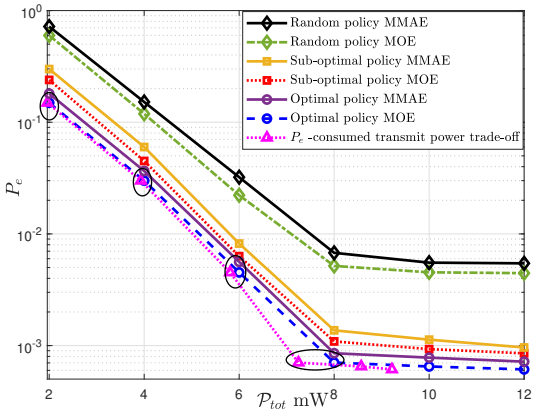

Figure 5.8: P_e versus $\mathcal{P}_{tot}$ for $K=5$, $N=3$, $b_u=$ 1mJ, $\gamma_g=2$, $L=3$, $\text{SNR}_s=3$dB.

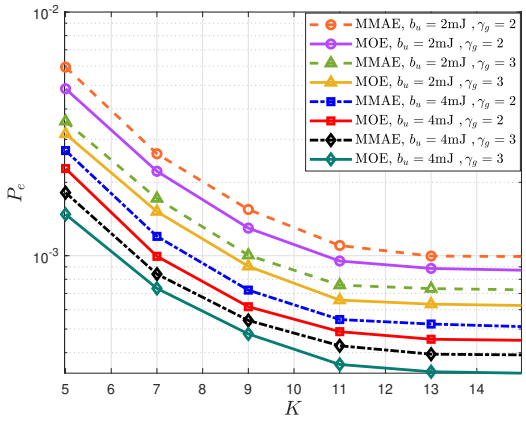

Figure 5.9: P_e vs. K for $N=10, \mathcal{P}_{tot}=15$mW, $L=4$, $\text{SNR}_s=5$dB.

runs. For random policy, we randomly choose $\alpha_{n,t}^2$ such that the two constraints in (5.33) are satisfied, i.e., (i) $\alpha_{n,t}^2 T_s/b_u \leq b_{n,t},\ \forall t,n$, (ii) $\sum_{n=1}^{N}\alpha_{n,t}^2 \leq \mathcal{P}_{tot},\ \forall t$. Fig. 5.6 illustrates that, given a K value, the average J-divergence increases in b_u, however, it remains almost the same after b_u reaches and exceeds a certain value. This is due to the fact that, for larger b_u values transmit power is not limited by energy harvesting and stored energy. Instead, it is limited by the communication channel noise variance σ_w^2. Fig. 5.7 shows that the average J-divergence increases in SNR_s. This is due to the fact that as SNR_s increases, $P_{f_n}=P_f, \forall n$ in (5.4) decreases (given a P_d value). Decreasing P_f leads into increasing the average J-divergence, where P_f and $J_{n,t}$ are related through (5.20) and (5.21). In both figures, average J-divergence achieved by the sub-optimal policy is smaller than average J-divergence achieved by the optimal policy, and larger than average J-divergence achieved by the random policy.

• **P_e corresponding to optimal and sub-optimal policies, and P_e-consumed transmit power trade-off**: Fig. 5.8 shows P_e versus $\mathcal{P}_{tot}$. To plot the curves we set transmit power $\alpha_{n,t}^2$ corresponding to the optimal and the sub-optimal policies, and then we consider 10^4 independent Monte Carlo runs to find P_e, i.e., we generate 10^4 realizations of random

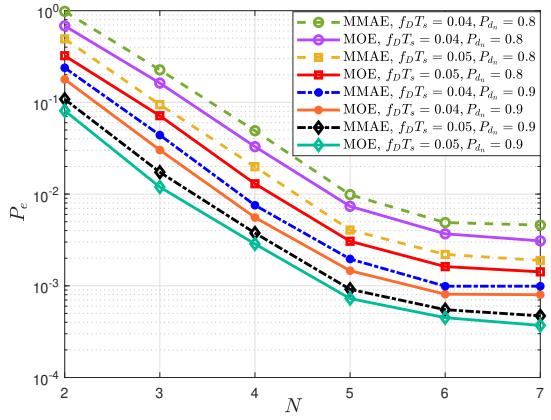

Figure 5.10: P_e vs. N for $K = 10, \mathcal{P}_{tot} = 15$mW, $b_u = 2$mJ $\gamma_g = 1.5, L = 4$, $\text{SNR}_s = 3$dB.

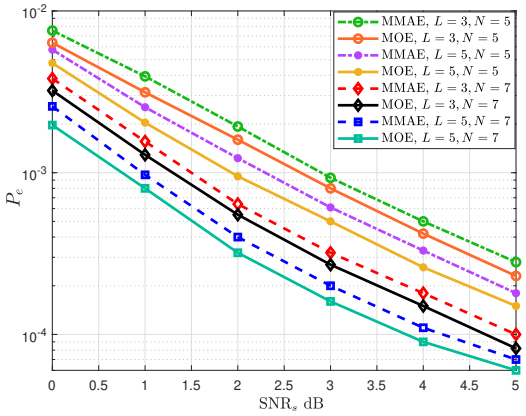

Figure 5.11: P_e vs. SNR_s for $K = 10, \mathcal{P}_{tot} = 15$mW, $b_u = 2$mJ, $\gamma_g = 2$

noises and fading channels and count the errors, $\dot{P}_e$ is the number of errors occurred divided by 10^4. Fig. 5.8 reveals two important points: (i) "optimal policy MOE" and "optimal policy MMAE" achieve the lowest P_e, followed by "sub-optimal policy MOE" and "sub-optimal policy MMAE", followed by "random policy MOE" and "random policy MMAE", (ii) "sub-optimal policy" performs very close to "optimal policy". Note that for all curves, P_e decreases as $\mathcal{P}_{tot}$ increases, however, it reaches an error floor after $\mathcal{P}_{tot}$ exceeds a certain value. This is due to the fact that for larger $\mathcal{P}_{tot}$ values, P_e is not limited by $\mathcal{P}_{tot}$. Instead, it is limited by σ_w^2. Fig. 5.8 also allows us to examine the existing trade-off between the consumed transmit power and P_e. Consider the curve labeled "P_e-consumed transmit power trade-off" in Fig. 3.3b, which shows how much transmit power is required to provide a certain P_e value. This curve is obtained from examining the points on "optimal policy MOE" and checking whether the constraint $\sum_{n=1}^{N} \alpha_{n,t}^2 \leq \mathcal{P}_{tot}, \ \forall t.$ is active or inactive. At a given point, when this constraint is active (inactive), the consumed transmit power is equal to (less than) $\mathcal{P}_{tot}$. Note that as $\mathcal{P}_{tot}$ increases and P_e reaches an error floor, the consumed transmit power is less than $\mathcal{P}_{tot}$. Since finding the sub-optimal policy has a much lower computational complexity than that of the optimal policy, and its performance is very close to the optimal

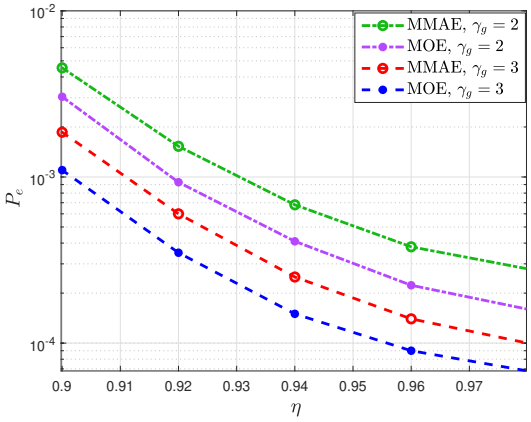

Figure 5.12: P_e vs. η for $K = 10, N = 5, \mathcal{P}_{tot} = 15\text{mW}, b_u = 1, L = 4, \text{SNR}_s = 3\text{dB}$.

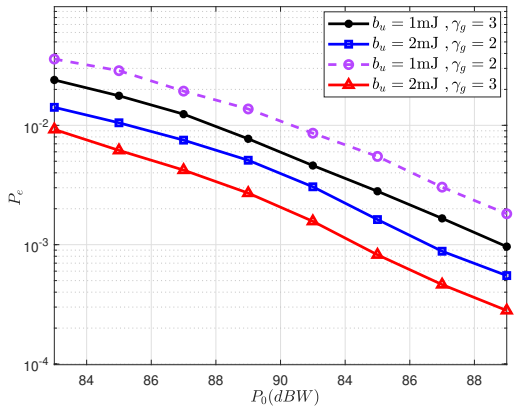

Figure 5.13: P_e vs. P_0 for $K = 10, N = 5, \mathcal{P}_{tot} = 15\text{mW}, L = 4, (r_0, r_1) = (1\text{m}, 100\text{m})$.

policy, from this point forward, we focus on the sub-optimal policy.

• **Dependency of P_e on different system parameters**: Fig. 5.9-5.12 plot P_e corresponding to sub-optimal policy in terms of different system parameters. Fig. 5.9 depicts P_e versus K as γ_g and b_u change. Given the pair (γ_g, b_u), P_e decreases as K increases, until it reaches an error floor. The error floor becomes smaller as (i) γ_g increases, given b_u, (ii) b_u increases, given γ_g. The presence of error floor is due to the fact that, for larger K values P_e is no longer restricted by K, and instead it is restricted by σ_w^2, leading to an error floor. Fig. 5.10 depicts P_e versus N as $f_D T_s$ and P_d vary. We observe that, given the pair $(f_D T_s, P_\text{d})$, P_e reduces when N increases, however, it reaches an error floor after cretin value of N. This is due to the fact that for larger N values, P_e becomes limited by $\mathcal{P}_{tot}$ and σ_w^2. Furthermore, we notice that P_e decreases when (i) given the pair (N, P_d), $f_D T_s$ increases; (ii) given the pair (N, $f_D T_s$), P_d increases. Fig. 5.11 shows P_e versus SNR_s as L, N change. Examination of this figure shows that P_e reduces when (i) given the pair (L, N), SNR_s increases. This is because as SNR_s increases, $P_{f_n} = P_f, \forall n$ in (5.4) decreases, (ii) given the pair (SNR_s, L), N increases, (iii) given the pair (SNR_s, N), L increases. This is because as L increases the feedback information from the FC to the sensors on channel gain increases. Fig. 5.12

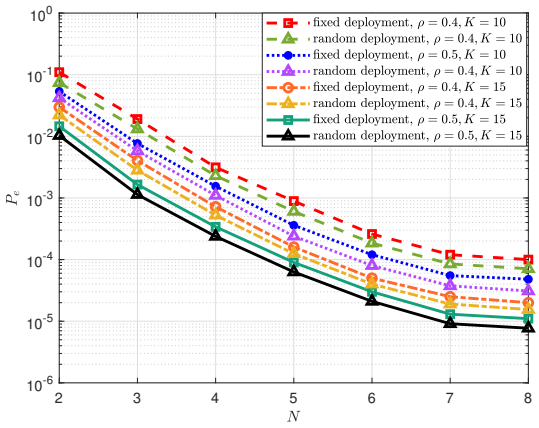

Figure 5.14: P_e vs. N for $\mathcal{P}_{tot} = 15\text{mW} b_u = 4\text{mJ}, \gamma_g = 1.5, L = 4$ (i) for fixed deployment $\text{SNR}_s = 5\text{dB}$, $P_\text{d} = 0.9$, (ii) for random deployment $(r_0, r_1) = (1\text{m}, 100\text{m})$, $P_0 = 84\text{dBW}$.

shows P_e versus η as γ_g varies. Given γ_g, P_e decreases in η. This is due to the fact that, as η increases, the sub-optimal $\alpha_{n,t}^2$ values increases, leading to a decrease in P_e. We note that there is a performance-computational complexity trade-off as η increases. Recall the mean of the network lifetime T is $\mathbb{E}\{T\} = 1/(1-\eta)$. As η increases, the number of iterations required for the value iteration algorithm (i.e., step 3 of Algorithm 4)) to converge increases.

• **Effect of random deployment of sensors on P_e**: We consider a circle field where the signal source with power P_0 is located at its center. Sensors are randomly deployed in the field such that the distance of sensor n from the source, r_n, is uniformly distributed in the interval of $(r_0, r_1) = (1\text{m}, 100\text{m})$. We assume the quantization thresholds are obtained via MMAE. Fig. 5.13 illustrates P_e versus P_0 as γ_g and b_u change. We observe that P_e decreases when: (i) given the pair (γ_g, b_u), P_0 increases, (ii) given the pair $(P_0,\ b_u)$, γ_g increases, (iii) given the pair $(P_0,\ \gamma_g)$, b_u increases. These observations are all expected. Fig. 5.14 illustrates P_e versus N for fixed and random deployment, as ρ and K vary. For the given set of parameters, the performance of fixed and random deployments is close to each other. Also, given the pair (ρ, K), P_e reduces when N increases, however, it reaches an error floor after N exceeds a certain value. This is due to the fact that for larger N values, P_e becomes

limited by $\mathcal{P}_{tot}$ and σ_w^2. Furthermore, we notice that P_e decreases when (i) given the pair (N, K), ρ increases, (ii) given the pair (N, ρ), K increases.

5.5 Conclusions

Considering an EH-enabled WSN with N sensors and a feedback channel from the FC to the sensors, tasked with binary distributed detection, we developed adaptive channel-dependent transmit power control policies such that the detection performance is optimized, subject to total transmit power constraint. Modeling the quantized fading channel, the energy arrival, and the dynamics of the battery as homogeneous FSMCs, and the network lifetime as a random variable with geometric distribution, we formulated our power control optimization problem as a discounted infinite-horizon constrained MDP problem, where sensors' transmit powers are functions of the battery state, quantized CSI, and the arrived energy. We developed the optimal policy, using dynamic programming and utilizing the Lagrangian approach to transform the constrained MDP problem into an equivalent unconstrained MDP problem. Determining the optimal policy, however, requires the knowledge of the global state at the FC, which imposes a significant signaling overhead to the sensors. To eliminate this overhead, we developed the sub-optimal policy, using a uniform Lagrangian multiplier to transform the constrained MDP problem into N unconstrained MDP problems. Different from the optimal policy, in the sub-optimal policy each sensor sets its transmit power based on its local state information. We showed that the computational complexity of finding the sub-optimal policy scales linearly in N and this policy has a close-to-optimal performance. We studies the error probability P_e in terms of different system parameters, including $K, N, \mathcal{P}_{tot}$, SNR_s. Although P_e decreases as each of these parameters increases, there is an error floor that ultimately depends on the communication channel noise variance and $\mathcal{P}_{tot}$. We expanded our work

to random deployment of sensors and examined how it affects the error probability. The insights obtained in this work are useful for adaptive transmit power control of EH-enabled WSNs tasked with distributed detection.

CHAPTER 6: EH-ENABLED DISTRIBUTED DETECTION OVER TEMPORALLY CORRELATED MARKOVIAN MIMO CHANNELS

We address distributed detection problem in a wireless sensor network, where each sensor harvests and stores randomly arriving energy units in a finite-size battery. Sensors transmit their symbols *simultaneously* to a fusion center (FC) with $M > 1$ antennas, over temporally correlated fading channels. Each sensor knows the quantized Frobenius norm of channel gain matrix, acquired via a feedback channel from the FC. Modeling the randomly arriving energy units as a Poisson process and the quantized channel state information (CSI) and the battery dynamics as homogeneous finite-state Markov chains, we propose an adaptive transmit power control strategy such that the J-divergence based detection metric is maximized at the FC, subject to an average transmit power per-sensor constraint. The proposed strategy is parameterized in terms of the scale factors (optimization variables) corresponding to the quantization intervals. This strategy allows each sensor to adapt its power based on its battery state and available CSI.

6.1 System Model

6.1.1 Observation Model at Sensors

Suppose the time horizon is divided into slots of equal length T_s. Each time slot is indexed by an integer t for $t = 1, 2, ..., \infty$. We model the underlying binary hypothesis H_t in time slot t as a binary random variable $H_t \in \{0, 1\}$ with a-priori probabilities $\Pi_0 = \Pr(H_t = 0)$ and $\Pi_1 = \Pr(H_t = 1) = 1 - \Pi_0$. We assume that the hypothesis H_t varies over time slots in an

independent and identically distributed (i.i.d.) manner. Let $x_{n,t}$ denote the local observation at sensor n in time slot t. We assume that sensors' observations given each hypothesis with conditional distribution $f(x_{n,t}|H_t=h_t)$ for $h_t \in \{0,1\}$ are independent across sensors. This model is relevant for WSNs that are tasked with detection of a known signal in uncorrelated Gaussian noises with the following signal model

$$\begin{aligned} H_t = 1: &\quad x_{n,t} = \mathcal{A} + v_{n,t}, \\ H_t = 0: &\quad x_{n,t} = v_{n,t}, \quad \text{for } n = 1, \ldots, N, \end{aligned} \tag{6.1}$$

where Gaussian observation noises $v_{n,t} \sim \mathcal{N}(0, \sigma^2_{v_n})$ are independent over time slots and across sensors. Given observation $x_{n,t}$ sensor n computes its local log-likelihood ratio (LLR)

$$\xi_n(x_{n,t}) \triangleq \log\left(\frac{f(x_{n,t}|H_t=1)}{f(x_{n,t}|H_t=0)}\right), \tag{6.2}$$

and compares it against a given local threshold θ_n to choose its non-negative transmission symbol $\alpha_{n,t}$. When $\xi_n(x_{n,t}) < \theta_n$, sensor n lets $\alpha_{n,t} = 0$. When $\xi_n(x_{n,t}) > \theta_n$, sensor n chooses $\alpha_{n,t}$ according to the rule in (6.10). We have

$$\begin{aligned} \widehat{\Pi}_{n,0} &= \Pr(\alpha_{n,t}=0) = \Pi_0(1-P_{\mathrm{f}_n}) + \Pi_1(1-P_{\mathrm{d}_n}), \\ \widehat{\Pi}_{n,1} &= \Pr(\alpha_{n,t}\neq 0) = \Pi_0 P_{\mathrm{f}_n} + \Pi_1 P_{\mathrm{d}_n}, \end{aligned} \tag{6.3}$$

where the probabilities P_{f_n} and P_{d_n} are

$$\begin{aligned} P_{\mathrm{f}_n} &= \Pr(\xi_n(x_{n,t}) > \theta_n | H_t = 0) = Q\Big(\frac{\theta_n + \mathcal{A}^2/2\sigma^2_{v_n}}{\mathcal{A}/\sigma_{v_n}}\Big), \\ P_{\mathrm{d}_n} &= \Pr(\xi_n(x_{n,t}) > \theta_n | H_t = 1) = Q\Big(\frac{\theta_n - \mathcal{A}^2/2\sigma^2_{v_n}}{\mathcal{A}/\sigma_{v_n}}\Big). \end{aligned} \tag{6.4}$$

6.1.2 Markovian Battery State and Energy Harvesting Models

We assume sensors are equipped with identical batteries of finite size K cells (units), where each cell corresponds to b_u Joules of stored energy. Therefore, each battery is capable of storing at most Kb_u Joules of harvested energy. Let $B_{n,t} \in \{0, 1, ..., K\}$ denote the discrete random process indicating the battery state of sensor n at the beginning slot t. Note that $B_{n,t} = 0$ and $B_{n,t} = K$ represent the empty battery and full battery levels, respectively. Also, $B_{n,t} = k$ implies that the battery is at state k, i.e., k cells of the battery is charged and the amount of stored energy in the battery is kb_u Joules.

Let $\mathcal{E}_{n,t}$ denote the randomly arriving energy units during time slot t at sensor n, where each unit is b_u Joules. We assume $\mathcal{E}_{n,t}$'s are i.i.d. over time slots and across sensors. We model $\mathcal{E}_{n,t}$ as a Poisson random variable with parameter ρ, and probability mass function (pmf) $p_m \triangleq \Pr(\mathcal{E}_{n,t} = m) = e^{-\rho}\rho^m/m!$ for $m = 0, 1, \ldots, \infty$. Note that parameter ρ is the average number of arriving energy units during one time slot at each sensor. Let $\mathcal{S}_{n,t}$ be the number of stored (harvested) energy units in the battery at sensor n during time slot t. Note that the harvested energy $\mathcal{S}_{n,t}$ cannot be used during slot t. Since the battery has a finite capacity of K cells, we have $\mathcal{S}_{n,t} \in \{0, 1, ..., K\}$. Also, $\mathcal{S}_{n,t}$ are i.i.d. over time slots and across sensors. The two random variables $\mathcal{S}_{n,t}$ and $\mathcal{E}_{n,t}$ are related as the following

$$\mathcal{S}_{n,t} = \begin{cases} \mathcal{E}_{n,t}, & \text{if } 0 \leq \mathcal{E}_{n,t} \leq K-1, \\ K, & \text{if } \mathcal{E}_{n,t} \geq K. \end{cases} \tag{6.5}$$

Based on (6.5) we can find the pmf of $\mathcal{S}_{n,t}$ in terms of the pmf of $\mathcal{E}_{n,t}$. Let $q_e \triangleq \Pr(\mathcal{S}_{n,t} = e)$

for $e = 0, 1, \ldots, K$. We have

$$q_e = \begin{cases} p_e, & \text{if } 0 \leq e \leq K-1, \\ \sum_{m=K}^{\infty} p_m, & \text{if } e = K. \end{cases} \tag{6.6}$$

The battery state at the beginning of slot $t+1$ depends on the battery state at the beginning of slot t, the harvested energy during slot t, and the transmission symbol $\alpha_{n,t}$, i.e.,

$$B_{n,t+1} = \min\left\{[B_{n,t} + \mathcal{S}_{n,t} - \alpha_{n,t}^2 T_s / b_u]^+, K\right\}, \tag{6.7}$$

where $[x]^+ = \max\{0, x\}$. Considering the dynamic battery state model in (6.7) we note that, conditioned on $\mathcal{S}_{n,t}$ and $\alpha_{n,t}$ the value of $B_{n,t+1}$ only depends on the value of $B_{n,t}$. Hence, the process $B_{n,t}$ can be modeled as a Markov chain. Let $\mathbf{\Phi}_{n,t}$ be the probability vector of battery state in slot t

$$\mathbf{\Phi}_{n,t} \triangleq \Big[\Pr(B_{n,t} = 0), \ldots, \Pr(B_{n,t} = K)\Big]^T, \tag{6.8}$$

where $\Pr(B_{n,t}=k)$ in (6.8) depends on $B_{n,t-1}$, $\mathcal{S}_{n,t-1}$ and $\alpha_{n,t-1}$. Assuming that the Markov chain is time-homogeneous, we let $\mathbf{\Psi}_n$ be the transition probability matrix of this chain with its (i,j)-th entry $[\mathbf{\Psi}_n]_{i,j} \triangleq \Pr(B_{n,t} = j | B_{n,t-1} = i)$ for $i, j = 0, \ldots, K$. We can express $[\mathbf{\Psi}_n]_{i,j}$ as (6.11). Since the Markov chain characterized by $\mathbf{\Psi}_n$ is irreducible and aperiodic, there exists a unique steady state distribution, regardless of the initial state [43]. Let $\mathbf{\Phi}_n = [\phi_{n,0}, \phi_{n,1}, ..., \phi_{n,K}]^T$ be the unique steady state probability vector with the entries $\phi_{n,k} = \lim_{t\to\infty} \Pr(B_{n,t} = k)$. This vector satisfies the eigenvalue equation $\mathbf{\Phi}_n = \mathbf{\Phi}_n \mathbf{\Psi}_n$.

6.1.3 Markovian Channel Gain Model and Transmission Symbol

We assume N sensors send their transmission symbols $\alpha_{n,t}$ simultaneously to the FC, that is equipped with M receive antennas. Let $g_{m,n,t}$ indicate the fading channel gain between sensor n and m-th antenna of the FC during time slot t. The $M \times N$ channel matrix $\boldsymbol{G}_t$ becomes

$$\boldsymbol{G}_t = \begin{bmatrix} g_{1,1,t} & g_{1,2,t} & \cdots & g_{1,N,t} \\ g_{2,1,t} & g_{2,2,t} & \cdots & g_{2,N,t} \\ \vdots & \vdots & \vdots & \vdots \\ g_{M,1,t} & g_{M,2,t} & \cdots & g_{M,N,t} \end{bmatrix}. \tag{6.9}$$

We assume block fading model and $g_{m,n,t}$'s are i.i.d. over time slots and independent across sensors. We define the *channel gain* as the Frobenius norm of $\boldsymbol{G}_t$, i.e., $s_t = ||\boldsymbol{G}_t||_F^2$ [62]. We consider a scalar quantizer at the FC that maps s_t into a point in set $\mathbb{S} = \{\hat{s}_1, \hat{s}_2, ..., \hat{s}_L\}$, which contains L *quantized channel gain* values. The points in set $\mathbb{S}$ can be found such that a certain distortion function is minimized. The FC partitions the positive real line $\mathbb{R}^+$ into L intervals (Voronoi cells of the quantizer) using L quantization thresholds $\{\mu_l\}_{l=1}^{L}$, where $0 = \mu_1 < \mu_2 < \ldots < \mu_{L-1} < \mu_L = \infty$, and associates interval $\mathcal{I}_l = [\mu_l, \mu_{l+1})$ with point $\hat{s}_l$, i.e., if s_t lies in the interval $\mathcal{I}_l$ then the quantized channel gain $Q(s_t)$ becomes $\hat{s}_l$. The FC informs all sensors of the quantized channel gain through a *feedback channel*. Sensor n chooses $\alpha_{n,t}$ according to its *battery state* k and the available *quantized channel gain*, using the following rule

$$\alpha_{n,t}^2 = \begin{cases} 0, & \xi_n(x_{n,t}) < \theta_n, \\ \lfloor c_1 k \rfloor b_u / T_s, & \xi_n(x_{n,t}) \geq \theta_n,\ Q(s_t) = \hat{s}_1, \\ \vdots & \vdots \\ \lfloor c_L k \rfloor b_u / T_s, & \xi_n(x_{n,t}) \geq \theta_n,\ Q(s_t) = \hat{s}_L, \end{cases} \tag{6.10}$$

$$[\boldsymbol{\Psi}_n]_{i,j} = \widehat{\Pi}_{n,1} \sum_{k=0}^{K} \sum_{l=1}^{L} \pi_l q_k I_{i\to j}(\mathcal{S}_{n,t}, \lfloor c_l i \rfloor) + \widehat{\Pi}_{n,0} \sum_{k=0}^{K} q_k I_{i\to j}(\mathcal{S}_{n,t}, 0).$$

$$\text{where } I_{i\to j}(\mathcal{S}_{n,t}, \alpha_{n,t}^2 T_s/b_u) = \begin{cases} 1, & \text{if } j = \min\left\{[i + \mathcal{S}_{n,t} - \alpha_{n,t}^2 T_s/b_u]^+, K\right\}, \\ 0, & \text{o.w.} \end{cases} \tag{6.11}$$

where $\lfloor . \rfloor$ is the floor function and the scale factors $\{c_l\}_{l=1}^{L}$ are between zero and one and are *our optimization variables*.

We model the time variation of the quantized channel gain using a Markov chain [63]. The Markov chain has L states and the states are the points in set $\mathbb{S}$. To obtain this Markov model, similar to [62], we make the following two assumptions: **(AS1)** The entries of $\boldsymbol{G}_t$ have the Clark's correlation function [64], i.e., we have $\mathbb{E}\left[g_{i,j,t}^* \; g_{i,j,t+\tau}\right] = J_0(2\pi f_D \tau), \forall i, j$, where J_0 is Bessel function of zeroth-order and f_D is the maximum Doppler frequency [52]. **(AS2)** Inter-state transitions only occur between adjacent states in the chain. Let $\pi_l = \Pr(Q(s_t) = \hat{s}_l)$ be the steady-state probability of state l of the Markov chain. We have $\pi_l = \int_{\mu_l}^{\mu_{l+1}} f_s(s) ds$, where $f_s(s)$ is the probability density function (pdf) of s_t. Assuming that the elements of $\boldsymbol{G}_t$ are i.i.d and distributed as $\mathcal{CN}(0, 1)$, the channel gain s_t follows a chi-squared distribution with degree of freedom equal to MN. Hence, π_l can be written as

$$\pi_l = \Pr(Q(s_t) = \hat{s}_l) = \sum_{i=0}^{Z-1} \frac{\exp(-\mu_l)\mu_l^i - \exp\left(-\mu_{l+1}\right)\mu_{l+1}^i}{i!}, \tag{6.12}$$

where $Z = 2MN$. Let Θ be the transition probability matrix of this chain with its (i, j)-th

entry $[\Theta]_{i,j}=\Pr(Q(s_t)=\hat{s}_i|Q(s_{t-1})=\hat{s}_j)$. We have

$$[\Theta]_{i,j}=\begin{cases}\frac{\beta(\mu_{l+1}^2)}{\pi_{n,l}}, & i=l+1,\ j=1,...,L-1\\ \frac{\beta(\mu_l^2)}{\pi_{n,l}}, & i=l-1,\ j=2,...,L\\ 1-\frac{\beta(\mu_l^2)}{\pi_{n,l}}-\frac{\beta(\mu_{l+1}^2)}{\pi_{n,l}}, & i=l,\ j=2,...,L-1\\ 1-\frac{\beta(\mu_2^2)}{\pi_{n,1}}, & i=1,\ j=1\\ 1-\frac{\beta(\mu_L^2)}{\pi_{n,L}}, & i=L,\ j=L\\ 0, & \text{O.W.}\end{cases} \tag{6.13}$$

where β is the level crossing rate of the random process s_t^2 at the level x and is given by [62] $\beta(x)=\frac{\sqrt{2\pi}f_D T_s x^{(Z-1/2)}}{(Z-1)!\exp(x)}$.

6.1.4 Received Signals at FC and Optimal Bayesian Fusion Rule

In each time slot, sensors send their symbols simultaneously to the FC. The received signal at the FC corresponding to time slot t is $\boldsymbol{y}_t=\boldsymbol{G}_t\boldsymbol{\alpha}_t+\boldsymbol{w}_t$, where $\boldsymbol{y}_t=[y_{1,t},y_{2,t},,...,y_{M,t}]^T$, $\boldsymbol{\alpha}_t=[\alpha_{1,t},\alpha_{2,t},,...,\alpha_{N,t}]^T$, $\boldsymbol{w}_t=[w_{1,t},w_{2,t},,...,w_{M,t}]^T$, and $\boldsymbol{w}_t$ is a zero mean complex Gaussian vector with covariance matrix $\boldsymbol{R}$. The FC applies the optimal Bayesian fusion rule $\Gamma_0(.)$ to obtain a global decision $u_{0,t}$ [16]. In particular, we have

$$u_{0,t}=\Gamma_0(\boldsymbol{y}_t)=\begin{cases}1,\ \Delta_t>\tau,\\ 0,\ \Delta_t<\tau,\end{cases}\ \Delta_t=\log\left(\frac{f(\boldsymbol{y}_t|H_t=1)}{f(\boldsymbol{y}_t|H_t=0)}\right) \tag{6.14}$$

where $f(\boldsymbol{y}_t|H_t=h_t)$ is the conditional pdf of $\boldsymbol{y}_t$ and the decision threshold $\tau=\log(\frac{\Pi_0}{\Pi_1})$. From Bayesian perspective, the natural choice to measure the detection performance is the

error probability, defined as $P_e = \Pi_0 \Pr(\Delta_t > \tau | H_t = 0) + \Pi_1 \Pr(\Delta_t < \tau | H_t = 1)$. However, finding a closed form expression for P_e is mathematically intractable. Instead, we choose the J-divergence between the distributions of the detection statistics at the FC under different hypotheses, as our detection performance metric. This choice allows us to provide a tractable analysis. Given the local thresholds $\{\theta_n\}_{n=1}^N$ in (6.10) and the channel gain quantizer at the FC, *our problem of optimizing transmit power control strategy reduces to finding the optimal scale factors* $\{c_l\}_{l=1}^L$ *in (6.10) such that the J-divergence at the FC is maximized, subject to per-sensor average transmit power constraints.*

6.2 J-Divergence Derivation and Our Constrained Optimization Problem

By definition [18,30], the J-divergence between two pdfs $\eta_1(x)$ and $\eta_0(x)$, denoted as $J(\eta_1, \eta_0)$, is $J(\eta_1, \eta_0) = D(\eta_1||\eta_0) + D(\eta_0||\eta_1)$, where $D(\eta_i||\eta_j)$ is the non-symmetric Kullback-Leibler (KL) distance between $\eta_i(x)$ and $\eta_j(x)$. The KL distance $D(\eta_i||\eta_j)$ is defined as $D(\eta_i||\eta_j) = \int_{-\infty}^{\infty} \log\left(\frac{\eta_i(x)}{\eta_j(x)}\right) \eta_i(x) dx$. Therefore, we obtain

$$J(\eta_1, \eta_0) = \int_{-\infty}^{\infty} [\eta_1(x) - \eta_0(x)] \log\left(\frac{\eta_1(x)}{\eta_0(x)}\right) dx. \tag{6.15}$$

In our problem setup, $f(\boldsymbol{y}_t|\boldsymbol{G}_t, H_t = 1)$ and $f(\boldsymbol{y}_t|\boldsymbol{G}_t, H_t = 0)$ play the role of $\eta_1(x)$ and $\eta_0(x)$, respectively. Given $\boldsymbol{G}_t$ we note that H_t, $\boldsymbol{\alpha_t}$, $\boldsymbol{y}_t$ satisfy the Markov property, i.e., $H_t \to \boldsymbol{\alpha_t} \to \boldsymbol{y}_t$ [18,30]. This implies that $\boldsymbol{y}_t$ and H_t, given $\boldsymbol{\alpha_t}$, are conditionally independent. Therefore, we can write $f(\boldsymbol{y}_t|\boldsymbol{G}_t, H_t = i) = f(\boldsymbol{y}_t|\boldsymbol{G}_t, \boldsymbol{\alpha_t} = 0) \Pr(\boldsymbol{\alpha}_t|H_t = i) + f(\boldsymbol{y}_t|\boldsymbol{G}_t, \boldsymbol{\alpha_t} \neq 0) \Pr(\boldsymbol{\alpha}_t|H_t = i)$ for $i = 0, 1$. We have

$$f(\boldsymbol{y}_t|\boldsymbol{G}_t, \boldsymbol{\alpha}_t) = \frac{1}{|2\pi \boldsymbol{R}|^{\frac{1}{2}}} \exp[-\frac{1}{2}(\boldsymbol{y}_t - \boldsymbol{G}_t\boldsymbol{\alpha}_t)\boldsymbol{R}^{-1}(\boldsymbol{y}_t - \boldsymbol{G}_t\boldsymbol{\alpha}_t)] \tag{6.16}$$

Although $f(\boldsymbol{y}_t|\boldsymbol{G}_t, \boldsymbol{\alpha}_t)$ is Gaussian, $f(\boldsymbol{y}_t|\boldsymbol{G}_t, H_t = 0), f(\boldsymbol{y}_t|\boldsymbol{G}_t, H_t = 1)$ are Gaussian mixtures. Unfortunately, the J-divergence between two Gaussian mixture densities does not have a general closed-form expression. Similar to [18, 30], we approximate the J-divergence between two Gaussian mixture densities by the J-divergence between two Gaussian densities $f^G(\boldsymbol{y}_t|\boldsymbol{G}_t, H_t = i) \sim \mathcal{N}(\boldsymbol{m}_i, \boldsymbol{\Upsilon}_i)$, where the mean and the variance of the approximate distributions are obtained from matching the first and second order moments of the actual and the approximate distributions. For our problem setup, the parameters $\boldsymbol{m}_0, \boldsymbol{m}_1, \boldsymbol{\Upsilon}_0, \boldsymbol{\Upsilon}_1$ become

$$\begin{aligned} \boldsymbol{m}_0 &= \boldsymbol{G}_t \boldsymbol{A}_t \boldsymbol{P}_{\mathrm{f}}, \quad \boldsymbol{\Upsilon}_0 = \boldsymbol{R} + \boldsymbol{G}_t \boldsymbol{A}_t \widehat{\boldsymbol{P}}_{\mathrm{f}} \boldsymbol{A}_t^T \boldsymbol{G}_t^T, \\ \boldsymbol{m}_1 &= \boldsymbol{G}_t \boldsymbol{A}_t \boldsymbol{P}_{\mathrm{d}}, \quad \boldsymbol{\Upsilon}_1 = \boldsymbol{R} + \boldsymbol{G}_t \boldsymbol{A}_t \widehat{\boldsymbol{P}_{\mathrm{d}}} \boldsymbol{A}_t^T \boldsymbol{G}_t^T. \end{aligned} \tag{6.17}$$

in which $\boldsymbol{A}_t = \mathrm{diag}\{\alpha_{1,t}, ..., \alpha_{N,t}\}$, $\boldsymbol{P}_{\mathrm{f}} = [P_{\mathrm{f}_1}, ..., P_{\mathrm{f}_N}]^T$, $\boldsymbol{P}_{\mathrm{d}} = [P_{\mathrm{d}_1}, ..., P_{\mathrm{d}_N}]^T$, $\widehat{\boldsymbol{P}}_{\mathrm{f}} = \mathrm{diag}\{P_{\mathrm{f}_1}(1 - P_{\mathrm{f}_1}), ..., P_{\mathrm{f}_N}(1 - P_{\mathrm{f}_N})\}$, and $\widehat{\boldsymbol{P}_{\mathrm{d}}} = \mathrm{diag}\{P_{\mathrm{d}_1}(1 - P_{\mathrm{d}_1}), ..., P_{\mathrm{d}_N}(1 - P_{\mathrm{d}_N})\}$. After some algebra, we obtain

$$\begin{aligned} J\big(f^G(\boldsymbol{y}_t|\boldsymbol{G}_t, H_t = 1), f^G(\boldsymbol{y}_t|\boldsymbol{G}_t, H_t = 0)\big) &= \frac{1}{2}\mathrm{Tr}\big[\boldsymbol{\Upsilon}_0 \boldsymbol{\Upsilon}_1^{-1} + \boldsymbol{\Upsilon}_1 \boldsymbol{\Upsilon}_0^{-1} \\ + (\boldsymbol{\Upsilon}_1^{-1} + \boldsymbol{\Upsilon}_0^{-1})(\boldsymbol{m}_1 - \boldsymbol{m}_0)(\boldsymbol{m}_1 - \boldsymbol{m}_0)^T\big] - M \end{aligned} \tag{6.18}$$

Note that J in (6.18) depends on $\boldsymbol{G}_t$, whereas $\alpha_{n,t}^2$ in (6.10) depends on the quantization interval to which $s_t = ||\boldsymbol{G}_t||_F^2$ belongs. Let $\bar{J}^{(i)} = \mathbb{E}\{J|s_t \in [\mu_i, \mu_{i+1}]\}$ and $\bar{\mathcal{P}}_n^{(i)} = \mathbb{E}\{\alpha_{n,t}^2|s_t \in [\mu_i, \mu_{i+1}]\}$, respectively, denote the expectations of J in (6.18) and $\alpha_{n,t}^2$ in (6.10) over s_t, conditioned that $s_t \in [\mu_i, \mu_{i+1}]$. Since $\bar{J}^{(i)}$ does not have a closed-form expression we compute it via Monte Carlo simulation. Using (6.10) we find $\bar{\mathcal{P}}_n^{(i)} = \widehat{\Pi}_{n,1} \sum_{k=0}^{K} \phi_{n,k} \pi_i \lfloor c_i k \rfloor$. Our constrained optimization problem of maximizing the J-divergence, subject to per-sensor average transmit power constraints, with respect to the optimization variables $\{c_l\}_{l=1}^{L}$ in

(6.10) become

$$\text{(6.P1)} \qquad \max_{\{c_l\}_{l=1}^{L}} \sum_{i=1}^{L} \bar{J}^{(i)}$$
$$\text{s.t. } c_l \in [0,1], \forall l, \ \sum_{i=1}^{L} \bar{\mathcal{P}}_n^{(i)} \leq \mathcal{P}_0, \forall n.$$

where $\mathcal{P}_0$ is the maximum allowed average transmit power per-sensor. We note that (6.P1) is *not concave* with respect to the optimization variables. Moreover, the objective function and the constraints in (6.P1) are *not differentiable* with respect to the optimization variables. Hence, existing gradient-based algorithms for solving non-convex optimization problems cannot be used to solve (6.P1). We resort to a grid-based search method, which requires L-dimensional search over the search space $[0,1]^L$. Clearly, the accuracy of this solution depends on the resolution of the grid-based search. Suppose the intervals $[0,1]$ is divided into N_c sub-intervals. Therefore, the search space of (P1), denoted as $\mathcal{D}$, consists of $(N_c)^L$ discrete points in the original L-dimensional search space.

Computational complexity of solving (6.P1): We note that the FC needs to perform two tasks for each point in $\mathcal{D}$: task (i) forming $\mathbf{\Psi}_n$ and $\mathbf{\Phi}_n$, task (ii) calculating $\bar{J}^{(i)}$ and $\bar{\mathcal{P}}_n^{(i)}$. Our numerical results show that for a fixed $\{c_l\}_{l=1}^{L}$ the computational complexity of task (i) and task (ii) are $\mathcal{O}(K^{3.2})$ and $\mathcal{O}(M \times N \times K^{2.7})$, respectively. Hence, the computational complexity of solving (P1) is $\mathcal{O}\left((N_c)^L(K^{3.2} + M \times N \times K^{2.7})\right)$. To curb he computational complexity of the grid-based search method, we plan to explore random search algorithms (in which only a randomly chosen subset of the points in $\mathcal{D}$ is searched to find a solution) that have a low-computational complexity and provide a close-to-optimal performance for our future work.

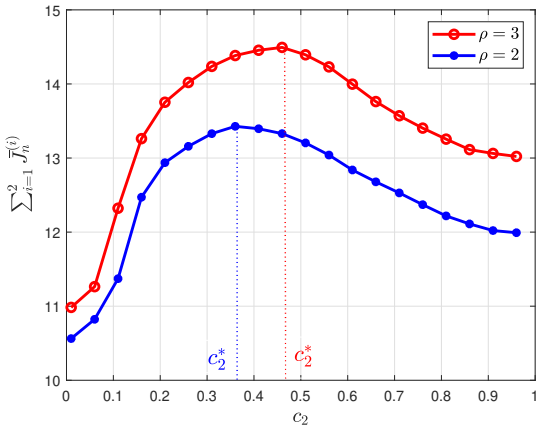

Figure 6.1: $L=2$, $\mathcal{P}_0=2$mW.

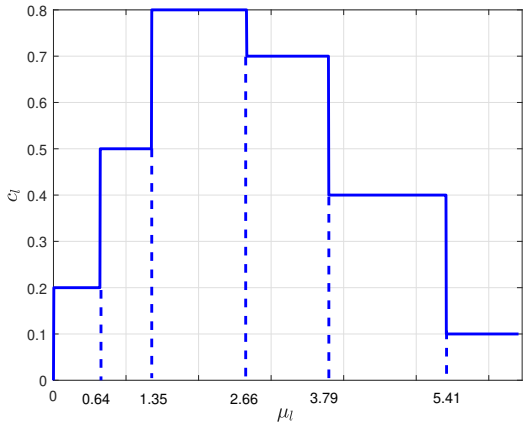

Figure 6.2: $L=6, \mathcal{P}_0=2$mW, $\rho=2$.

6.3 Simulation results and Concluding Remarks

In our simulations, we let $\boldsymbol{R}=\boldsymbol{I}\sigma_w^2$ and define the SNR corresponding to observation channel as $\text{SNR}_s = 20\log(\mathcal{A}/\sigma_v)$. We let $P_{d_n} = 0.9, \forall n, K = 5, M = 4, N = 3, \text{SNR}_s = 3\text{dB}$, $\sigma_w^2 = 1$. For $L=2$ the optimization variables are $\{c_1, c_2\}$. Fig. 6.1 illustrates the objective function $\bar{J}^{(1)} + \bar{J}^{(2)}$ versus the scale factor c_2 given $c_1=0.5$. We observe that the objective function is not a concave function of c_2. Still there exists a point, denoted as c_2^*, at which the function attains its maximum. Starting from small values of c_2, as c_2 increases (until it reaches c_2^*), the function value increases, because the harvested energy can recharge the battery and can yield more power for data transmission. However, when c_2 exceeds c_2^*, the harvested and stored energy cannot support the data transmission and the function value decreases.

Fig. 6.2 depicts the optimized $\{c_l\}$'s versus the quantization thresholds $\{\mu_l\}$'s for $L=6$. We note that, as l increases (i.e., channel gain s_t increases), c_l first increases and then decreases. Considering (6.10) this implies that, given the battery state k, as s_t increases $\alpha_{n,t}^2$ first increases and then decreases. Fig. 6.3 shows the error probability P_e versus $\mathcal{P}_0$, in which P_e values are obtained from Monte-Carlo simulations. As $\mathcal{P}_0$ increases P_e decreases, which

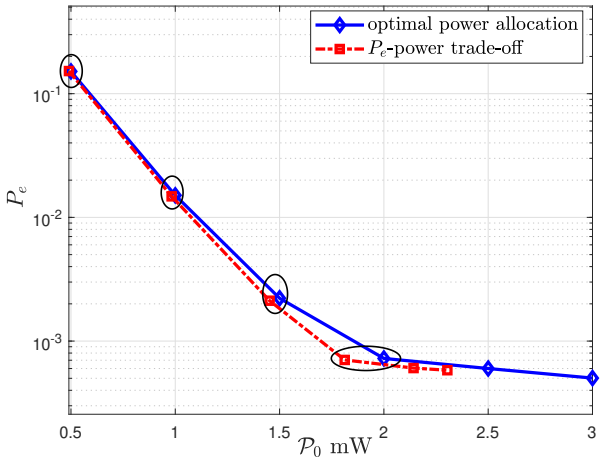

Figure 6.3: $L=4, \rho=2$.

is expected. Fig. 6.3 also allows us to examine the existing trade-off between the average transmit power and the detection performance. Consider the curve labeled "P_e-power trade-off" in Fig. 6.3, which shows how much average transmit power is required to provide a certain P_e value. This curve is obtained from checking whether the power constraint in (3.P1) is active or inactive. At a given point, when this constraint is active (inactive), the average transmit power is equal to (less than) $\mathcal{P}_0$. Note that as $\mathcal{P}_0$ increases and P_e reaches an error floor, the average transmit power is less than $\mathcal{P}_0$.

CHAPTER 7: CONCLUSION AND FUTURE WORK DIRECTIONS

In this dissertation we studied the distributed detection in energy harvesting wireless sensor networks (WSNs). In EH-powered WSNs, where sensors are capable of harvesting and storing energy, power control is necessary to balance the rates of energy harvesting and energy consumption for data transmission. In addition, wireless communication channels change randomly in time due to fading. These together prompt the need for developing new power control strategies for an EH-enabled transmitter that can best exploit and adapt to the random energy arrivals and time-varying fading channels. We consider parallel structure EH-powered WSNs tasked with solving a binary distributed detection problem. Sensors process locally their observations, adapt their transmission according to the battery and fading channel states, and transmit their data symbols to the fusion center (FC) over orthogonal fading channels. We study adaptive transmission schemes that optimize detection performance metrics at the FC, subject to certain battery and transmit power constraints.

7.1 Conclusions

In the following, we summarize our contributions in Chapters 2-6, and provide some ideas for future works.

In chapter 2, we studied a distributed detection problem in a wireless network with N heterogeneous energy harvesting sensors and investigated the optimal local decision thresholds for given transmission and battery state models. Our numerical results indicate that the thresholds obtained from maximizing the Kullback-Leibler distance are near-optimal. Find-

ing these thresholds is computationally very efficient, as it requires only N one-dimensional searches, as opposed to a N-dimensional search required to find the thresholds that maximize the detection probability.

In chapter 3, we developed a power control strategy for an EH-enabled WSN, that is tasked with solving a binary distributed detection problem. Our proposed strategy is parameterized in terms of the channel gain quantization thresholds and the scale factors, which play key roles in balancing the rates of energy harvesting and energy consumption for transmission. We explored the optimal and sub-optimal strategies such that the J-divergence based detection metric is maximized, subject to an average transmit power per sensor constraint. These optimization problems can be solved offline and allow each sensor to adapt its power based on its battery state and its quantized CSI (acquired via limited feedback from the FC). Since our non-convex optimization problem is not differentiable with respect to the optimization variables, we explored deterministic, random, and hybrid grid-based search methods, and showed that our proposed hybrid search methods have a low-computational complexity and near-optimal performance. The structure of the optimized scale factors reveals that, given the battery state, the optimized power level is not a monotonic function of the channel gain. We examined the existing trade-off between the average transmit power and the detection performance. We also demonstrated that increasing K or ρ do not necessarily lower the detection error, and it depends on the communication channel noise.

In chapter 4, we considered a binary distributed detection system where each sensor is capable of harvesting and storing randomly arrived energy in its battery. We formulated the problem of finding the optimal power control policy that optimizes the detection performance as a finite-horizon MDP problem, and solved the problem via finite horizon dynamic programming. The optimal policy allows each sensor to adapt its transmission symbol based on its current quantized CSI and battery state.

In chapter 5, considering an EH-enabled WSN with N sensors and a feedback channel from the FC to the sensors, tasked with binary distributed detection, we developed adaptive channel-dependent transmit power control policies such that the detection performance is optimized, subject to total transmit power constraint. Modeling the quantized fading channel, the energy arrival, and the dynamics of the battery as homogeneous FSMCs, and the network lifetime as a random variable with geometric distribution, we formulated our power control optimization problem as a discounted infinite-horizon constrained MDP problem, where sensors' transmit powers are functions of the battery state, quantized CSI, and the arrived energy. We developed the optimal policy, using dynamic programming and utilizing the Lagrangian approach to transform the constrained MDP problem into an equivalent unconstrained MDP problem. Determining the optimal policy, however, requires the knowledge of the global state at the FC, which imposes a significant signaling overhead to the sensors. To eliminate this overhead, we developed the sub-optimal policy, using a uniform Lagrangian multiplier to transform the constrained MDP problem into N unconstrained MDP problems. Different from the optimal policy, in the sub-optimal policy each sensor sets its transmit power based on its local state information. We showed that the computational complexity of finding the sub-optimal policy scales linearly in N and this policy has a close-to-optimal performance. We studied the error probability P_e in terms of different system parameters, including $K, N, \mathcal{P}_{tot}$, SNR_s. Although P_e decreases as each of these parameters increases, there is an error floor that ultimately depends on the communication channel noise variance and $\mathcal{P}_{tot}$. We expanded our work to random deployment of sensors and examined how it affects the error probability. The insights obtained in this chapter are useful for adaptive transmit power control of EH-enabled WSNs tasked with distributed detection.

In chapter 6, considering a WSN, composed of EH-enabled sensors and a fusion center (FC), in [3] we developed an adaptive channel-dependent transmit power control strategy

for sensors such that J-divergence detection metric at the FC is maximized. In [3] we assumed that the FC has a single antenna, sensors transmit over orthogonal channels, and fading channels between sensors and the FC are independent and identically distributed (i.i.d.) over time slots. In this chapter we extended [3] to temporally correlated Markovian MIMO channels where the FC has $M > 1$ antennas, sensors transmit their symbols to the FC simultaneously, and fading channels between sensors and the FC are correlated over time slots.

7.2 Future work

In this section, we provide some interesting issues that can be addressed in the future.

In cooperative communication networks, the source node transmits its data to the destination either directly or cooperatively with a cooperating node. When using energy harvesting technology, where nodes collect their energy from the environment, the energy availability at the nodes becomes unpredictable due to the stochastic nature of energy harvesting processes. As a result, when the source has a transmission, it cannot immediately transmit its data cooperatively with the cooperating node. It first needs to determine whether the cooperating node has sufficient energy to forward its transmission or not. Otherwise, its transmitted data may get lost. Therefore, when using energy harvesting, the challenge is for the source to schedule its transmissions whether directly or cooperatively, such that the fraction of its events (sensed data) that are successfully reported to the destination is maximized.

We propose to address the problem of cooperating node scheduling in energy harvesting sensor networks. We can study the problem for the case of a single cooperating node and the case of multiple cooperating nodes, as well as the scenarios of one-way and two-way

cooperative communications. A simple scheduling scheme, called feedback scheme, which enables the source to optimally schedule its transmissions whether directly or cooperatively can be investigated.

APPENDIX A: BIOGRAPHICAL SKETCH

The author was born in Shiraz, Iran in 1990. She received her Bachelor of Science degree and Master of Science degree from Shiraz University, Shiraz, Iran in 2013 and 2017; both in Electrical Engineering. In her master's program, she worked on relaying schemes in molecular communication. In August 2017, she joined the Department of Electrical Engineering and Computer Science in University of Central Florida as a PhD student under direction of Dr. Azadeh Vosoughi. Her current research interests include distributed detection, statistical signal processing, energy harvesting in wireless sensor networks, and array signal processing.

APPENDIX B: PUBLICATIONS

Journal papers

• G. Ardeshiri and A. Vosoughi, "On Distributed Detection in EH-WSNs With Finite-State Markov Channel and Limited Feedback," submitted in *IEEE Transactions on Green Communications and Networking*.

• G. Ardeshiri and A. Vosoughi, "On Adaptive Transmission for Distributed Detection in Energy Harvesting Wireless Sensor Networks with Limited Fusion Center Feedback," in *IEEE Transactions on Green Communications and Networking*, vol. 6, no. 3, pp. 1764–1779, 2022.

Conference papers

• G. Ardeshiri and A. Vosoughi, "EH-Enabled Distributed Detection Over Temporally Correlated Markovian MIMO Channels," submitted in *2023 IEEE International Conference on Acoustics, Speech, and Signal Processing (ICASSP 2023)*

• G. Ardeshiri and A. Vosoughi, "Learning-based Distributed Detection with Energy Harvesting," *2021 55th Asilomar Conference on Signals, Systems, and Computers*, 2021, pp. 747-751, doi: 10.1109/IEEECONF53345.2021.9723378.

• G. Ardeshiri, H. Yazdani and A. Vosoughi, "Power adaptation for distributed detection in energy harvesting WSNs with finite-capacity battery," in *2019 IEEE Global Communications Conference (GLOBECOM)*, 2019, pp. 1–6.

• G. Ardeshiri, H. Yazdani and A. Vosoughi, "Optimal local thresholds for distributed detection in energy harvesting wireless sensor networks," *2018 IEEE Global Conference on Signal and Information Processing (GlobalSIP)*, Anaheim, CA, USA, 2018, pp. 813-817.

APPENDIX C: COPYRIGHT PERMISSIONS

Optimal Local Thresholds for Distributed Detection in Energy Harvesting Wireless Sensor Networks

Conference Proceedings:
2018 IEEE Global Conference on Signal and Information Processing (GlobalSIP)

Author: Ghazaleh Ardeshiri

Publisher: IEEE

Date: November 2018

Thesis / Dissertation Reuse

The IEEE does not require individuals working on a thesis to obtain a formal reuse license, however, you may print out this statement to be used as a permission grant:

Requirements to be followed when using any portion (e.g., figure, graph, table, or textual material) of an IEEE copyrighted paper in a thesis:

1) In the case of textual material (e.g., using short quotes or referring to the work within these papers) users must give full credit to the original source (author, paper, publication) followed by the IEEE copyright line © 2011 IEEE.
2) In the case of illustrations or tabular material, we require that the copyright line © [Year of original publication] IEEE appear prominently with each reprinted figure and/or table.
3) If a substantial portion of the original paper is to be used, and if you are not the senior author, also obtain the senior author's approval.

Requirements to be followed when using an entire IEEE copyrighted paper in a thesis:

1) The following IEEE copyright/ credit notice should be placed prominently in the references: © [year of original publication] IEEE. Reprinted, with permission, from [author names, paper title, IEEE publication title, and month/year of publication]
2) Only the accepted version of an IEEE copyrighted paper can be used when posting the paper or your thesis on-line.
3) In placing the thesis on the author's university website, please display the following message in a prominent place on the website: In reference to IEEE copyrighted material which is used with permission in this thesis, the IEEE does not endorse any of [university/educational entity's name goes here]'s products or services. Internal or personal use of this material is permitted. If interested in reprinting/republishing IEEE copyrighted material for advertising or promotional purposes or for creating new collective works for resale or redistribution, please go to http://www.ieee.org/publications_standards/publications/rights/rights_link.html to learn how to obtain a License from RightsLink.

If applicable, University Microfilms and/or ProQuest Library, or the Archives of Canada may supply single copies of the dissertation.

BACK CLOSE WINDOW

LIST OF REFERENCES

[1] G. Ardeshiri, H. Yazdani, and A. Vosoughi, "Optimal local thresholds for distributed detection in energy harvesting wireless sensor networks," in *2018 IEEE Global Conference on Signal and Information Processing (GlobalSIP)*, Nov 2018, pp. 813–817.

[2] G. Ardeshiri, H. Yazdani, and A. Vosoughi, "Power adaptation for distributed detection in energy harvesting wsns with finite-capacity battery," in *2019 IEEE Global Communications Conference (GLOBECOM)*. IEEE, 2019, pp. 1–6.

[3] G. Ardeshiri and A. Vosoughi, "On adaptive transmission for distributed detection in energy harvesting wireless sensor networks with limited fusion center feedback," *IEEE Transactions on Green Communications and Networking*, vol. 6, no. 3, pp. 1764–1779, 2022.

[4] P. K. Varshney, "Distributed detection and data fusion," 1996.

[5] J. N. Tsitsiklis, "Decentralized detection by a large number of sensors," *Mathematics of Control, Signals and Systems*, vol. 1, no. 2, pp. 167–182, 1988.

[6] R. Viswanathan and P. K. Varshney, "Distributed detection with multiple sensors part i. fundamentals," *Proceedings of the IEEE*, vol. 85, no. 1, pp. 54–63, 1997.

[7] R. S. Blum, S. A. Kassam, and H. V. Poor, "Distributed detection with multiple sensors ii. advanced topics," *Proceedings of the IEEE*, vol. 85, no. 1, pp. 64–79, 1997.

[8] S. S. Gupta, S. K. Pallapothu, and N. B. Mehta, "Ordered transmissions for energy-efficient detection in energy harvesting wireless sensor networks," *IEEE Transactions on Communications*, vol. 68, no. 4, pp. 2525–2537, 2020.

[9] S. Sudevalayam and P. Kulkarni, "Energy harvesting sensor nodes: Survey and implications," *IEEE Communications Surveys Tutorials*, vol. 13, no. 3, pp. 443–461, Third 2011.

[10] A. Tarighati, J. Gross, and J. Jaldén, "Decentralized hypothesis testing in energy harvesting wireless sensor networks," *IEEE Transactions on Signal Processing*, vol. 65, no. 18, pp. 4862–4873, Sep. 2017.

[11] T. Li, P. Fan, and K. B. Letaief, "Outage probability of energy harvesting relay-aided cooperative networks over rayleigh fading channel," *IEEE Transactions on Vehicular Technology*, vol. 65, no. 2, pp. 972–978, 2015.

[12] S. Ulukus, A. Yener, E. Erkip, O. Simeone, M. Zorzi, P. Grover, and K. Huang, "Energy harvesting wireless communications: A review of recent advances," *IEEE Journal on Selected Areas in Communications*, vol. 33, no. 3, pp. 360–381, March 2015.

[13] A. Tarighati, J. Gross, and J. Jaldén, "Decentralized detection in energy harvesting wireless sensor networks," in *2016 24th European Signal Processing Conference (EUSIPCO)*, Aug 2016, pp. 567–571.

[14] V. Sharma, U. Mukherji, V. Joseph, and S. Gupta, "Optimal energy management policies for energy harvesting sensor nodes," *IEEE Transactions on Wireless Communications*, vol. 9, no. 4, pp. 1326–1336, April 2010.

[15] B. Chen, L. Tong, and P. K. Varshney, "Channel-aware distributed detection in wireless sensor networks," *IEEE Signal Processing Magazine*, vol. 23, no. 4, pp. 16–26, 2006.

[16] H. R. Ahmadi and A. Vosoughi, "Distributed detection with adaptive topology and nonideal communication channels," *IEEE transactions on signal processing*, vol. 59, no. 6, pp. 2857–2874, 2011.

[17] N. Maleki and A. Vosoughi, "On bandwidth constrained distributed detection of a known signal in correlated gaussian noise," *IEEE Transactions on Vehicular Technology*, 2020.

[18] X. Zhang, H. V. Poor, and M. Chiang, "Optimal power allocation for distributed detection over MIMO channels in wireless sensor networks," *IEEE Transactions on Signal Processing*, vol. 56, no. 9, pp. 4124–4140, Sep. 2008.

[19] H.-s. Kim and N. A. Goodman, "Power control strategy for distributed multiple-hypothesis detection," *IEEE Transactions on Signal Processing*, vol. 58, no. 7, pp. 3751–3764, 2010.

[20] V. W. Cheng and T.-Y. Wang, "Performance analysis of distributed decision fusion using a censoring scheme in wireless sensor networks," *IEEE Transactions on Vehicular Technology*, vol. 59, no. 6, pp. 2845–2851, 2010.

[21] S. Maleki, G. Leus, S. Chatzinotas, and B. Ottersten, "To and or to or: On energy-efficient distributed spectrum sensing with combined censoring and sleeping," *IEEE Transactions on Wireless Communications*, vol. 14, no. 8, pp. 4508–4521, 2015.

[22] R. S. Blum and B. M. Sadler, "Energy efficient signal detection in sensor networks using ordered transmissions," *IEEE Transactions on Signal Processing*, vol. 56, no. 7, pp. 3229–3235, 2008.

[23] M.-L. Ku, W. Li, Y. Chen, and K. R. Liu, "Advances in energy harvesting communications: Past, present, and future challenges," *IEEE Communications Surveys & Tutorials*, vol. 18, no. 2, pp. 1384–1412, 2015.

[24] Z. Wang, V. Aggarwal, and X. Wang, "Iterative dynamic water-filling for fading multiple-access channels with energy harvesting," *IEEE Journal on Selected Areas in Communications*, vol. 33, no. 3, pp. 382–395, 2015.

[25] H. Yazdani and A. Vosoughi, "Steady-state rate-optimal power adaptation in energy harvesting opportunistic cognitive radios with spectrum sensing and channel estimation errors," *IEEE Transactions on Green Communications and Networking*, 2021.

[26] M. Nourian, S. Dey, and A. Ahlén, "Distortion minimization in multi-sensor estimation with energy harvesting," *IEEE Journal on Selected Areas in Communications*, vol. 33, no. 3, pp. 524–539, 2015.

[27] J. Geng and L. Lai, "Non-bayesian quickest change detection with stochastic sample right constraints," *IEEE Transactions on Signal Processing*, vol. 61, no. 20, pp. 5090–5102, 2013.

[28] H. R. Ahmadi and A. Vosoughi, "Impact of channel estimation error on decentralized detection in bandwidth constrained wireless sensor networks," in *MILCOM 2008-2008 IEEE Military Communications Conference*. IEEE, 2008, pp. 1–7.

[29] ——, "Channel aware sensor selection in distributed detection systems," in *2009 IEEE 10th Workshop on Signal Processing Advances in Wireless Communications*. IEEE, 2009, pp. 71–75.

[30] Z. Hajibabaei, A. Vosoughi, and N. Mastronarde, "Optimal power allocation for M-ary distributed detection in the presence of channel uncertainty," *Signal Processing*, vol. 169, p. 107400, 2020.

[31] X. Guo, Y. He, S. Atapattu, S. Dey, and J. S. Evans, "Power allocation for distributed detection systems in wireless sensor networks with limited fusion center feedback," *IEEE Transactions on Communications*, vol. 66, no. 10, pp. 4753–4766, Oct 2018.

[32] A. G. Marques, X. Wang, and G. B. Giannakis, "Minimizing transmit-power for coherent communications in wireless sensor networks using quantized channel state information," in *2007 IEEE International Conference on Acoustics, Speech and Signal Processing-ICASSP'07*, vol. 3. IEEE, 2007, pp. III–529.

[33] M. Shirazi and A. Vosoughi, "On distributed estimation in hierarchical power constrained wireless sensor networks," *IEEE Transactions on Signal and Information Processing over Networks*, vol. 6, pp. 442–459, 2020.

[34] G. Ardeshiri and A. Vosoughi, "On distributed detection in eh-wsns with finite-state markov channel and limited feedback," in *arXiv:2210.04953*, 2022.

[35] T. Banerjee, P. Gurram, and G. T. Whipps, "A bayesian theory of change detection in statistically periodic random processes," *IEEE Transactions on Information Theory*, vol. 67, no. 4, pp. 2562–2580, 2021.

[36] K. Premkumar and A. Kumar, "Optimal sleep-wake scheduling for quickest intrusion detection using wireless sensor networks," in *IEEE INFOCOM 2008-The 27th Conference on Computer Communications*. IEEE, 2008, pp. 1400–1408.

[37] I. S. Gradshteyn and I. M. Ryzhik, *Table of integrals, series, and products*, 7th ed., 2007.

[38] A. Goldsmith, *Wireless Communications*. Cambridge University Press, 2005.

[39] R. Valentini, M. Levorato, and F. Santucci, "Aging aware random channel access for battery-powered wireless networks," vol. 5, no. 2, April 2016, pp. 176–179.

[40] Y. Lin, B. Chen, and P. K. Varshney, "Decision fusion rules in multi-hop wireless sensor networks," *IEEE Transactions on Aerospace and Electronic Systems*, vol. 41, no. 2, pp. 475–488, 2005.

[41] D. Bajoivć, B. Sinopoli, and J. Xavier, "Sensor selection for hypothesis testing in wireless sensor networks: a kullback-leibler based approach," in *Proceedings of the 48h IEEE Conference on Decision and Control (CDC) held jointly with 2009 28th Chinese Control Conference*, Dec 2009, pp. 1659–1664.

[42] B. Chen, R. Jiang, T. Kasetkasem, and P. K. Varshney, "Fusion of decisions transmitted over fading channels in wireless sensor networks," in *Conference Record of the Thirty-Sixth Asilomar Conference on Signals, Systems and Computers, 2002.*, vol. 2, Nov 2002, pp. 1184–1188 vol.2.

[43] J. F. Shortle, J. M. Thompson, D. Gross, and C. M. Harris, *Fundamentals of queueing theory*. John Wiley & Sons, 2018, vol. 399.

[44] A. Winkelbauer, "Moments and absolute moments of the normal distribution," *arXiv preprint arXiv:1209.4340*, 2012.

[45] W. Lindeberg, "Eine neue herleitung des exponentialgesetzes in der wahrscheinlichkeitsrechnung," *Mathematische Zeitschrift*, vol. 15, no. 1, pp. 211–225, 1922.

[46] T. Ye and S. Kalyanaraman, "A recursive random search algorithm for large-scale network parameter configuration," in *Proceedings of the 2003 ACM SIGMETRICS International conference on Measurement and modeling of computer systems*, 2003, pp. 196–205.

[47] G. Ardeshiri and A. Vosoughi, "Learning-based distributed detection with energy harvesting," in *2021 55th Asilomar Conference on Signals, Systems, and Computers*, 2021, pp. 747–751.

[48] M. Ku, Y. Chen, and K. J. R. Liu, "Data-driven stochastic models and policies for energy harvesting sensor communications," *IEEE Journal on Selected Areas in Communications*, vol. 33, no. 8, pp. 1505–1520, Aug 2015.

[49] C. K. Ho, P. D. Khoa, and P. C. Ming, "Markovian models for harvested energy in wireless communications," in *2010 IEEE International Conference on Communication Systems*, 2010, pp. 311–315.

[50] F. Zhang, T. Jing, Y. Huo, and K. Jiang, "Joint Optimization of Spectrum Sensing and Transmit Power in Energy Harvesting Cognitive Radio Sensor Networks," *The Computer Journal*, vol. 62, no. 2, pp. 215–230, 02 2019.

[51] F. Amirnavaei and M. Dong, "Online power control optimization for wireless transmission with energy harvesting and storage," *IEEE Transactions on Wireless Communications*, vol. 15, no. 7, pp. 4888–4901, July 2016.

[52] Hong Shen Wang and N. Moayeri, "Finite-state markov channel-a useful model for radio communication channels," *IEEE Transactions on Vehicular Technology*, vol. 44, no. 1, pp. 163–171, Feb 1995.

[53] P. Sadghi, R. Kennedy, P. Rapajic, and R. Shams, "Finite-state markov modeling of fading channels," *IEEE signal processing magazine*, vol. 57, 2008.

[54] S. Mao, M. H. Cheung, and V. W. S. Wong, "Joint energy allocation for sensing and transmission in rechargeable wireless sensor networks," *IEEE Transactions on Vehicular Technology*, vol. 63, no. 6, pp. 2862–2875, July 2014.

[55] M. L. Puterman, *Markov decision processes: discrete stochastic dynamic programming*. John Wiley & Sons, 2014.

[56] M. Moghadari, E. Hossain, and L. B. Le, "Delay-optimal distributed scheduling in multi-user multi-relay cellular wireless networks," *IEEE Transactions on Communications*, vol. 61, no. 4, pp. 1349–1360, April 2013.

[57] F. Fu and M. V. Der Schaar, "A systematic framework for dynamically optimizing multi-user wireless video transmission," *IEEE Journal on Selected Areas in Communications*, vol. 28, no. 3, pp. 308–320, April 2010.

[58] D. Bertsekas, *Dynamic programming and optimal control: Volume I*. Athena scientific, 2012, vol. 1.

[59] D. G. Luenberger, Y. Ye *et al.*, *Linear and nonlinear programming*. Springer, 1984, vol. 2.

[60] N. Maleki, A. Vosoughi, and N. Rahnavard, "Distributed binary detection over fading channels: Cooperative and parallel architectures," *IEEE Transactions on Vehicular Technology*, vol. 65, no. 9, pp. 7090–7109, 2015.

[61] R. Niu and P. K. Varshney, "Target location estimation in sensor networks with quantized data," *IEEE Transactions on Signal Processing*, vol. 54, no. 12, pp. 4519–4528, 2006.

[62] K. Huang, B. Mondal, W. Heath, and J. Andrews, "Markov models for limited feedback mimo systems," in *2006 IEEE International Conference on Acoustics Speech and Signal Processing Proceedings*, vol. 4, 2006, pp. IV–IV.

[63] S. Akoum and R. W. Heath, "Limited feedback beamforming for temporally correlated mimo channels with other cell interference," in *2010 IEEE International Conference on Acoustics, Speech and Signal Processing*, 2010, pp. 3054–3057.

[64] W. C. Jakes and D. C. Cox, *Microwave mobile communications*. Wiley-IEEE press, 1994.